

**Novel Techniques for Rayleigh Noise Suppression and
Multicast Transmission in Wavelength Division
Multiplexed Passive Optical Networks**

XU, Jing

A Thesis Submitted in Partial Fulfillment
of the Requirements for the Degree of
Doctor of Philosophy

in

Information Engineering
The Chinese University of Hong Kong

July 2011

UMI Number: 3497761

All rights reserved

INFORMATION TO ALL USERS

The quality of this reproduction is dependent on the quality of the copy submitted.

In the unlikely event that the author did not send a complete manuscript and there are missing pages, these will be noted. Also, if material had to be removed, a note will indicate the deletion.



UMI 3497761

Copyright 2012 by ProQuest LLC.

All rights reserved. This edition of the work is protected against unauthorized copying under Title 17, United States Code.



ProQuest LLC.
789 East Eisenhower Parkway
P.O. Box 1346
Ann Arbor, MI 48106 - 1346

Acknowledgement

Time flies, and my four-year Ph.D study is coming to a close. At this moment, I owe the deepest gratitude to my thesis supervisor, Professor Lian-Kuan Chen, for his excellent guidance, continuous support, and providing me with an enjoyable atmosphere for doing research. His extensive knowledge, scientific foresight, and insight into the crux of difficult problems were pivotal in this work as well as in my development as an independent researcher. His high standard in research and teaching has set before me the best role model in academic integrity and ethics. I feel privileged to have had the opportunity to study under his guidance.

I would also like to thank Professor Chun-Kit Chan. My research benefited immensely from many enlightening discussions with him. I highly appreciate his continuous encouragement in my research, kind caring during oversea conferences, and warm support in my job hunting. I also gratefully acknowledge Professor Chester Shu, Professor Kwok-Wai Cheung and Professor Chao Lu for their valuable advices and providing experimental facilities.

I am grateful to Dr. Ning Deng, Mr. Yin Zhang, Mr. Zhenchang Xie, Dr. Ming Li, Dr. Guowei Lu, Dr. Jian Zhao, Dr. Ho Li and Mr. Jordan Tse, for their guidance on my experimental skills, fruitful discussions and help in daily life. It is my pleasure to have a chance to work with many talented fellow postgraduate students in Lightwave Communications Laboratory in the Department of Information Engineering. In particular, thanks must go to all my lab mates, including Mr. Yang Qiu, Mr. Kin-Man Chong, Mr. Kam-Hon Tse, Mr. Shuqiang Zhang, Ms. Pulan Li, Mr. Piu-hung Yuen, Mr.

Zhixin Liu, Mr. Wei Jia, Mr. Dong Shen, Mr. Qike Wang and Mr. Hon-tong Luk, for creating a dynamic and collaborative culture for research and study.

Last but not least, I cordially thank my family and friends for their long-term support, tolerance and encouragement. This thesis is dedicated to them.

Abstract

Foreseeing the rapidly growing demand for multimedia services and the trend of service convergence, the penetration of optical fiber in access network is an ultimate solution to break the last-mile bottleneck imposed by the 100-year-old copper network. One of the most promising solutions to realize optical access is the passive optical network (PON), in which the network infrastructure is shared by many subscribers and has no active elements between the central office and the customer. Thus a PON requires neither electrical power nor active management, leading to effective reduction in operational expenses. Time-division-multiplexed passive optical networks (TDM-PONs) such as Ethernet PON (EPON) and Gigabit PON (GPON) are being widely deployed in current fiber-based access networks for providing broadband access, offering triple-play services including video, data and voice. In the near future, wavelength-division-multiplexed passive optical network (WDM-PON) can be the enabler of the next-generation optical broadband access that requires large dedicated and symmetric bandwidth, data privacy, and upgrade flexibility. TDM-PONs also can benefit from WDM technologies for capacity upgrade.

Centralized light source (CLS) at the central office is an attractive solution for low-cost implementation of WDM-PON, as it eliminates the need of wavelength-specific transmitters and wavelength management at the optical network units (ONU). CLS can be realized by either a carrier-distributed scheme or a remodulation scheme. In both schemes, however, the upstream signal is susceptible to the interferometric crosstalk induced by the beating between the upstream signal and the back-reflected light due to the intrinsic Rayleigh Backscattering (RB), both of

which are of the same wavelength. We propose and demonstrate a simple and novel scheme to suppress the RB noise in the carrier-distributed WDM-PON. Differential phase-shift keying (DPSK) is used as the upstream modulation format and the destructive port of the delay-interferometer (DI) is employed to demodulate the upstream DPSK signal. As the spectrum of RB towards the OLT is narrow due to the very narrow spectrum of the distributed carrier, the RB noise can be considerably rejected by the notch filter-like destructive port of the DI at the OLT, which is used simultaneously to demodulate the upstream DPSK signal. The scheme can also be extended to the application in the remodulation-based WDM-PON, as long as the downstream signal has a narrow spectrum (i.e. via reducing downstream modulation depth). A unique feature of the DPSK signal with reduced modulation depth (RMD-DPSK) is that it can be demodulated by DI's destructive port without extinction ratio (ER) degradation, whereas the demodulated signal from DI's destructive port has a very low ER and can be used as the source for upstream remodulation. We also proposed a novel offset-Manchester coding to suppress Rayleigh noise in electrical domain via a postdetection high-pass filter.

With more diverse multimedia and data services available for broadband access, the access network has to be flexible enough to cope with various data or video delivery such as broadcast/multicast services, in addition to the point-to-point traffic. Multicast is more attractive, compared to broadcast, as it allows selective control of the connection for each subscriber individually. Multicast can be easily realized in TDM-PONs as it employs power-splitting at the remote node (RN). However, it is more challenging in WDM-PONs, due to the dedicated connection between the optical line terminal (OLT) and each ONU. Many studies have been carried out to solve this problem. The prior schemes either need relatively complicated multicast control

and/or cannot support future proof 10-Gb/s symmetric point-to-point (PtP) transmission. We proposed a novel multicast control scheme for a WDM-PON with 10-Gb/s symmetric bit rate. The multicast data encoded in DPSK format is superimposed onto all PtP channels modulated in inverse return-to-zero format. With an athermal DI being used at the ONU to demodulate the DPSK signal, the multicast data can be effectively disabled by slight detuning the laser wavelength at OLT, which has negligible effect on the PtP data. The proposed scheme differs from all the previous schemes in that, the multicast control is realized via the inherent wavelength management of WDM systems, rather than via any other additional adjustment such as ER, synchronization, and polarization.

摘要

使用具有 100 年歷史的通信電纜作為接入媒介必然導致最後一英里瓶頸，考慮到多媒體業務需求的迅速增長和業務融合的趨勢，光纖在接入網中的延伸是打破最後一英里瓶頸的最終解決辦法。無源光網絡是最有前途的實現光纖接入的解決方案之一。每個無源光網絡的網絡基礎設施可以被多個用戶共享，而且在中央基站和用戶之間沒有任何有源器件。因此，一個無源光網絡既不需要電力，也不需要太多的管理維護，有效地降低了運營費用。時分複用無源光網絡，例如以太網無源光網絡和千兆無源光網絡，正在被廣泛部署在當前的寬帶光纖接入網絡中，用於提供三網融合業務，包括視頻，數據和語音。下一代光接入網要求具有大量的專用和對稱帶寬，數據隱私性和升級的靈活性。在不久的將來，波分複用無源光網絡的將成為下一代光接入網的推動者。當然時分複用無源光網絡也可以和波分複用技術相結合以升級帶寬。

把光源集中在中央基站是一個有吸引力的低成本的波分複用無源光網絡實施方案，因為它消除了光網絡單元中的特定波長發射器和波長管理。可以通過載波遠程分配和重調製這兩個方案把光源集中在中央基站。但是，在這兩個方案中，下行信號的瑞利散射光和上行信號具有相同波長，二者的拍噪聲將會對上行信號產生相干竄擾。我們提出並實驗驗證了一種簡單新穎的抑制基於載波遠程分配的波分複用無源光網絡中瑞利噪聲的方案。在該方案中，上行調製格式使用差分相移鍵控並使用延遲干涉儀的相消端口解調上行差分相移鍵控信號。由於送往光網絡單元的光載波具有很窄的線寬，它的傳往光線路終端的瑞利散射光也具有很窄的光譜，從而可以用上述的具有陷波濾波器特性的延遲干涉儀的相消端口有效地抑制瑞利散射光。只要下行信號的功率集中於低頻（例如可通過降低下行信號的調製），該方案也可以推廣到基於重調製的波分複用無

源光網絡。低調製深度差分相移鍵控信號具有一個獨特的性質：如果它被延遲干涉儀的相消端口解調，所得解調信號的消光比不會由於調製深度降低而惡化，同時如果它被延遲干涉儀的相長端口解調，所得解調信號的消光比會很低，從而可以用作實現上行重調製的光源。我們還提出了一個新穎的時移曼徹斯特編碼方案，並通過電子高通濾波器實現對瑞利噪聲的抑制。

隨著接入網中多媒體和寬帶數據服務的多樣化發展，接入網必須具有足夠的靈活性，以應對各種數據或視頻傳輸。比如它除了支持點到點傳輸外還應支持廣播或組播服務。相比之下，組播比廣播更具吸引力，因為它允許選擇性地控制為每個用戶的單獨連接。時分複用無源光網絡在遠程節點中放置了分光器，所以它很容易實現組播功能。但是，由於在波分複用無源光網絡中光線路終端和每個光網絡單元之間的信道都是專用的，在波分複用無源光網絡中實現組播功能是很困難的。為解決這一難題，人們進行了很多的研究。但是，這些已經提出的方案要么需要比較複雜的組播控制，要么不能支持面向未來的十吉比特每秒對稱的點到點傳輸。我們提出了一個新的用於波分複用無源光網絡中的組播控制方案，同時它可以支持十吉比特每秒對稱的點到點傳輸。該方案中，組播信號使用差分相移鍵控編碼並通過正交調製疊加到下行的使用反轉歸零編碼的點到點信號上。差分相移鍵控信號在光網絡單元中被一個無源的延遲干涉儀解調。通過在光線路終端微調激光器波長，組播信號可以被有效地關閉，與此同時點到點信號基本不受影響。該方案有一個區別於所有已知方案的優點，那就是在該方案中組播控制是基於波分複用系統固有的波長管理，而不是基於對一些額外參數的調整，比如對消光比、同步和偏振的調整。

Table of contents

Acknowledgement.....	i
Abstract	iii
摘要.....	vi
Table of contents	viii
List of figures and tables	xii
Chapter 1 Introduction	1
1.1. Introduction to WDM-PON	1
1.1.1. Increasing Bandwidth Demand in Access network.....	2
1.1.2. PON Systems Overview.....	5
1.2. Research challenges of WDM-PON	8
1.2.1. Colorless ONU	9
1.2.2. Rayleigh noise in WDM-PON	10
1.2.3. Broadcast/ Multicast service in WDM-PON.....	12
1.3. Major contributions of this thesis	12
1.3.1. Using DI's destructive port to suppress Rayleigh noise.....	12
1.3.2. Unique features of RMD-DPSK signal.....	13
1.3.3. Flexible multicast control in WDM-PONs with symmetric point-to-point bit rate.....	14
1.4. Outline of this thesis	14
References	15
Chapter 2 WDM-PONs with Centralized Light Sources	21
2.1. Carrier-distributed scheme.....	22
2.2. Remodulation scheme	22

2.3.	Demodulation of downstream DPSK signals by a partial-bit delay interferometer.....	24
2.3.1.	System architecture and operation principle.....	24
2.3.2.	Experimental demonstration.....	26
2.4.	Reducing the modulation depth of downstream DPSK signal.....	29
2.4.1.	Operation principle and system architecture.....	30
2.4.2.	Experimental demonstration.....	32
2.5.	Summary.....	38
	References.....	38
	Chapter 3 Rayleigh Noise Suppression in Optical Domain.....	42
3.1.	Rayleigh noise suppression in carrier-distributed WDM-PONs based on in-band optical filtering.....	42
3.1.1.	Introduction.....	42
3.1.2.	Application in a 20-km WDM-PON.....	44
3.1.3.	Application in a long-reach WDM-PON.....	50
3.1.4.	Multiple Rayleigh Backscattering.....	64
3.2.	Optical phase remodulation with enhanced tolerance to Rayleigh noise	67
3.2.1.	Introduction.....	67
3.2.2.	System architecture.....	68
3.2.3.	Operation principle.....	69
3.2.4.	Experimental demonstration.....	76
3.3.	Summary.....	80
	References.....	81
	Chapter 4 Rayleigh Noise Suppression in Electrical Domain.....	87
4.1.	Offset Manchester coding for Rayleigh noise suppression in carrier-distributed WDM-PONs.....	87

4.1.1.	Introduction	87
4.1.2.	System architecture and operation principle	88
4.1.3.	Experimental demonstration	90
4.2.	A novel chirp-free optical Manchester signal transmitter	95
4.2.1.	Introduction	95
4.2.2.	Operation principle.....	97
4.2.3.	Experimental demonstration	98
4.2.4.	Enhanced dispersion tolerance	100
4.3.	Summary	102
	References	103
	Chapter 5 Multicast Transmission in WDM-PON	105
5.1.	Introduction to broadcast/multicast Overlay	105
5.2.	Hybrid- OTDM-based broadcast overlay	106
5.2.1.	Introduction	106
5.2.2.	System architecture	107
5.2.3.	Experimental demonstration	108
5.2.4.	Delay-interferometer based timing alignment monitoring for RZ-transmitters	111
5.3.	Broadcast transmission using time-interleaved phase remodulation	122
5.3.1.	Introduction	122
5.3.2.	System architecture and operation principles	122
5.3.3.	Experimental demonstration	125
5.4.	A delay-based multicast control scheme for WDM-PONs with 10-Gb/s symmetric two-way traffics.....	127
5.4.1.	Introduction	127
5.4.2.	Proposed system architecture and multicast control	128

5.4.3.	Experimental demonstration	130
5.4.4.	Discussions.....	136
5.5.	A wavelength detuning-based multicast control scheme	142
5.5.1.	Introduction.....	142
5.5.2.	System architecture and multicast control	142
5.5.3.	Experimental demonstration	144
5.6.	Summary	146
	References	148
	Chapter 6 Conclusion	152
6.1.	Summary of the thesis.....	152
6.2.	Suggestion on future work.....	154
	References	155
	Appendix:.....	157
A.	List of abbreviations	157
B.	List of publications	161

List of figures and tables

Fig. 1.1 Nielsen’s Law of Internet Bandwidth [1].	1
Fig. 1.2 FTTH households & penetration in major economies (end of 2013) [7].	1
Fig. 1.3 Worldwide FTTH deployment forecast (2007-2013) [7].....	1
Fig. 1.4 PON timeline [9].....	1
Fig. 2.1 WDM-PON architecture using the proposed simplified ONU structure with partial-bit-delay DI (PBD-DI).....	1
Fig. 2.2 Eye diagrams of (a) the demodulated downstream 10-Gb/s DPSK signal from the destructive port of the 0.25-bit DI, (b) IRZ-shaped output from the constructive port of the 0.25-bit DI, (c) the detected upstream OOK signal. Time scale: 20 ps/div. (d) BER degradation (from 10^{-9}) caused by wavelength offset between the laser source and the DI.	1
Fig. 2.3 BER measurement results for both down- and up-stream signals.	1
Fig. 2.4 (a) Eye diagram of the 10-Gb/s FMD-DPSK signal after transmission in 20-km SMF without demodulation by DI. Time scale: 20ps/div. (b) Spectrum comparison between two DPSK signals with different driving voltages (Raised-cosine driving signal is assumed).	1
Fig. 2.5 Proposed re-modulation architecture using downstream RMD-DPSK and upstream OOK. Tx/R: transceiver.	1
Fig. 2.6 BER measurements of both DS and US signals when using dual-fiber configuration. Inset: corresponding eye diagrams for different cases. Time scale: 20ps/div. DS: downstream, US: upstream.....	1

Fig. 2.7 Power penalty of upstream signal induced by remodulation timing misalignment.	1
Fig. 2.8 : BER measurements of both DS and US signals using single-fiber configuration . Inset: corresponding eye diagrams for different cases. Time scale: 20ps/div. DS: downstream, US: upstream, ch: channel.	1
Fig. 3.1 Proposed loopback architecture using DPSK as the upstream modulation format to suppress Rayleigh noise. The downstream channels are omitted here for simplicity.	1
Fig. 3.2 (a) Experimental setup. (b) The relationship between the average reflection power (P_r) and the average power of the input CW light to the 20-km SMF (P_{in}). Inset: measured spectrum of the RB noise with (the dashed line) or without (the solid line) using the destructive port of the DI to suppress the RB noise.	1
Fig. 3.3: Eye diagrams of the detected upstream DPSK signal by a 10-Gb/s p-i-n receiver in both back-to-back (a) and (c), and transmission case (b) and (d). Time scale: 20ps/div.	1
Fig. 3.4 BER measurements. The received signal power was measured before the p-i-n receiver. Inset: eye diagram of the detected upstream OOK signal. Time scale: 20ps/div.	1
Fig. 3.5 Proposed loopback architecture using DPSK as the upstream modulation format to suppress Rayleigh noise for long-reach WDM-PON. The downstream channels are omitted here for simplicity. OA: optical amplifier, PM: phase modulator, DI: delay-interferometer, DCM: dispersion compensation module, PIN: p-i-n receiver.	1
Fig. 3.6 Required ONU gain, and P_{CB}/P_{SB} , for different feeder-fiber lengths. The upstream receiver sensitivity is set to be -32 dBm for the dashed line, and -27 dBm for the solid line, respectively.....	1

Fig. 3.7 Experimental setup to investigate the effectiveness of the proposed scheme on the suppression of (a) carrier RB, and (b) signal RB.	1
Fig. 3.8 Power penalty as a function of signal-to-crosstalk ratio (SCR). Insets: measured spectra (resolution bandwidth=0.06 nm) of signal (DPSK) RB and carrier RB before and after DI.	1
Fig. 3.9 BER measurement results. Insets: upstream eye diagrams in the proposed scheme and in the conventional scheme. Time scale: 20ps/div.	1
Fig. 3.10 The relation between the upstream receiver sensitivity and ONU gain.	1
Fig. 3.11 The maximum system margin and the required optimal ONU gain for different system reaches. The length ratio between the feeder and distribution fiber is assumed to be 5:1.	1
Fig. 3.12 Generation of second-order RB.	1
Fig. 3.13 Power ratio between signal-RB1 and signal-RB2 _(b) as the function of ONU gain.	1
Fig. 3.14 Proposed optical phase remodulation architecture.	1
Fig. 3.15 Eye diagrams with different downstream modulation depths: (a)-(c), downstream DPSK signal demodulated from DI's destructive port; (d)-(f), downstream DPSK signal demodulated from DI's constructive port; (g)-(i) downstream OOK signal in conventional optical amplitude remodulation scheme. ...	1
Fig. 3.16 The insertion loss of the DI's destructive port for the downstream RMD-DPSK signal and for its RB, at different downstream modulation depths. Inset: the simulated spectrum of the downstream RMD-DPSK signal with different modulation depths.	1
Fig. 3.17 (a) The impact of the downstream modulation depth on the receiver sensitivity of both downstream and upstream signals when using different remodulation schemes. Eye diagrams of the detected upstream FMD-DPSK signal that	

is remodulated (b) on the DI's constructive port output (c) on part of the downstream RMD-DPSK signal. (d) Eye diagrams of the detected upstream FMD-OOK signal when using the conventional optical amplitude remodulation (downstream RMD-OOK, upstream FMD-OOK). The downstream modulation depth in Fig. 3 (c)-(e) is 0.4 1

Fig. 3.18 (a) experimental setup used to investigate the effectiveness of DI's two output ports on RB suppression, CP: constructive port, DP: destructive port. (b)-(d), measured spectrum (resolution bandwidth=0.06 nm) of the RB before and after the DI when the downstream modulation depth (MD) is 0.18, 0.31 and 0.43, respectively... 1

Fig. 3.19 Eye diagrams of the detected downstream RMD-DPSK and upstream FMD-DPSK signals in B2B and transmission cases. B2B: back-to-back, DS: downstream, US: upstream, DP: destructive port of the DI, CP: constructive port..... 1

Fig. 3.20 (a) BER measurement results when the downstream modulation depth is 0.22. (b) BER measurement results when the downstream modulation depth is 0.18 and a SOA is used at ONU. DS: downstream, US: upstream..... 1

Fig. 4.1 Proposed loopback architecture using Manchester coding and postdetection electrical high-pass filter in upstream to suppress Rayleigh noise. The downstream channels are omitted here for simplicity. 1

Fig. 4.2 Experimental setup to investigate the Rayleigh-noise tolerance. 1

Fig. 4.3 Eye diagrams of the OMC-signal, the MC-signal and the NRZ signal at 2.5-Gb/s with different SCR values. Time scale: 100ps/div. 1

Fig. 4.4 The upstream power penalty (BER=10⁻⁹) as a function of SCR. 1

Fig. 4.5 BER measurement results..... 1

Fig. 4.6 The impact of ONU gain on the upstream receiver sensitivity (at BER=10⁻⁹). 1

Fig. 4.7 (a) Proposed optical Manchester signal transmitter. (b) simulated spectrum of

the optical Manchester signal.....	1
Fig. 4.8. Operation principle of the proposed optical Manchester signal transmitter. .	1
Fig. 4.9: BER measurements. Inset: eye diagram of the detected optical Manchester signal by a 10-Gb/s p-i-n receiver.	1
Fig. 4.10 Dispersion tolerance comparison between the proposed scheme and the prior scheme using dual-drive MZM, (a) direct detection, (b) differential detection [14]. . .	1
Fig. 4.11 Eye diagrams of the detected 10-Gb/s optical Manchester signal generated by the proposed scheme, (a) back to back, direct detection; (b) back to back, differential detection; (c) after the transmission in 20-km SMF, direct detection; (d) after the transmission in 20-km SMF, differential detection;.....	1
Fig. 4.12: Eye diagrams of the detected 10-Gb/s optical Manchester signal generated by the prior dual-drive MZM based scheme, (a) back to back, direct detection; (b) back to back, differential detection; (c) after the transmission in 20-km SMF, direct detection; (d) after the transmission in 20-km SMF, differential detection;	1
Fig. 5.1 The proposed WDM-PON architecture with hybrid-OTDM based broadcast overlay.	1
Fig. 5.2 Eye diagrams of (a), (b) before DI (for downstream unicast signal detection); (c), (d) after DI (for broadcast signal detection); (e),(f) the detected upstream signal. Time scale: 20 ps/div.....	1
Fig. 5.3 BER curves for downstream unicast signal, broadcast signal and upstream signal.	1
Fig. 5.4 RZ-DPSK signals in the two arms of the DI before combining by the output 3-dB coupler for (a) aligned and (b) half-bit misaligned cases.....	1
Fig. 5.5: MPDR versus the delay of DI. The duty cycle of the RZ pulse train in simulation was 50%. DP: destructive port, CP: constructive port, DM: differential monitoring.	1

Fig.5.6 Experimental setup. Inset: Eye diagrams of the detected RZ-DPSK signals from each port of the DI when the pulse carver and data modulator are well aligned or have half-bit misalignment. Time scale: 20ps/div. DP: destructive port, CP: constructive port.....	1
Fig.5.7 Experimental results of output monitoring power for different timing misalignments using a 94-ps DI.....	1
Fig. 5.8 MPDR vs. the delay of DI. The duty cycle of the RZ pulse train in simulation was 33%. DP: destructive port, CP: constructive port, DM: differential monitoring..	1
Fig. 5.9 MPDR versus the delay of DI when the RZ-DPSK/ RZ-OOK signals are generated by single modulator. DP: destructive port, CP: constructive port, DM: differential monitoring.	1
Fig. 5.10 Proposed WDM-PON architecture with symmetric bit rates and broadcast overlay. CR: clock recovery.	1
Fig. 5.11 (a) Eye diagrams of (i) the detected downstream unicast data when the broadcast signal is off, (ii) the detected broadcast data when the unicast signal is off, (iii) the detected downstream unicast and broadcast data, (iv) the constructive port output with optical power in each bit. Time scale: 50 ps/div. (b) Operation principles of time-interleaved phase remodulation.	1
Fig. 5.12 BER results of (a) the downstream unicast and broadcast signals. (b) the upstream signal. Inset: the corresponding eye diagrams for different cases. Time scale: 50ps/div.	1
Fig. 5.13 The proposed WDM-PON architecture with symmetric bit-rates and multicast overlay. Tx/R: transceiver, P-t-P Data: point-to-point data, IM: intensity modulator, OLT: optical line terminal, EDFA: Erbium Doped Fiber Amplifier, DI: delay interferometer, PIN: p-i-n photodetector, PM: phase modulator, RN: remote node, ONU: optical network unit.	1

Fig. 5.14 Eye diagrams of (a) the detected 10-Gb/s downstream point-to-point data in IRZ format, (b) the detected upstream data with proper delay at the Delay-2, (c) (i) – (vi) the 10-Gb/s demodulated DPSK multicast signal with timing misalignment adjusted from 0 to 50 ps with a 10-ps step. Time scale: 20 ps/div.	1
Fig. 5.15 BER measurements of downstream IRZ point-to-point signals and multicast DPSK signals with multicast enabled (0-ps time misalignment) and disabled (50-ps time misalignment) cases. The solid and dashed lines correspond to the cases that the ERs of the IRZ signal are ~ 4.5 dB and ~ 6 dB, respectively.	1
Fig. 5.16 BER measurements of upstream signals. The solid and dashed lines correspond to the cases that the ERs of the IRZ signal are ~ 4.5 dB and ~ 6 dB, respectively.....	1
Fig. 5.17 Power penalty of multicast signal versus misaligned time between the downstream IRZ signals and the multicast DPSK signals. The solid and dashed lines correspond to the cases that the ERs of the IRZ signal are ~ 4.5 dB and ~ 6 dB, respectively.....	1
Fig. 5.18 Power penalty of upstream signal versus misaligned time between the downstream IRZ signals and the upstream signals. The solid and dashed lines correspond to the cases that the ERs of the IRZ signal are ~ 4.5 dB and ~ 6 dB, respectively.....	1
Fig. 5.19 Power penalty (at BER= 10^{-9}) versus the 3-dB channel bandwidth of AWGs used at the OLT and the RN. The solid and dashed lines correspond to the cases that the ERs of the IRZ signal are ~ 4.5 dB and ~ 6 dB, respectively.	1
Fig. 5.20. Power penalty (at BER= 10^{-9}) versus residual dispersion in the distribution fiber. The solid and dashed lines correspond to the cases that the ERs of the IRZ signal are ~ 4.5 dB and ~ 6 dB, respectively.	1
Fig. 5.21. (a) Optical eye diagram of the detected 5-Gb/s multicast data with timing	

misalignment of 50 ps. (b) Optical eye diagram of the detected 5-Gb/s multicast data with timing misalignment of 0 ps. (c) Detected electrical eye diagram of the 5-Gb/s multicast data with 50-ps timing misalignment using a 4-GHz receiver. (d) Detected electrical eye diagram of the 5-Gb/s multicast data with 0-ps timing misalignment using a 4-GHz receiver..... 1

Fig. 5.22. BER measurements of the 2.5-Gb/s multicast data for timing misalignment of 50 ps and 0 ps. The ER of the 10-Gb/s downstream point-to-point data is 10 dB. . 1

Fig. 5.23 Proposed WDM-PON architecture with wavelength tuning-based multicast control. I&T control: diving current and temperature control of the DFB Laser..... 1

Fig. 5.24 Power penalty versus laser driving current and wavelength tuning for multicast control..... 1

Fig. 5.25 BER measurements. B2B: back-to-back. 1

Chapter 1 Introduction

1.1. Introduction to WDM-PON

The worldwide high-speed wired access network nowadays is still mainly based on Digital Subscriber Line (DSL) technology. However, the limited bandwidth-distance product of the copper based network will be the bottleneck for future bandwidth-intensive multimedia-services, such as super-high-definition TV and even 3D TV. For example, the typical bandwidth provided by DSL is 1.5 Mbps and 128 kbps in downstream and upstream, respectively, when subscribers distribute within 18,000 ft from the central office (CO). Foreseeing the rapidly growing demand for bandwidth, it is obvious that fiber-based access network will be the ultimate solution. At the same time, wireless communication is also entering a new phase, shifting the focus from conventional voice service to the emerging multimedia communications. In this scenario optical access network is an attractive solution to provide higher capacity for base station back-haul communications.

One of the most promising optical access architectures is the passive optical network (PON), in which the network infrastructure is shared by many subscribers and has no active elements between the central office and the customer. The outside passive plant consists of only optical fibers and optical passive components, and thus requires neither electrical power nor active management, leading to effective reduction in operational expenses. Time-division-multiplexed passive optical network (TDM-PON) systems such as Ethernet PON (EPON) and Gigabit PON (GPON) are being widely deployed in current fiber-based access networks for providing broadband

access, offering triple-play services including video, data and voice. In the near future, wavelength-division-multiplexed passive optical network (WDM-PON) can be the enabler of the next-generation optical broadband access that requires large dedicated and symmetric bandwidth, data privacy, and upgrade flexibility. TDM-PONs also can benefit from WDM technologies for capacity upgrade.

1.1.1. Increasing Bandwidth Demand in Access network

Moore’s Law tells us that computing power (the number of transistors on a processor, to be precise) will double every two years. While Moore saw such a pace of development in computer processing power, Nielsen postulated its telecommunications’ equivalent in 1998: Nielsen’s Law of Internet Bandwidth. Nielsen’s Law states that a high-end user’s connection speed grows by 50% per year [1]. Fig. 1.1 shows that Nielsen’s prediction agrees well with actual data points of bandwidth availability [2]. The Fiber to the Home Council has been testing out Nielsen’s law in a sample of European countries, including Poland, Spain, Sweden,

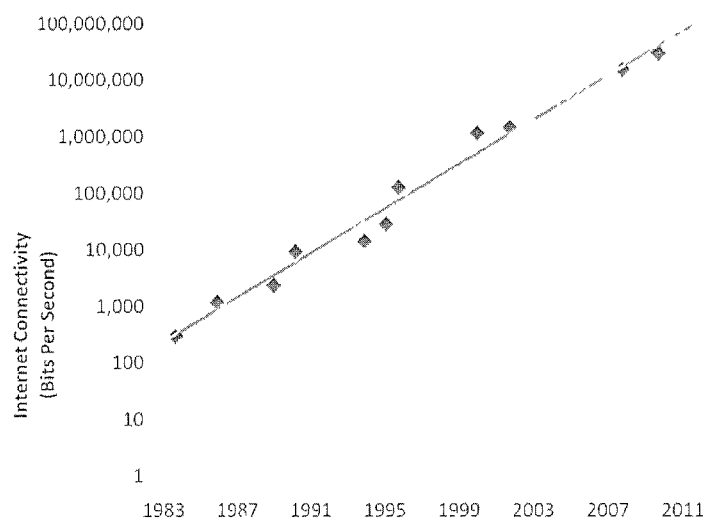
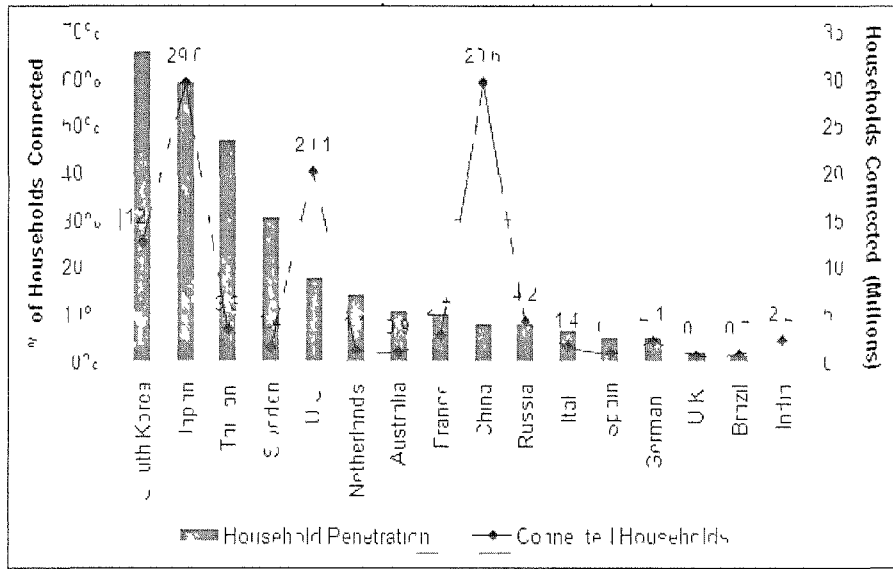


Fig. 1.1 Nielsen’s Law of Internet Bandwidth [1].

the UK and France. The results indicate that a decade after it was first postulated, Nielsen's Law is still working well as a guide to the trend in broadband access bandwidth, as the predicted growth rate of 50% per year held true as an average across the European countries evaluated [3].

In the near future, the access bandwidth is expected to be consumed by emerging subscriber services such as Internet protocol TV (IPTV), video-on-demand (VoD), video file swapping, peer-to-peer applications, teleworking, network storage, and real-time on-line games [4]. Take IPTV as an example, a standard-definition television signal requires a bandwidth of about 2 Mbps, a High-definition television (HDTV) signal requires a bandwidth of 4-8 Mbps with new compression technology, and 3D HDTV will further require 100 to 300 Mbps when it is widely sold to individual consumers, a few years from now [5]. Besides the aforementioned foreseeable applications, certain entirely new and unforeseen bandwidth-hungry services may suddenly appear and consequently frustrate end users whose network is not future-proof. YouTube, after appearing in February 2005, quickly became one of the five largest users of bandwidth on earth, and the largest single user of Internet bandwidth [5]. In addition to the rapid bandwidth increase as predicted by Nielsen's Law, symmetric bandwidth is also commonly required by some emerging applications [6]. Both DSL and CATV technologies, with limited and asymmetric capacity, cannot satisfy the explosive demand for bandwidth in emerging applications. This surging bandwidth demand can only be met by the deeper penetration of optical fiber in access networks.

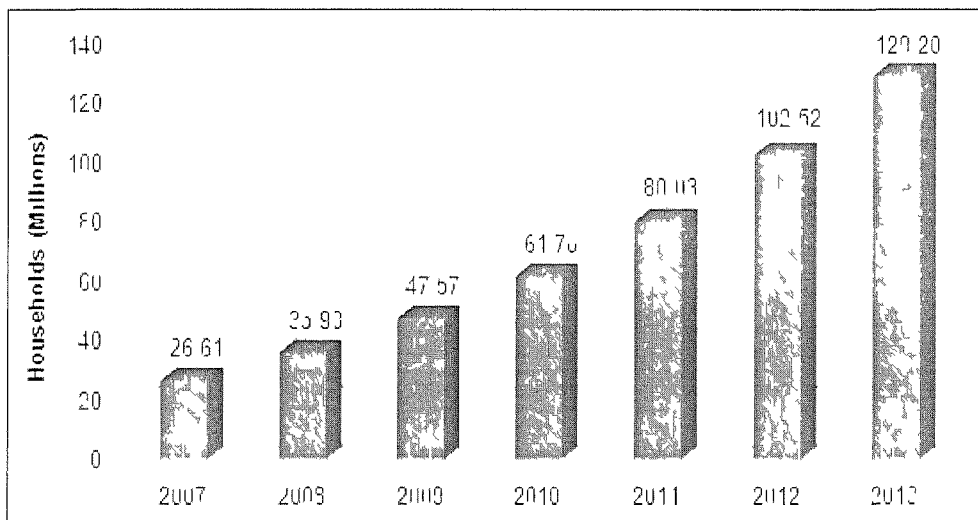
Although very promising, fiber-based broadband access is still at its initial stage. As shown in Fig. 1.2, only seven economies around the world will realize fiber to the



SOURCE: HEAVY RESEARCH

Fig 1 2 FTTH households & penetration in major economies (end of 2013) [7]

home (FTTH) with a household penetration greater than 10% till the end of 2013. By then, the household penetration of FTTH will be greater than 50% only in South Korea and Japan. Nevertheless, the developing trend of fiber-based broadband access around the world is encouraging. As shown in Fig 1 3, the worldwide FTTH deployment has been steadily increasing during recent years and the total number of



SOURCE: HEAVY RESEARCH

Fig 1 3 Worldwide FTTH deployment forecast (2007-2013) [7]

households connected with FTTH will reach around 130 million. [7]

1.1.2. PON Systems Overview

The deployment of optical fiber in access networks can be achieved in different ways, resulting in multiple FTTX models for optical access network -- FTTH, Fiber to the Curb (FTTC), Fiber to the Premises (FTTP), etc. These models are simply derived from different combinations of optical fiber and twisted pair or coaxial cable networks with variations in the penetration degree of optical fiber in the subscriber's side.

The optical access network is commonly deployed in two specific configurations. In the first one dedicated fiber runs from the central office (CO) to each subscriber. Although this point-to-point (PtP) network is the simplest design of optical access network, in most cases it is cost-prohibitive due to the extremely large amount of fibers deployed in the outside. To realize fiber gain, the other point-to-multipoint (PtMP) configuration can be adopted, with a remote node (RN) being placed close to the subscribers. In the PtMP network, one common feeder fiber is used to connect the CO and the RN, whereas dedicated distribution fiber is used for the connection between the RN and each subscriber. Bandwidth is split at the RN among all subscribers. The amount of fibers deployed in the outside plant can be substantially reduced in the PtMP configuration, thanks to the sharing of one common feeder fiber among all the subscribers. A consequent advantage of PtMP configuration over PtP configuration is that the mean-time-to-repair is significant reduced in case of fiber break.

Optical access networks using the PtMP configuration fall into two categories,

depending on whether active components are used at the RN or not. The optical access network is referred to as active optical network (AON) when an active switch together with transceiver pairs is placed at the RN, whereas it is referred to as PON when the RN consists of only passive components. The key advantage of PON over AON is that no electrical power is required in the outside plant, as the provisioning and maintaining of electrical power in the local loop are very costly and manpower intensive. For example, the backup batteries have life spans of 5-10 years and hence must be replaced regularly. While electrical power may seem like a mundane topic in the glamorous world of lasers, fiber, and high-speed data access, it is actually a substantial problem with no easy solution [8]. As PON is characterized by the attractive feature of fully passive outside plant, it is the most promising candidate for optical access network.

Time-division multiple access (TDMA) is currently the most popular method to share a single PON architecture among all its subscribers, and TDM-PON has been supported by a set of mature standards, such as two major state-of-the-art PON standards IEEE 802.3ah EPON and ITU-T G.984 GPON. Dynamic Bandwidth Allocation (DBA) algorithms are used in TDM-PON to share an aggregated bandwidth among all subscribers. This time-based separation of subscribers within fixed aggregated bandwidth has made TDM-PON difficult to keep pace with the rapidly changing bandwidth landscape predicted by Nielsen's Law. Today, bandwidth in the range of 10 Mbit/s may seem generous for a residential user. However, 100 Mbit/s is currently used by most operators as a more future-proof assumption in their Return on Investment (RoI) calculations, with future upgradability to 1 Gbit/s mandated for both residential communities and business users [9]. It is difficult for a TDM-PON to deliver 1-Gbit/s Committed Information Rate (CIR) to each subscriber,

as all transceivers at the end-points would need to operate at the aggregate bitrate, i.e., at 32 Gbit/s if the TDM-PON is shared by 32 subscriber. Standards bodies, equipment vendors and service providers have been struggling to keep pace with the increasing bandwidth demand, evolving from ATM PON (APON), Broadband PON (BPON), to current EPON and GPON, and now searching for future-proof alternatives.

Most challenging issues in TDM-PON can be avoided in WDM-PON, such as limited CIR and reach, poor security and inflexible migration. For this reason, WDM-PON has attracted extensive research interest from academia and industry [9-14]. Fig.1.4 shows the evolution path of PON, in which WDM-PON is regarded as a promising candidate for the next generation access network (NGA) [9]. In contrast to TDM-PON where a single pair of wavelengths is shared among all subscribers, in WDM-PON each subscriber is assigned a pair of dedicated wavelengths (or only one dedicated wavelength when the upstream signal is remodulated on part of the downstream signal). Thus, a WDM-PON actually provides a physical point-to-point

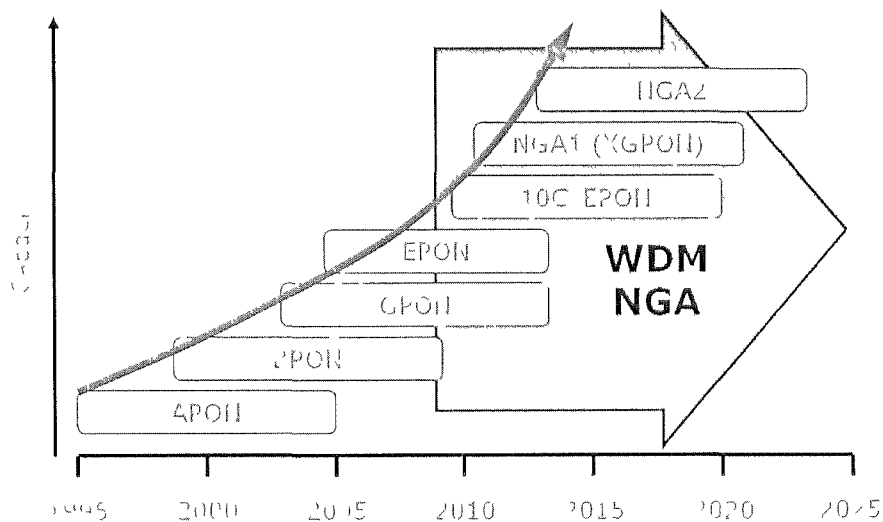


Fig. 1.4 PON timeline [9].

wavelength connection over a PtMP fiber plant, leading to much higher CIR than TDM-PON. Compared with TDM-PON, the only difference in the outside plant is that the power splitter at RN in a TDM-PON is replaced with an athermal arrayed waveguide grating (AWG) to demultiplex the downstream wavelengths and multiplex the upstream wavelengths. As the insertion loss of the AWG is much lower than a power splitter, WDM-PON can future-proof network operators' investment by delivering more bandwidth to more endpoints from fewer COs that sit farther back in the network.

Residential and business customers have traditionally been served from two separate networking platforms, due to their different requirements on bandwidth and service quality. When introducing WDM in the access and backhaul part of the network, two parallel purpose-built platforms are not necessary any longer, as different customer groups can be served on different wavelengths for which the bandwidth and service quality can be set independently. Thus, one common WDM-PON infrastructure can serve different customer groups, from residential communities to business customers and ultimately even wholesale carrier customers, yielding obvious and substantial savings [9]. The hardware-based traffic separation also makes it possible for WDM-PON to meet stringent requirements for data privacy.

1.2. Research challenges of WDM-PON

At first glance, the idea of WDM technology is somewhat simple. However, it has certainly been one of the greatest bandwidth enablers for modern optical communications. It is the WDM technology together with optical amplification that has paved the way to a new era of high speed optical communications. As WDM

technology matured, its footprint has moved from the core network toward the metropolitan network, eventually reaching the edge of access. However, the extension of WDM technology to cost-sensitive access network is not straightforward. Although WDM-PON has many technical advantages, several challenging issues have to be tackled before making it more attractive for practical deployment.

1.2.1. Colorless ONU

Athermal AWGs, once being a challenging issue for the practical deployment of WDM-PON, have been recently commercialized and can potentially be manufactured as cheap as power splitters using planar lightwave circuit (PLC) technology [15]. However, cost-effective light source at ONU remains the most challenging issue in WDM-PON. If wavelength-specific sources such as distributed fiber bragg (DFB) lasers were used at different ONUs, thermo-electric coolers (TEC) would be required to stabilize their wavelengths, resulting in expensive packaging as well as large power consumption. Furthermore, in this scheme different or “colored” transmitters would be required for different users, leading to high costs for inventory management and maintenance [16]. Spectrum-sliced incoherent light sources such as light-emitting diodes (LEDs) and amplified spontaneous emission sources have been proposed to use as low-cost and colorless ONU transmitters [17][18]. However, the bit rate of this scheme is limited to hundreds of Mb/s. Wavelength-tunable lasers can also be used as ONU transmitters to realize color-free operation [19], [20], enabling bit rates of >1 Gb/s and reach in excess of 50 km. Nevertheless, more technology advances are necessary to make tunable lasers cheap enough for the application in access network.

Meanwhile, color-free operation of ONU can also be realized by eliminating any

light source at ONU. Thus, to facilitate the wavelength management and maintenance, the WDM-PON architecture with centralized light sources (CLS) at OLT has emerged as an attractive solution [21]-[29]. The CLS architecture can be realized by either a carrier-distributed scheme or a remodulation scheme. In the carrier-distributed scheme, in addition to the downstream laser sources, extra laser diodes are installed at the OLT to remotely provide optical carrier to each ONU for the upstream data modulation. In the remodulation scheme, part of the downstream light is directly reused as the upstream carrier at the ONU. In the CLS architecture, only a wavelength-independent modulator is needed at each ONU. The ONU modulator can be either external modulator, Fabry-Perot laser diode (FP-LD) or reflective semiconductor optical amplifier (RSOA), depending on the required bit rate and power budget. With no wavelength registered light source incorporated at the ONU, wavelength provisioning, monitoring and stabilization at every ONU are unnecessary. As the ONU in the CLS architecture is colorless, identical modules can be used in all ONUs, and it would greatly facilitate mass production and the operation, administration, and maintenance (OA&M) functions.

1.2.2. Rayleigh noise in WDM-PON

Rayleigh scattering (named after the British physicist Lord Rayleigh) arises from small-scale (small compared with the light wavelength) inhomogeneities that are produced during fiber manufacture. Examples of inhomogeneities are compositional fluctuations (which results in minute refractive index change) and microscopic variations in the material density (fundamental and not improvable) [30], [31]. As light travels in the core, some scattered light is reflected back toward the light source and is named as Rayleigh backscattering (RB). For a input power of P_m , the mean

backscattered power P_{RB} is given by [32], [33],

$$P_{RB} = P_m \alpha_s S (1 - e^{-2\alpha_p L}) / 2\alpha_p$$

With α_s , α_p , S , L being the attenuation coefficient due to Rayleigh scattering, fiber attenuation coefficient, recapture factor, and fiber length, respectively.

The design of CLS architecture is a key technical issue for low-cost implementation of WDM-PON. However, in both aforementioned CLS schemes, when the optical carrier for upstream transmission is distributed from the OLT to the ONU, the back-reflected light generated by RB and Fresnel back-reflections will transmit to the upstream receiver together with the upstream signal. Due to the loss of the round-trip propagation between the OLT and the ONU, the received upstream signal normally has a relatively small power, and will be susceptible to the interferometric crosstalk induced by the beating between the upstream signal and the back-reflected light, in the case of bidirectional transmission over single fiber. Whereas Fresnel back-reflections could be prevented by using specially designed connectors, RB arising from the intrinsic refractive index inhomogeneities in the fiber is unavoidable.

The RB problem can be avoided via dual-fiber transmission. However, it will increase the network cost, as fiber deployment is manpower intensive and fiber links are very precious resource for network operators. In addition, a bandwidth provider seldom has direct fiber access to an area of subscribers, but rather must provide services over one or more networks owned by others, leasing the access on a per-fiber basis [9]. In this case, doubling the number of transmission fibers would directly double the operational cost of fiber leasing. Thus bidirectional transmission over

single fiber is highly desirable in the practical deployment of WDM-PON. For this reason, RB noise suppression, the enabler of bidirectional transmission over single fiber in CLS-based WDM-PON, is a major research challenge.

1.2.3. Broadcast/ Multicast service in WDM-PON

As the bandwidth-hungry video streams such as high-definition (HD) television are more and more pervasive in the access network, broadcast service is a very important issue in PON systems. Compared to broadcast service, multicast service can offer exclusive service to premium subscribers, thus generating more revenue. Broadcast can be easily realized in TDM-PON by power-splitting at the RN. However, it is more challenging for WDM-PON, due to the dedicated connection between the OLT and the ONU. Thus, broadcast or even multicast transmission is also a valuable research topic in WDM-PON [34]-[40].

1.3. Major contributions of this thesis

This research makes three important contributions to the realization of Rayleigh noise suppression and multicast transmission in WDM-PON. We then briefly elaborate on these contributions in the following sections.

1.3.1. Using DI's destructive port to suppress Rayleigh

noise

We propose and demonstrate a novel scheme to effectively suppress the carrier RB in

carrier-distributed WDM-PONs. By replacing the upstream modulation format of conventional on-off keying (OOK) with DPSK, the system tolerance to carrier RB is substantially enhanced by 19 dB, as the carrier RB can be considerably rejected by the notch filter-like destructive port of the delay-interferometer (DI) at the OLT, which is used simultaneously to demodulate the upstream DPSK signal. To my best knowledge, this scheme is the first proposal of using DI's destructive port to suppress Rayleigh noise. As no deliberate spectral up-shifting is required in this scheme, neither additional modulator nor complicated modulation/demodulation circuit is needed at ONU/OLT. Theoretical models related to Rayleigh noise suppression are also built in this work. They can predict well the system performance and are expected to serve as a design tool for optimizing the overall performance of a WDM-PON.

1.3.2. Unique features of RMD-DPSK signal

Intuitively, the extinction ratio (ER) of the demodulated signal should be degraded for the differential phase-shift keying (DPSK) signal with a reduced modulation depth (RMD-DPSK). Actually, I discover that the ER degradation depends on which port of the DI is used to demodulate the RMD-DPSK signal. The ER of the demodulated RMD-DPSK signal from the destructive port is independent of the phase modulation depth and is always infinite, theoretically. On the contrary, the ER of the output signal from the constructive port is substantially reduced and can be readily used as the source for upstream remodulation. Therefore, the RMD-DPSK signal can be used in the downstream in a WDM-PON, to simultaneously generate the downstream signal and the upstream carrier from DI's two output ports at ONU.

1.3.3. Flexible multicast control in WDM-PONs with symmetric point-to-point bit rate

Although many studies have been carried out on this topic, the prior schemes either need relatively complicated multicast control and/or cannot support future-proof 10-Gb/s symmetric point-to-point transmission. We propose a delay-based multicast overlay scheme to superimpose a multicast DPSK-modulated signal on a point-to-point downstream inverse-return-to-zero (IRZ)-modulated signal in a WDM-PON. By adjusting the synchronization of the DPSK and the IRZ modulation on the downstream carrier, simple and flexible multicast control could be realized. We have successfully demonstrated the proposed scheme for three different traffics, namely 10-Gb/s IRZ downstream point-to-point data, 10-Gb/s DPSK downstream multicast data, and 10-Gb/s non-return-to-zero (NRZ) upstream re-modulated data, respectively. To the best of my knowledge, this is world's first demonstration of 30-Gb/s transmission of three different traffics over one wavelength channel in a WDM-PON. This scheme further evolves to a simpler wavelength detuning-based multicast control scheme that is realized via the inherent wavelength management of WDM systems.

1.4. Outline of this thesis

The remaining chapters of this thesis are organized as the following:

Chapter 2 introduces the basic concept and recent research thrust on CLS-based WDM-PON, followed by two proposed remodulation schemes with enhanced

tolerance to wavelength offset, and to chromatic dispersion and re-modulation misalignment, respectively.

Chapter 3 proposes to use DI's destructive port to suppress Rayleigh noise in CLS-based WDM-PON. Its application in both carrier-distributed and remodulation structures will be investigated respectively. The unique property of the proposed optical phase remodulation will also be explored.

Chapter 4 proposes a novel offset Manchester coding for electrical-domain Rayleigh-noise suppression in a carrier-distributed WDM-PON. We also propose an interesting chirp-free optical Manchester signal transmitter with a simple structure.

Chapter 5 deals with the broadcast/multicast issue in WDM-PON. Two broadcast schemes and two multicast schemes are proposed, respectively.

Chapter 6 gives the summary of this thesis and suggests the possible future work.

References

- [1] Nielsen's Law of Internet Bandwidth, <http://www.useit.com/alertbox/980405.html> [online].
- [2] Nielsen's Law, <http://connectedhome2go.com/2008/03/18/nielsens-law/> [online].
- [3] Test of new law proves bandwidth will be used, <http://www.globaltelecomsbusiness.com/Article/2199345/Search/Results/Test-of-new-law-proves-bandwidth-will-be-used.html?Keywords=mobile%20ser>

vices [online].

- [4] H. Song, B.-W. Kim, and B. Mukherjee, “Long-reach optical access networks: A survey of research challenges, demonstrations, and bandwidth assignment mechanisms,” *Communications Surveys and Tutorials*, IEEE, vol. 12, no. 1, 2010.
- [5] Fiber to the Home, FTTH Council, 3rd, Spring 2009.
<http://s.ftthcouncil.org/files/FTTH%20Fiber%20Primer%20low%20res.pdf>
- [6] M. Wegleitner, “Maximizing the Impact of Optical Technology,” Keynote Address, Proc. IEEE/OSA Optical Fiber Communication Conference (OFC'07), Anaheim, CA, Mar. 2007.
- [7] FTTH to Improve US Ranking, <http://www.fttxtra.com/ftth/ftth-to-improve-us-ranking/> [online].
- [8] Steve Gorshe, Principal Engineer, “Introduction to Passive Optical Networks,” White paper PCM-Sierra, Issue No. 1: October 2006.
- [9] Jim Theodoras and Stephan Rettenberger, “Introducing WDM into Next-Generation Access Networks,” White paper ADVA, August 2006.
- [10] G. K. Chang, A. Chowdhury, Z. S. Jia, H. C. Chien, M. F. Huang, J. J. Yu, and G. Ellinas, “Key Technologies of WDM-PON for Future Converged Optical Broadband Access Networks [Invited],” *J. Opt. Commun. Netw.*, 1, C35-C50 (2009).
- [11] B. Kim, and B. W. Kim, “WDM-PON development and deployment as a present optical access solution,” OFC/NFOEC2009, OThP5, (2009).
- [12] W. Hung, C.K. Chan, L.K. Chen, and F. Tong, “An Optical Network Unit for WDM Access Networks with Downstream DPSK and Upstream Re-modulated OOK Data Using Injection-Locked FP Laser,” *IEEE Photon. Technol. Lett.*, 15, 1476–1478 (2003).

- [13] C. Antony, P. Ossieur, A. M. Clarke, A. Naughton, H. G. Krimmel, Y. Chang, A. Borghesani, D. Moodie, A. Poustie, R. Wyatt, B. Harmon, I. Lealman, G. Maxwell, D. Rogers, D. W. Smith, D. Nettet, R. P. Davey, P. D. Townsend, "Demonstration of a Carrier Distributed, 8192-Split Hybrid DWDM-TDMA Pon Over 124km Field-Installed Fibers," OFC/NFOEC2010, PDPD8, (2010).
- [14] T. Yoshida, S. Kimura, H. Kimura, K. Kumozaki, and T. Imai, "A new single-fiber 10-Gb/s optical loopback method using phase modulation for WDM optical access networks," *J. Lightwave Technol.*, 24, 786-796 (2006).
- [15] K. Okamoto, *Fundamentals of Optical Waveguides*. New York: Academic, 2006.
- [16] Chang-Hee Lee, Wayne Sorin, and Byung Yoon Kim, "Fiber to the Home Using a PON Infrastructure," *IEEE J. Lightwave Technol.*, vol. 24, no. 12, pp. 4568-4583, 2006.
- [17] M. H. Reeve, A. R. Hunwicks, S. G. Methley, L. Bickers, and S. Hornung, "LED spectral slicing for single-mode local loop application," *Electron. Lett.*, vol. 24, pp. 389-390, Mar. 1988.
- [18] D. K. Jung, S. K. Shin, C.-H. Lee, and Y. C. Chung, "Wavelength-division-multiplexed passive optical network based on spectrum slicing techniques," *IEEE Photon. Technol. Lett.*, vol. 10, pp. 1334-1336, June 1998.
- [19] S. H. Lee, A. Wonfor, R. V. Penty, I. H. White, G. Busico, R. Cush and M.

- Wale, "Athermal Colourless C-band Optical Transmitter for Passive Optical Networks," ECOC 2010, Mo.1.B.2.
- [20] Markus Roppelt, Felix Pohl, Klaus Grobe, Michael Eiselt and Jörg-Peter Elbers, "Tuning Methods for Uncooled Low-Cost Tunable Lasers in WDM-PON," OFC/NFOEC 2011, NTuB1.
- [21] L.Y. Chan, C.K. Chan, D. T. K. Tong, F. Tong, L.K. Chen, "Upstream Traffic Transmitter Using Injection-Locked Fabry-Perot Laser Diode as Modulator for WDM Access Networks," IEE Electronics Letters, vol. 38, no. 1, pp. 43-45, Jan. 2002
- [22] H. S. Chung, B. K. Kim, and K. Kim, "Effects of Upstream Bit Rate on a Wavelength-Remodulated WDM-PON Based on Manchester or Inverse-Return-to-Zero Coding," ETRI Journal, Volume 30, Number 2, April 2008.
- [23] X. F. Cheng, Y. K. Yeo, Z. W. Xu, Y. X. Wang, "A Novel Hybrid WDM/TDM-PON using Downlink DPSK and Uplink Remodulated OOK Signals Based on a Shared DI," ECOC 2009, 20-24 September, 2009, Vienna, Austria.
- [24] J. Zhao, L.K. Chen, and C.K. Chan, "A Novel Re-modulation Scheme to Achieve Colorless High-Speed WDM-PON with Enhanced Tolerance to Chromatic Dispersion and Re-modulation Misalignment," in Proc. OFC /NFOEC'07, Anaheim, CA, 2007, Paper OWD.
- [25] J. Xu, L.K. Chen, "A New Remodulation Scheme for WDM-PONs With Enhanced Tolerance to Chromatic Dispersion and Remodulation Misalignment," IEEE Photonics Technology Letters, vol. 22, no. 7, pp. 456 - 458, 2010.
- [26] C. W. Chow, Y. Liu, and C. Kwok, "Signal Remodulation with High

- Extinction Ratio 10-Gb/s DPSK signal for DWDM-PONs,” in Proc. OFC /NFOEC’08, San Diego, CA, 2008, Paper OTHT2.
- [27] J. Prat et al., “Full-Duplex Single Fiber Transmission Using FSK Downstream and IM Remote Upstream Modulations for Fiber-to-the-Home,” IEEE Photon. Technol. Lett. 17, 702-704 (2005).
- [28] A. Chowdhury et al., “Rayleigh Backscattering Noise-Eliminated 115-km Long-Reach Bidirectional Centralized WDM-PON With 10-Gb/s DPSK Downstream and Remodulated 2.5-Gb/s OCS-SCM Upstream Signal,” IEEE Photon. Technol. Lett. 20, 2081-2083 (2008).
- [29] J. Xu, L.K. Chen, “Optical Phase Remodulation for 10-Gb/s WDM-PON with Enhanced Tolerance to Rayleigh Noise,” IEEE/OSA Optical Fiber Communication Conference / National Fiber Optic Engineers Conference, OFC/NFOEC 2010, Paper OThG3, San Diego, California, USA, 2010.
- [30] G. Keiser, Optical Fiber Communications, 3rd ed. New York: McGraw-Hill, 2000.
- [31] Optical Fiber Loss and Attenuation,
<http://www.fiberoptics4sale.com/wordpress/optical-fiber-loss-and-attenuation/> [Online].
- [32] P. Gysel and R.K. Staubli, “Statistical Properties of Rayleigh Backscattering in Single-Mode Fibers,” J. Lightwave Technol., Vol. 8, no. 4, pp. 561-567, Apr. 1990.
- [33] S. K. Liaw, S. L. Tzeng and Y. J. Hung, “Rayleigh backscattering induced power penalty on bidirectional wavelength-reuse fiber systems,” Opt. Commun., Vol. 188, no. 1-4, pp. 63-67, Feb. 2001.
- [34] T. Luk, J. Goodchild, and R. Habel, “WDM PON RF/Video Broadcast Overlay,” US Patent 20100021164, Jan. 2010.

- [35] M. Khanal, C. J. Chae, and R. S. Tucker, "Selective broadcasting of digital video signals over a WDM passive optical network," *IEEE Photon. Technol. Lett.*, 17, 1992–1994 (2005).
- [36] Y. Tian, Q. J. Chang, and Y. K. Su, "A WDM passive optical network enabling multicasting with color-free ONUs," *Opt. Exp.*, 16, 10434-10439 (2008).
- [37] Q. J. Chang, J. M. Gao, Q. Li, and Y. K. Su, "Simultaneous transmission of point-to-point data and selective delivery of video services in a WDM-PON using ASK/SCM modulation format," *OFC/NFOEC2008, OWH2* (2008).
- [38] Y. Zhang, N. Deng, C.K. Chan, and L.K. Chen, "A multicast WDM-PON architecture using DPSK/NRZ orthogonal modulation," *IEEE Photon. Technol. Lett.*, 20, 1479-1481 (2008).
- [39] N. Deng, C.K. Chan, L.K. Chen, C.L. Lin, "A WDM passive optical network with centralized light sources and multicast overlay," *IEEE Photon. Technol. Lett.*, 20, 114-116 (2008).
- [40] J. Xu, Y. Zhang, L.K. Chen, and C.K. Chan, "A WDM-PON with 10-Gb/s Symmetric Bit-Rates and Multicast Overlay with Delay-based Multicast Control," *OFC/NFOEC2009, NME5* (2009).
- [41] J. Xu, L.K. Chen, C.K. Chan, "Enhancement of Wavelength Offset Tolerance for Downstream DPSK Signals Demodulation in 10-Gb/s WDM-PONs," *OptoElectronics and Communications Conference, OECC 2010, Paper 6A1-4, Sapporo, Hokkaido, Japan, Jul. 2011.*
- [42] J. Xu, L.K. Chen, C.K. Chan, "Phase Modulation Based Loopback Scheme for Rayleigh Noise Suppression in 10-Gb/s Carrier-Distributed WDM-PONs" *IEEE Photonics Technology Letters*, vol. 22, no. 18, pp. 1343-1345, Sep. 2010.
- [43] J. Xu, Z.X. Liu, W. Jia, L.K. Chen, "A Novel Chirp-free Optical Manchester

Signal Transmitter with Enhanced Dispersion Tolerance,” Asia Communications and Photonics Conference and Exhibition (ACP) 2010, Paper SA 2, Shanghai, China, Dec. 2010.

- [44] J. Xu, Z.X. Liu, L.K. Chen, C.K. Chan, “Time-Interleaved Phase Remodulation to Enable Broadcast Transmission in Bidirectional WDM-PONs without Additional Light Sources,” *IEEE/OSA Optical Fiber Communication Conference / National Fiber Optic Engineers Conference, OFC/NFOEC 2011, Paper OThK4, Los Angeles, California, USA, 2011*
- [45] J. Xu, Y.Zhang, L.K. Chen, C.K. Chan, “A Delay-based Multicast Overlay Scheme for WDM Passive Optical Networks with 10-Gb/s Symmetric Two-way Traffic,” *IEEE OSA Journal of Lightwave Technology*, vol. 28, no. 18, pp.2660-2666, Sep. 2010.
- [46] J. Xu, K.M.Chong, L.K. Chen, “Delay-interferometer based timing alignment monitoring for data and clock signal in optical RZ-DPSK and RZ-OOK systems,” *Optical Fiber Technology*, vol. 16, no. 4, pp. 236 - 239, 2010.

Chapter 2 WDM-PONs with

Centralized Light Sources

2.1. Carrier-distributed scheme

In this scheme centralized optical carriers are distributed from the OLT to each ONU, modulated, and sent back to the OLT. The centralized optical carrier can be either incoherent broadband amplified spontaneous emission (ASE) light or coherent light. There are three major advantages in using incoherent light: no stringent wavelength control is needed for broadband ASE sources; the Rayleigh backscattering (RB) of broadband ASE light will induce smaller beating noise in the upstream signal; and broadband ASE light does not require the upstream transmitter to be polarization-insensitive [1]-[3]. However, its main shortcoming is the limited bit-rate that can be supported by an incoherent optical carrier.

For broadband (10 Gbit/s or above) operation coherent light sources are necessary [4]. In this scheme, however, the upstream signal is susceptible to the interferometric crosstalk induced by the beating between the upstream signal and the RB of the distributed carrier in downstream, both of which are of the same wavelength [5]. This challenging issue will be tackled in chapter 3.

2.2. Remodulation scheme

In the carrier-distributed scheme, in addition to the downstream light sources, extra light sources are installed at the OLT to remotely provide optical carrier to each ONU for the upstream data, thus higher system cost is incurred. In the remodulation scheme,

part of the downstream light is directly reused as the upstream carrier at the ONU [6]-[11]. Therefore, remodulation of downstream signal to generate upstream signal can further save the wavelengths and light sources by wavelength reuse. However, as a tradeoff, the remodulation scheme normally has a smaller power budget than the carrier-distributed scheme.

The key challenging issue of the remodulation scheme is how to alleviate the upstream signal degradation caused by the residual downstream data. One straightforward approach is to reserve certain optical power in the downstream signal, by using on-off keying with reduced modulation depth (RMD-OOK), inverse return-to-zero (IRZ) OOK or Manchester coding as the downstream modulation format [12] ,[13]. However, the downstream receiver sensitivity will be degraded by the reserved constant optical power that carries no signal. A more elegant approach has been proposed by using downstream differential phase shift keying (DPSK) and upstream OOK with full modulation depth (FMD-OOK) [7] [14]. As the modulation format in downstream is of constant amplitude, it can be reused for upstream OOK remodulation. In addition, the constant-intensity nature of the DPSK modulation format reduces various nonlinear phenomena during transmission, thus improving the system power budget.

In most of the prior remodulation schemes using DPSK in downstream, a power splitter is needed at ONU for the separation of the downstream signal and the signal for re-modulation. Meanwhile only one output port of the delay interferometer (DI) is used since balance detector is expensive to be used at the customer's side. The power from the other output port of the DI is wasted, and proper termination is also required for the unused output port. In the following part of this chapter, two novel schemes are

proposed to solve this problem. And more importantly, the proposed schemes also have enhanced tolerance to wavelength offset, or to chromatic dispersion and re-modulation misalignment.

2.3. Demodulation of downstream DPSK signals by a partial-bit delay interferometer

In this work, we propose the use of the destructive port of a DI with partial-bit delay to demodulate the 10-Gb/s downstream DPSK signal with enhanced tolerance to wavelength offset between the laser source and the DI, whereas the constructive port output is used as the source for upstream re-modulation. Thus, the ONU structure is also simplified, as one power splitter is saved. The DI is used for both downstream signal demodulation and the separation of the downstream signal and the upstream source.

2.3.1. System architecture and operation principle

Fig. 2.1 illustrates the architecture of a WDM PON using downstream DPSK and upstream OOK with our proposed ONU structure. For each downstream wavelength at the OLT, differentially precoded data are used to drive an optical phase modulator (PM) to generate the downstream DPSK signal. After transmission, the downstream signal from the OLT is wavelength routed toward different ONUs, by an arrayed waveguide grating (AWG) at the remote node (RN). At an ONU, the downstream DPSK signal is

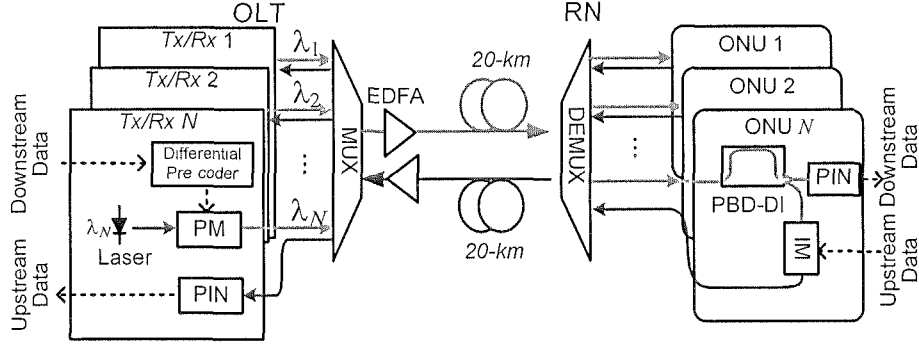


Fig. 2.1 WDM-PON architecture using the proposed simplified ONU structure with partial-bit-delay DI (PBD-DI).

demodulated by the destructive port of the DI with partial-bit delay between two arms before direct detection, while light from the constructive port is fed into an optical intensity modulator (IM) for upstream data re-modulation.

Assume the delay between two arms of the DI is kT , where $0 < k < 1$ and T is the bit-period. As the relative delay of the DI used at ONU is shorter than one bit period, the leading part of any bit will interfere with the trailing part of the previous bit at the DI output port within the overlap duration of kT . In the remaining $(1-k)T$ part, the two signals on the two arms of DI are from the same bit, thus leading to a constant 1 and 0 for the constructive and destructive ports, respectively. Thus, the output from the destructive port of the DI should be return-to-zero (RZ) shaped, whereas the output from the constructive port should be inverse-return-to-zero (IRZ) shaped. The IRZ shaped output from the constructive port of the DI, which always has optical power in each bit, can be readily re-modulated by the upstream data. As the phase error within DI, caused by the wavelength offset between the laser source and the DI, is proportional to the relative delay of the DI [15], using partial-bit DI to demodulate the downstream DPSK signal is more robust to wavelength offset.

For a smaller K , the downstream DPSK demodulation will be more robust to wavelength offset between the laser source and the DI. The insertion loss of DI's constructive port as well as the ER of the IRZ signal from DI's constructive port will also become smaller, resulting in improved upstream power budget. However, the tradeoff is that a smaller K will induce larger insertion loss to DI's and the RZ-shaped signal is less robust to dispersion.

2.3.2. Experimental demonstration

We have experimentally demonstrated the proposed ONU structure based on the architecture shown in Fig. 2.1. At the OLT, continuous-wave (CW) lights at 1549.3 and 1550.1 nm were coupled into a PM driven by a 10-Gb/s $2^{31}-1$ pseudorandom binary sequence (PRBS). The phase modulated output was then amplified to 4 dBm per channel and was coupled into a 20-km dispersion-shifted fiber (DSF) to emulate the dispersion-compensated transmission between the OLT and the RN. At the RN, an AWG with a channel spacing of 0.8 nm and a 3-dB bandwidth of 0.35 nm was used to separate the two channels. The 1549.3-nm channel was input into a DI with 25-ps relative delay (40-Gb/s DI). The demodulated downstream data from the destructive port of the DI was then directly detected by a 10-Gb/s p-i-n receiver. Light from the constructive port was combined with the 1550.1-nm channel from the AWG via a 3-dB coupler and then fed into an optical IM, driven by a 10-Gb/s $2^{31}-1$ PRBS as the upstream data, before being transmitted back to the OLT via another piece of 20-km dispersion-shifted fiber. The two channels were modulated by the same IM at the ONU and the same PM at the OLT due to equipment availability.

As the two WDM channels had very similar performance, only the eye diagrams

and bit error rate (BER) measurements for the 1549.3-nm channel are shown. Fig. 2.2(a) shows the clearly open RZ-shaped eye diagram of the demodulated downstream DPSK signal from the destructive port of DI. Fig. 2.2(b) shows the IRZ-shaped output from the constructive port. As there is constant optical power in each bit for upstream re-modulation, as denoted by the area of the dashed trapezoid in Fig. 2.2(b), the detected upstream signal shows wide-open eye diagram in Fig. 2.2(c). By using the

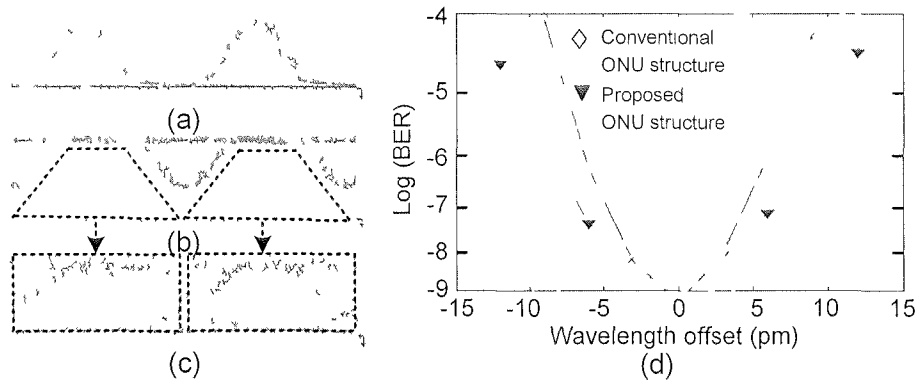


Fig. 2.2 Eye diagrams of (a) the demodulated downstream 10-Gb/s DPSK signal from the destructive port of the 0.25-bit DI, (b) IRZ-shaped output from the constructive port of the 0.25-bit DI, (c) the detected upstream OOK signal. Time scale: 20 ps/div. (d) BER degradation (from 10^{-9}) caused by wavelength offset between the laser source and the DI.

proposed ONU structure, the DPSK signal demodulation is less sensitive to wavelength offset between the laser source and the DI, as shown by the smaller slope in Fig. 2.2(d). It was measured that for less than 1-dB power penalty at BER of 10^{-9} , the DPSK signal can tolerate 25% larger wavelength offset, by using the proposed ONU structure than the conventional one. The BER measurement results are shown in Fig. 2.3 After 20-km transmission in DSF fiber, around 0.5-dB and 1-dB power penalty at BER of 10^{-9} are observed for the downstream and the upstream data,

respectively.

For comparison, we also measured the BER curve using the conventional ONU structure as in [7], where the downstream DPSK signal was demodulated by a DI with one-bit delay, and a power splitter was used to tap part of the downstream DPSK signal as the source for upstream re-modulation. Around 0.8-dB and 1.2-dB power penalty at

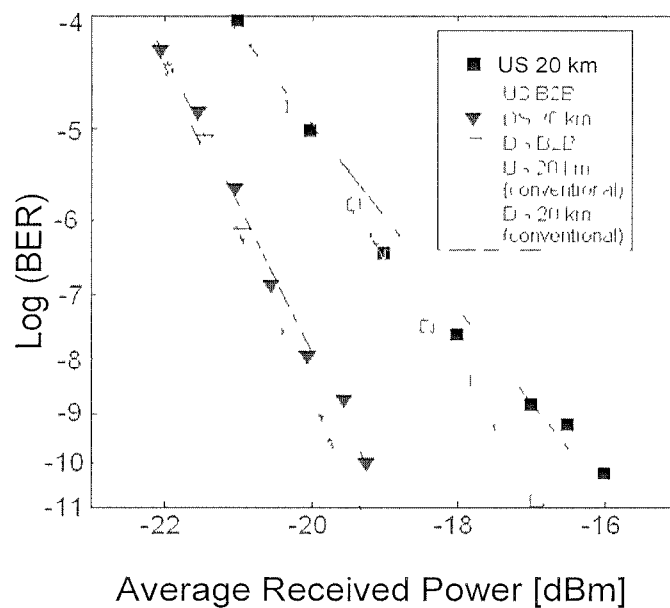


Fig. 2.3 BER measurement results for both down- and up-stream signals.

BER of 10^{-9} were observed for the downstream and the upstream data, respectively, using the proposed ONU structure. Note that the major power penalty of the upstream data can be compensated by the reduced insertion loss of the proposed ONU. In the experiment, measured insertion loss of the constructive port for the 0.25-bit DI was 2.4 dB. As the 3.5-dB insertion loss of the power splitter is eliminated in the proposed ONU structure, power budget for the proposed ONU structure was only reduced by around 0.1 dB for the upstream transmission.

In conclusion, we have demonstrated the novel use of a partial-bit DI's destructive port to demodulate the 10-Gb/s downstream DPSK signal with enhanced tolerance to wavelength offset. Meanwhile, the IRZ-shaped output from the constructive port can be readily used for 10-Gb/s upstream re-modulation to simplify the ONU structure. Note that as the 40-Gb/s DI's destructive port is used for 10-Gb/s downstream data demodulation, dispersion tolerance of the downstream data is compromised. The dispersion issue will be addressed in the next section.

2.4.Reducing the modulation depth of downstream

DPSK signal

As discussed above, several re-modulation schemes that support 10-Gb/s operation have been proposed, including downstream DPSK and upstream on-off keying (OOK), downstream frequency shift keying and upstream OOK, downstream inverse return-to-zero and upstream OOK, and downstream DPSK and upstream DPSK. However, these schemes have the disadvantages of either poor chromatic dispersion (CD) tolerance for 10-Gbit/s upstream transmission or the need of synchronization for re-modulation. In practice, it is highly desirable to operate a robust WDM-PON without CD compensation and re-modulation synchronization at each ONU, thus reducing the implementation complexity and system cost. For this purpose, one scheme using low- extinction-ratio (ER) OOK downstream and DPSK upstream has been proposed [11]. However, the ER reduction of the downstream OOK signal will degrade the downstream receiver sensitivity.

In this part, we propose a novel re-modulation scheme using downstream DPSK,

with a reduced modulation depth (RMD), and upstream OOK to enhance the tolerance to CD for upstream signal and the tolerance to re-modulation timing misalignment. Despite the use of RMD-DPSK for downstream transmission, in each ONU the demodulated RMD-DPSK signal from the destructive port of the delay-interferometer (DI) can still achieve a high ER, whereas the constructive port output has a very low ER and can be employed as the source for upstream re-modulation. Compared to prior re-modulation schemes, the ONU structure is further simplified, as the power splitter is eliminated and the DI is used for both downstream signal demodulation and the separation of the downstream/upstream signals. As RMD-DPSK requires a smaller driving voltage, a lower cost driver for the phase modulation can be used.

2.4.1. Operation principle and system architecture

For the conventional scheme using downstream DPSK with full modulation depth (FMD) and upstream OOK, the inferior tolerance to CD and re-modulation misalignment might not be intuitive. The constant-intensity nature of the DPSK modulation format reduces various nonlinear phenomena during transmission and greatly facilitates the re-modulation by the upstream OOK signal. However, such constant intensity is distorted during transmission due to CD. Fig. 2.4(a) shows the severe intensity fluctuation of a traditional 10-Gb/s DPSK signal with FMD after 20-km transmission in single mode fiber (SMF) without demodulation by DI. Due to such periodic intensity variation, rigorous timing alignment at the ONU is required for OOK re-modulation. The upstream OOK signal also suffers substantial power penalty [11]. By reducing the modulation depth of the downstream DPSK signal, the optical power will be shifted from sidebands to the central carrier tone, as shown in Fig. 2.4 (b) by simulation. Here we propose to use the DI's destructive port to demodulate the downstream RMD-DPSK signal, whereas the DI's constructive port is used to filter

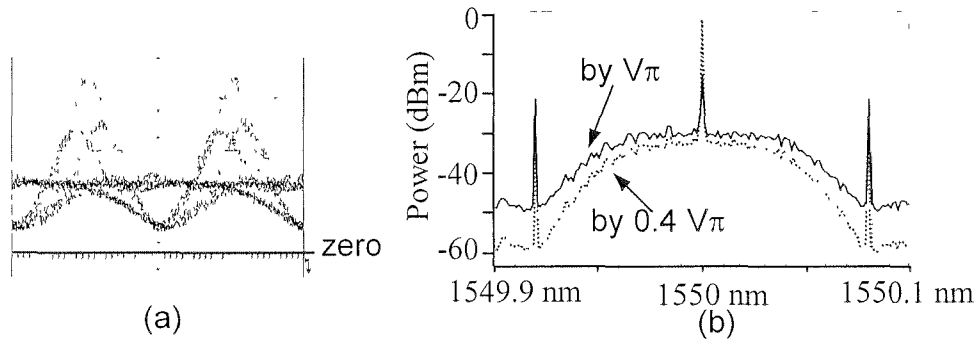


Fig. 2.4 (a) Eye diagram of the 10-Gb/s FMD-DPSK signal after transmission in 20-km SMF without demodulation by DI. Time scale: 20ps/div. (b) Spectrum comparison between two DPSK signals with different driving voltages (Raised-cosine driving signal is assumed).

out the carrier tone as the source for re-modulation. Thus, the tolerance to CD and remodulation misalignment for upstream signal can be significantly enhanced, compared with prior schemes using part of the FMD-DPSK signal as the source for re-modulation [11].

One issue is the possible ER degradation of the demodulated signal caused by the modulation depth reduction. The ER degradation actually depends on which port of the DI is used for the DPSK demodulation. For the destructive port, the demodulated '0' is the same as that in the case of FMD, as '0' denotes that the adjacent bits have the same phase, disregarding the specific phase values of the adjacent bits. Thus, the ER of the demodulated RMD-DPSK signal from the destructive port, theoretically, is independent of the phase modulation depth and is always infinite, as the demodulated '0' of the RMD-DPSK signal is perfectly null. On the contrary, the ER of the output signal from the constructive port is substantially reduced, which greatly facilitates upstream remodulation.

The other issue is that the insertion loss is larger if the destructive port is used for RMD-DPSK demodulation, due to the reduced ‘1’ level. However, the reduced optical power actually appears at the constructive port, from the principle of conservation of energy. Here we propose to use the constructive port output as the source for phase remodulation, thus its power increase by downstream modulation depth reduction will benefit the upstream power budget that generally is more crucial.

Fig. 2.5 illustrates the proposed re-modulation architecture for a WDM PON using downstream RMD-DPSK and upstream OOK. For each downstream wavelength at the OLT, differentially precoded data with low driving voltage is used to drive an optical PM to generate the downstream RMD-DPSK signal. After transmission, at the ONU the downstream RMD-DPSK signal is demodulated from the destructive port of the DI before direct detection, while light from the constructive port is fed into an optical intensity modulator (IM) for upstream data re-modulation.

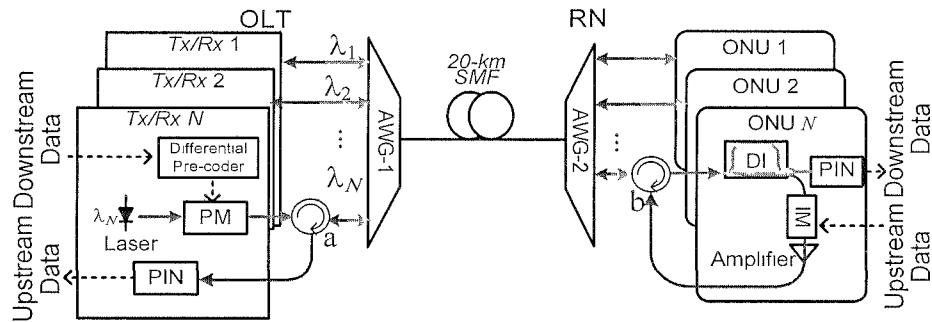


Fig. 2.5 Proposed re-modulation architecture using downstream RMD-DPSK and upstream OOK. Tx/R: transceiver.

2.4.2. Experimental demonstration

We have experimentally demonstrated the proposed re-modulation scheme based on

the architecture shown in Fig. 2.5. At the OLT, continuous-wave (CW) lights at 1549.3 and 1550.1 nm were coupled into a PM driven by a 10-Gb/s $2^{31}-1$ pseudorandom binary sequence (PRBS) with the driving voltage of $\sim 0.4 V_{\pi}$. The partially phase modulated output was then amplified to 6 dBm per channel and was coupled into a 20-km SMF. At the remote node (RN), an AWG with a channel spacing of 0.8 nm and a 3-dB bandwidth of 0.35 nm was used to separate the two channels. The 1549.3-nm channel was input into a DI with 94-ps relative delay. The demodulated downstream data from the destructive port of the DI was then directly detected by a 10-Gb/s p-intrinsic-n (PIN) receiver. Light from the constructive port was combined with the 1550.1-nm channel from the AWG via a 3-dB coupler and then fed into an optical IM, driven by a 10-Gb/s $2^{31}-1$ PRBS as the upstream data. The two channels were modulated by the same IM at the ONU and the same PM at the OLT due to equipment availability. To investigate the enhanced tolerance of the proposed re-modulation scheme to chromatic dispersion and re-modulation timing misalignment, first the effect from Rayleigh backscattering was isolated by using another piece of 20-km SMF for upstream transmission. At the OLT, another AWG with the same parameter was used to route the upstream channel at 1549.3 nm to a 10-Gb/s PIN receiver for direct detection and performance measurement. Then the 1550.1-nm channel was evaluated similarly.

As the two WDM channels had very similar performance, only the eye diagrams and BER measurements for the 1549.3-nm channel are shown. Although the driving voltage of the PM was as low as $0.4 V_{\pi}$, the eye of the demodulated DPSK signal from the destructive port of the DI is still wide-open, with a measured ER of 13.6 dB, as shown in the inset of Fig. 2.6. Meanwhile, the constructive port output had an ER as low as 1.9 dB, ready for upstream re-modulation with enhanced tolerance to re-modulation timing misalignment.

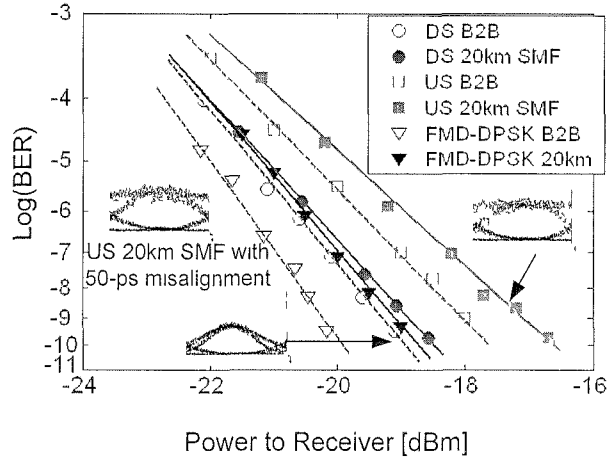


Fig. 2.6 BER measurements of both DS and US signals when using dual-fiber configuration. Inset: corresponding eye diagrams for different cases. Time scale: 20ps/div. DS: downstream, US: upstream.

The BER measurement results for both down- and up-stream signals (with optimal re-modulation synchronization) are shown in Fig. 2.6. After 20-km SMF transmission, the CD caused power penalty was ~ 0.4 dB and ~ 1 dB for the downstream RMD-DPSK signal and the upstream OOK signal, respectively. The BER curve for FMD-DPSK signals is also shown in Fig. 2.6. In the back-to-back (B2B) case, compared with the FMD-DPSK signal, the modulation depth reduction impaired the receiver sensitivity (at BER of 10^{-9}) by only around 1 dB, due to the high ER of the demodulated RMD-DPSK signal. After 20-km SMF transmission, the sensitivity difference between the RMD-DPSK and FMD-DPSK signal was further reduced to 0.2 dB. We should mention that compared to FMD-DPSK, the RMD-DPSK signal can tolerate less phase error in the DI, because the phase shift between different symbols is 0.4π instead of π . We measured the tolerance (for 1-dB power penalty at BER of 10^{-9})

of both FMD-DPSK and RMD-DPSK signals to the frequency offset between the laser source and the DI. Compared to the FMD-DPSK signal, the RMD-DPSK signal was more sensitive to frequency offset by a factor of 3.5. To investigate the tolerance of upstream signal to re-modulation timing misalignment we have deliberately adjusted the re-modulation synchronization through an electronic delay within one bit period. Less than 1-dB power penalty is observed as shown in Fig. 2.7. The eye diagram corresponding to the worst re-modulation synchronization (50-ps misalignment) is also shown in the inset of Fig. 2.6, with only slight distortion compared with the eye with optimal re-modulation synchronization.

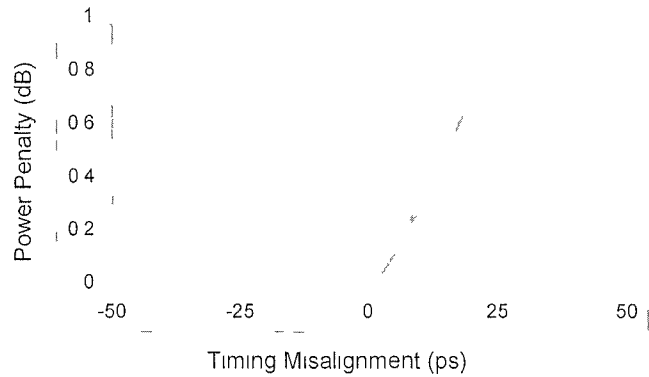


Fig. 2.7 Power penalty of upstream signal induced by remodulation timing misalignment.

We then demonstrated the proposed re-modulation scheme based on the setup in Fig. 2.5, using more practical, single-fiber configuration. At the OLT, CW light at 1547.8 nm was fed into a PM driven by a 10-Gb/s $2^{31}-1$ PRBS with the driving voltage of $\sim 0.4 V_{\pi}$. The RMD-DPSK signal was fed into AWG-1 (~ 4 -dB loss) at the OLT through circulator-a. The output from AWG-1 was amplified to 5 dBm before feeding into a 20-km SMF (~ 4 -dB loss). After propagating through AWG-2 (~ 4 -dB loss) at the RN and circulator-b (~ 0.6 -dB loss), -3.6 -dBm optical power was fed into the DI at

ONU. The output power from the destructive port of the DI was -13.9 dBm and was detected for downstream signal. Optical power of -4.9-dBm from the constructive port of the DI was fed into a Mach-Zehnder IM driven by a 10-Gb/s $2^{31}-1$ PRBS as the upstream data. The signal with a power of -13.3 dBm from the IM was amplified to 5.2 dBm, and then transmitted back to the OLT with -8-dBm received power by the receiver. The amplification increased the power ratio of the upstream signal to the Rayleigh backscattered signal [16]. For practical implementation, the Mach-Zehnder IM and the optical amplifier in this proof-of-concept experiment can be replaced by an electro-absorption modulator integrated with a semiconductor optical amplifier for 10-Gb/s polarization-insensitive operation [17]. The BER measurement results and the corresponding eye diagrams for single-fiber configuration are shown in Fig. 2.8. Rayleigh backscattering induced around 5-dB power penalty for the upstream signal. The receiver sensitivity at BER of 10^{-9} for the upstream signal was -11.3 dBm, implying a 2.3-dB margin even for the worst re-modulation synchronization (1-dB power penalty at BER of 10^{-9}). Negligible power penalty induced by Rayleigh backscattering was observed for the downstream signal. The receiver sensitivity at BER of 10^{-9} for the downstream signal was -18.8 dBm, implying 4.9-dB margin.

It is worth mentioning that using downstream DPSK (RMD-DPSK or FMD-DPSK) makes it possible to launch higher optical power to increase the maximum reach of PON, thanks to its nearly constant power [10]. To investigate the tolerance of the proposed scheme to nonlinear distortion, five downstream RMD-DPSK channels at the wavelength from 1546.2 nm to 1549.4 nm, spaced by 0.8 nm were first multiplexed by AWG-1 into 10-km SMF to decorrelate each channel. Then after being amplified to 13 dBm (around 6 dBm per channel), the decorrelated signals are fed into 20-km SMF. Negligible nonlinear distortion was observed for all

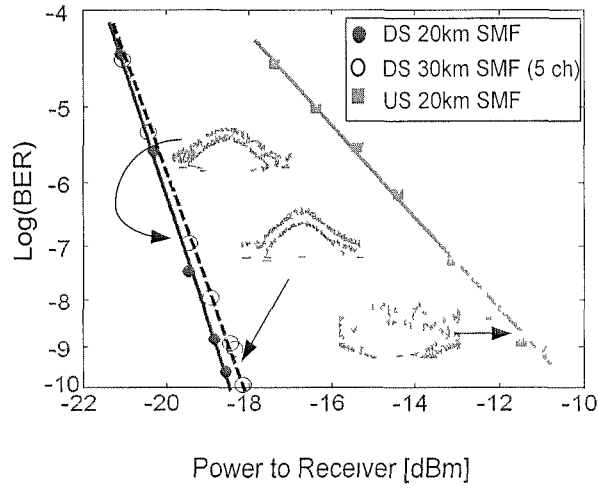


Fig. 2.8 : BER measurements of both DS and US signals using single-fiber configuration . Inset: corresponding eye diagrams for different cases. Time scale: 20ps/div. DS: downstream, US: upstream, ch: channel.

the five demodulated channels at the ONU. For the middle channel at 1547.8 nm, the BER measurement result as well as its eye diagram is shown in Fig. 2.8. Simulation investigation for 16 downstream RMD-DPSK channels was also conducted, showing the same results.

In conclusion, we have proposed a novel re-modulation scheme for WDM-PONs using downstream DPSK with a reduced modulation depth and upstream OOK to enhance system tolerance to chromatic dispersion and re-modulation misalignment. Error-free operation of both down- and up-stream signals, at 10 Gb/s without re-modulation synchronization, are achieved after the transmission of 20-km SMF. In addition to the robustness to chromatic dispersion and re-modulation misalignment, the proposed scheme also features simple ONU structure and lower driving voltage for phase modulation.

2.5. Summary

In this chapter, two CLS architectures are introduced. Particularly, two novel remodulation schemes are proposed and experimentally demonstrated. As a unique feature, in both schemes the DI at ONU is used for both downstream DPSK signal demodulation and the separation of the downstream/upstream. The first scheme is based on a partial-bit DI and has enhanced tolerance to wavelength offset between the laser source and the DI, whereas the second scheme is based on modulation depth reduction and has enhanced tolerance to chromatic dispersion and remodulation misalignment. An interesting feature of RMD-DPSK signal is observed: the demodulated signal from the destructive port of DI can still achieve a high ER despite of the modulation depth reduction. Note that if single feeder fiber is used, large power penalty induced by Rayleigh backscattering is observed. How to circumvent this problem will be the focus in the following two chapters.

References

- [1] H. D. Kim, S.-G. Kang, and C.-H. Lee, "A low-cost WDM source with an ASE injected Fabry-Pérot semiconductor laser," *IEEE Photon. Technol. Lett.*, vol. 12, no. 8, pp. 1067–1069, Aug. 2000.
- [2] H. Healey, P. Townsend, C. Ford, L. Johnston, P. Townley, I. Lealman, L. Rivers, S. Perrin, and M. Moore, "Spectral slicing WDM-PON using wavelength-seeded reflective SOAs," *Electron. Lett.*, vol. 37, no. 19, pp. 1181–1182, Sep. 2001.
- [3] H. S. Shin, D. K. Jung, H. S. Kim, D. J. Shin, S. B. Park, S. T. Hwang, Y. J. Oh,

- and C. S. Shin, "Spectrally pre-composed ASE injection for a wavelength-seeded reflective SOA in a WDM-PON," in Proc. ECOC, 2005, vol. 3, pp. 459–460.
- [4] B. Zhang, C.L. Lin, L. Huo, Z.X. Wang, C.K. Chan, "A Simple High-Speed WDM PON Utilizing a Centralized Supercontinuum Broadband Light Source for Colorless ONUs," IEEE/OSA Optical Fiber Communication Conference / National Fiber Optic Engineers Conference , OFC/NFOEC 2006, Paper OTuC6, Anaheim, California, United States, Mar. 2006.
- [5] T. H. Wood, R. A. Linke, B. L. Kasper, and E. C. Carr, "Observation of coherent Rayleigh noise in single-source bidirectional optical fiber systems," *J. Lightw. Technol.*, vol. 6, no. 2, pp. 346–352, Feb. 1988.
- [6] W. Hong, C.-K. Chan, L.-K. Chen, and F. Tong, "An optical network unit for WDM access networks with downstream DPSK and upstream remodulated OOK data using injection-locked FP laser," *IEEE Photon. Technol. Lett.*, vol. 15, no. 10, pp. 1476–1478, Oct. 2003.
- [7] W. Hung, C.K. Chan, L.K. Chen, and F. Tong, "An optical network unit for WDM access networks with downstream DPSK and upstream re-modulated OOK data using injection-locked FP laser", *IEEE Photon. Technol. Lett.* 15, 1476-1478 (2003).
- [8] N. Deng, W. Hung, C.K. Chan, and L.K. Chen, et al., "A novel wavelength modulated transmitter and its application in WDM passive optical networks", *OFC*, MF79 (2004).
- [9] G.W. Lu, N. Deng, C.K. Chan, and L.K. Chen, "Use of Downstream Inverse-RZ Signal for Upstream Data Re-modulation in a WDM Passive Optical Network", *OFC*, OFI8 (2005).
- [10] C. W. Chow, Y. Liu, and C. Kwok, "Signal Remodulation with High

- Extinction Ratio 10-Gb/s DPSK signal for DWDM-PONs,” OFC, OTHT2 (2008).
- [11] J. Zhao, L.K. Chen, and C.K. Chan, “A Novel Re-modulation Scheme to Achieve Colorless High-Speed WDM-PON with Enhanced Tolerance to Chromatic Dispersion and Re-modulation Misalignment,” OFC, OWD (2007).
- [12] L.Y. Chan, C.K. Chan, D. T. K. Tong, F. Tong, L.K. Chen, “Upstream Traffic Transmitter Using Injection-Locked Fabry-Perot Laser Diode as Modulator for WDM Access Networks,” IEE Electronics Letters, vol. 38, no. 1, pp. 43-45, Jan. 2002
- [13] H. S. Chung, B. K. Kim, and K. Kim, “Effects of Upstream Bit Rate on a Wavelength-Remodulated WDM-PON Based on Manchester or Inverse-Return-to-Zero Coding,” ETRI Journal, Volume 30, Number 2, April 2008.
- [14] X. F. Cheng, Y. K. Yeo, Z. W. Xu, Y. X. Wang, “A Novel Hybrid WDM/TDM-PON using Downlink DPSK and Uplink Remodulated OOK Signals Based on a Shared DI,” ECOC 2009, 20-24 September, 2009, Vienna, Austria.
- [15] H. Kim, and P. J. Winzer, “Robustness to laser frequency offset in direct-detection DPSK and DQPSK system,” J. Lightwave Technol. vol. 21, no. 9, 1887–1891 (2003).
- [16] Wooram Lee, Mahn Yong Park, Seung Hyun Cho, Jihyun Lee, Chulyoung Kim, Geon Jeong, and Byoung Whi Kim, “Bidirectional WDM-PON Based on Gain-Saturated Reflective Semiconductor Optical Amplifiers,” IEEE Photon. Technol. Lett. 17, 2460–2462 (2005).
- [17] H. Suzuki, H. Nakamura, J. Kani, and K. Iwatsuki, “A carrier-distributed wide-area WDM-based passive optical network (WDM-PON) accommodating

10 gigabit Ethernet-based VPN services” ECOC, Tu4.6.3 (2004).

Chapter 3 Rayleigh Noise

Suppression in Optical Domain

3.1. Rayleigh noise suppression in carrier-distributed

WDM-PONs based on in-band optical filtering

3.1.1. Introduction

As discussed in last chapter, centralized carrier distribution is a promising approach to realize broadband (10 Gbit/s or above) colorless ONU, in which the upstream optical carriers are remotely distributed from the OLT to each ONU [1], [2]. In the carrier-distributed architecture, however, the upstream signal is susceptible to the interferometric crosstalk induced by the beating between the upstream signal and the Rayleigh backscattering (RB) of the distributed optical carrier, both of which are of the same wavelength [3]. Intensive studies have been carried out to mitigate this interferometric crosstalk. They are well summarized in [4] and [5]. Reducing the light source coherence is the most straightforward approach to reduce the impact of interference [6], [7]. However, this scheme is vulnerable to dispersion. As the optical spectra of both the RB light towards the OLT and the upstream on-off keying (OOK) signal have strong low-frequency components, after detection the beating noise mainly distributes at the low frequency region, thus can be suppressed by an electrical

high-pass filter (HPF) [8]-[10]. These schemes require only minor modifications to the PON structure. However, proper line coding [8], [9], or electronic equalization [10], is needed to alleviate the HPF-induced distortion to the upstream signal. In addition, the reported improvement in Rayleigh noise tolerance is limited to 5 dB [9], [11]. Although in [10] the improvement in Rayleigh noise tolerance can be more than 10 dB, the signal extinction ratio has to be lower than 6 dB. A 7-dB improvement in Rayleigh noise tolerance can be achieved by using a novel offset Manchester coding, which will be discussed in detail in the next chapter. Besides these electrical-domain approaches, the Rayleigh noise can also be circumvented directly in optical domain, which turns out to be more effective [11]-[15]. The carrier RB light towards the OLT, with a narrow spectrum, can be effectively suppressed by an optical notch filter. However, unlike the ASE noise, Rayleigh noise is an in-band noise and is challenging to be directly filtered out without impairing the upstream signal itself. Thus, to mitigate the impairment to the upstream signal induced by the optical notch filter, several approaches have been proposed to spectrally up-shift the upstream signal, using additional phase modulation [11]-[13], sub-carrier multiplexing (SCM) [14], or carrier suppressed subcarrier amplitude modulated phase modulation [15]. Although reported as very effective (the improvement in Rayleigh noise tolerance can be 17 dB), these approaches are constrained by poor dispersion tolerance [11]-[14], requiring additional external modulators at ONU [13], [14], and complicated de/modulation circuit [15]. These constraints actually originate from the spectral up-shifting of the upstream signal.

Here, we proposed a simple scheme, via in-band optical filtering, to suppress RB in the carrier-distributed WDM-PON [16]. By replacing the conventional OOK modulation format in upstream with DPSK, the upstream signal is able to pass through

an optical notch filter, which is used to suppress the RB light, without any impairment. At any rate an optical notch filter, such as the destructive port of a delay-interferometer (DI), is required to demodulate the upstream DPSK signal. As no deliberate spectral up-shifting is required in this scheme, neither additional modulator nor complicated modulation/demodulation circuit is needed at ONU/OLT. In terms of the optical notch filter used to suppress the RB light, the standard DI used in the proposed scheme is also more favorable than the non-standard filters that are either specially designed ultra-narrow notch filters or wavelength-detuned AWG used in the prior schemes [12], [13], [15].

3.1.2. Application in a 20-km WDM-PON

3.1.2.1. Operation principle and system architecture

The DI used for DPSK demodulation is functionally equivalent to a delay-and-subtract or delay-and-add filter, depending on whether the destructive or constructive port is used [17]. For the destructive port, it could act as a notch filter to reject the RB of the optical carrier, which has a very narrow spectral width. We use DPSK as the upstream modulation format in carrier-distributed WDM-PONs, so that the destructive port of the DI used for upstream DPSK demodulation could simultaneously suppress the RB of the optical carrier.

Fig. 3.1 illustrates the proposed loopback architecture. The optical carriers for upstream transmission at different wavelengths are generated by continuous-wave (CW) lasers at the OLT, and then multiplexed by an AWG. After the transmission in a 20-km SMF, the optical carriers from the OLT are wavelength routed toward different ONUs, by another AWG at the RN. At the ONU, the CW light is modulated by an

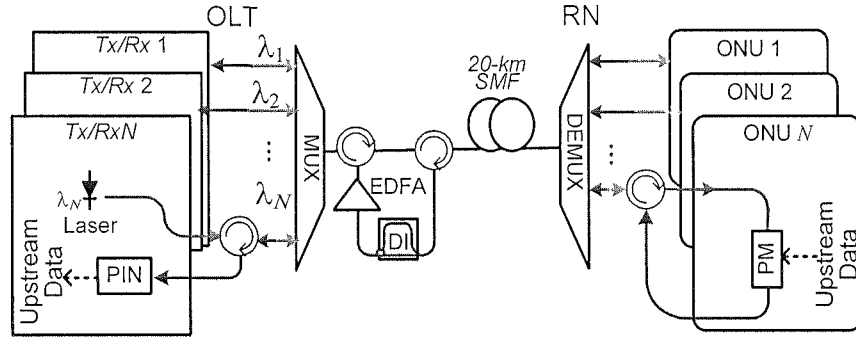


Fig. 3.1 Proposed loopback architecture using DPSK as the upstream modulation format to suppress Rayleigh noise. The downstream channels are omitted here for simplicity.

optical phase modulator, driven by differentially pre-coded upstream data, before being sent back to the OLT. Due to DI's periodic frequency response, all the upstream DPSK channels could be simultaneously demodulated by a common DI at the OLT [18], [19]. Athermal DIs, with C+L band coverage by a single device, are commercially available. The demodulated DPSK signals are pre-amplified by a shared erbium-doped fiber amplifier (EDFA) before direct detection.

3.1.2.2. Experimental demonstration

We first investigated the effectiveness of the destructive port of the DI on RB noise suppression based on the setup shown in Fig. 3.2(a). The 20-km SMF used in the setup was properly terminated by an optical terminator. The relationship between the average reflection power (P_r) and the average power of the input CW light to the 20-km SMF (P_{in}) was measured, as shown in Fig. 3.2(b). Two cases, with or without using the destructive port of the DI to suppress the RB, are depicted. The extinction

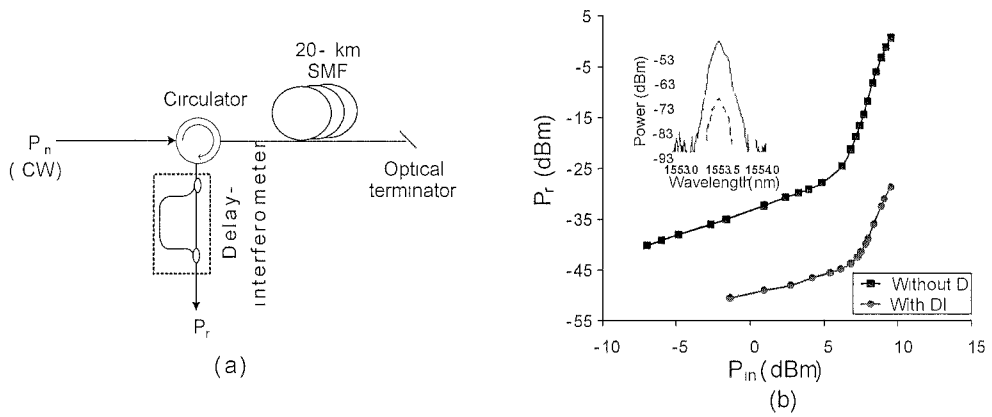


Fig. 3.2 (a) Experimental setup. (b) The relationship between the average reflection power (P_r) and the average power of the input CW light to the 20-km SMF (P_{in}). Inset: measured spectrum of the RB noise with (the dashed line) or without (the solid line) using the destructive port of the DI to suppress the RB noise.

ratio of the DI is 22 dB. With the assistance of DI, for any given P_{in} , the corresponding P_r was significantly reduced by more than 15 dB. The proposed scheme is actually based on the substantial difference in the insertion loss for the RB noise (~ 15 dB) and the upstream DPSK signal (~ 3.8 dB). P_r increases significantly when P_{in} is over 7 dBm, due to Stimulated Brillouin Scattering. The solid line in the inset of Fig. 3.2(b) shows the measured spectrum (resolution bandwidth=0.06 nm) of the RB without using the destructive port of the DI to suppress the RB. For comparison, the dashed line in the inset shows the substantially suppressed spectrum measured at the destructive port of the DI, demonstrating its effectiveness for RB suppression. The RB suppression will be enhanced for a DI with a higher extinction ratio as well as for a CW light with narrower linewidth.

We then conducted a proof-of-concept experiment to demonstrate the proposed loopback scheme, based on the architecture shown in Fig. 3.1. At the OLT, CW light at

1553.5 nm with a power of 3.5 dBm was fed into an AWG (4-dB insertion loss) with a channel spacing of 0.8 nm and a 3-dB bandwidth of 0.35 nm through a circulator (0.5-dB insertion loss). After propagating through another two circulators following the AWG, the CW light was coupled into a 20-km SMF (4-dB insertion loss) followed by another AWG (4-dB insertion loss) at the RN, with a channel spacing of 0.8 nm and a 3-dB bandwidth of 0.6 nm. At the ONU, through a circulator the CW light was fed into a polarization controller (0.8-dB insertion loss) followed by an optical PM (3.5-dB insertion loss). The PM was driven by a 10-Gb/s $2^{31}-1$ pseudorandom binary sequence (PRBS) as the upstream data. Following the PM, another polarization controller was used to assure that the system performance was investigated for the worst RB interference scenario. After transmitting back to the OLT, the upstream DPSK data were demodulated by a DI with 94-ps relative delay and pre-amplified to -8 dBm by a shared EDFA. The amplified signal transmitted through the AWG, the circulator and a tunable optical attenuator (for BER measurement) at the OLT, before being detected by a 10-Gb/s p-i-n receiver.

Fig. 3.3 depicts the eye diagrams of the detected upstream DPSK signals in both back-to-back (B2B) and transmission cases. In the transmission case, the eye of the upstream DPSK signal demodulated by the destructive port of the DI is clearly open, as shown in Fig. 3.3(b). Compared with the eye in the B2B case, shown in Fig. 3.3(a), only slight distortion, mainly due to the accumulated chromatic dispersion, is observed.

Although the two output ports of DI are generally equivalent in DPSK signal demodulation (Fig. 3.3 (a) and (c)), using the destructive port of DI to demodulate the upstream DPSK signal is essential to suppress the RB of the optical carrier. That is because the notch filter-like frequency response of destructive port of DI can

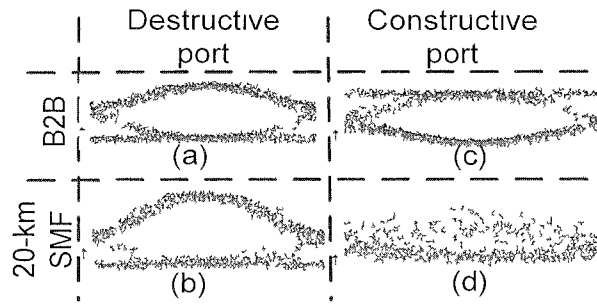


Fig. 3.3: Eye diagrams of the detected upstream DPSK signal by a 10-Gb/s p-1-n receiver in both back-to-back (a) and (c), and transmission case (b) and (d). Time scale: 20ps/div.

effectively suppress the RB of the optical carrier with a very narrow spectral width. On the contrary, the DPSK signal demodulated by the constructive port of the DI is vulnerable to RB, due to the low-pass frequency response of the constructive port which is complementary to that of the destructive port. Therefore it cannot prevent the RB entering the upstream receiver. For comparison, the much degraded eye diagram of the upstream DPSK signal demodulated by the constructive port of the DI is shown in Fig. 3.3(d).

The BER measurement result for the upstream DPSK signal in the transmission case based on the architecture in Fig. 3.1 is shown in Fig. 3.4. Compared with the BER curve of the B2B DPSK signal, around 1.5-dB power penalty at BER of 10^{-9} is observed. To prove that such power penalty was mainly due to the accumulated chromatic dispersion rather than the RB, the BER curve of the DPSK signal after 20-km SMF transmission was also measured. Compared to that, less than 0.2-dB power penalty at BER of 10^{-9} is shown for the upstream DPSK signal. Such a small power penalty demonstrates that the proposed loopback scheme is very robust to the interferometric crosstalk induced by the RB. We also compared the proposed scheme with the on-off keying (OOK) modulation case. We replaced the PM in Fig.

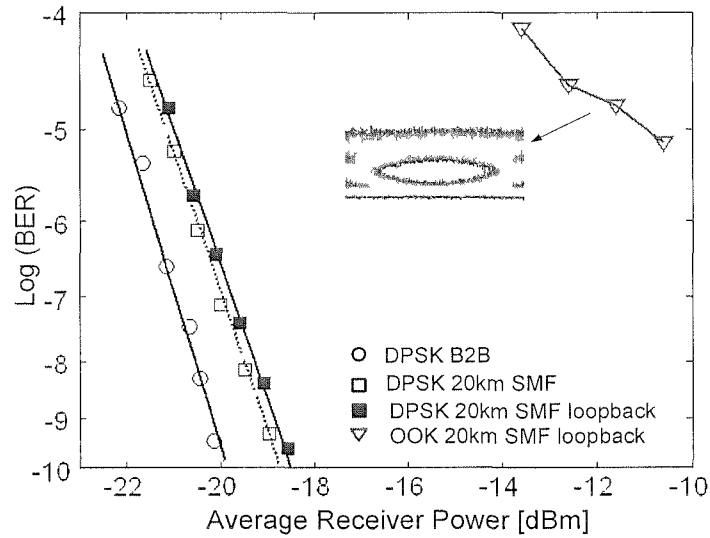


Fig. 3.4 BER measurements. The received signal power was measured before the p-i-n receiver. Inset: eye diagram of the detected upstream OOK signal.

Time scale: 20ps/div.

3.1 by an optical intensity modulator and utilized OOK as the upstream modulation format. The BER measurement result for the upstream OOK signal after 20-km SMF transmission is also shown in Fig. 3.4. An error floor above 10^{-6} and a much degraded eye diagram are observed for the upstream OOK signal, due to the interferometric crosstalk caused by the beating between the signal and the RB.

By placing the tunable optical attenuator before the shared EDFA, the preamplified receiver sensitivity ($\text{BER}=10^{-9}$) of the upstream DPSK signal after 20-km transmission in SMF, was measured to be -34.7 dBm. The received upstream power before the shared EDFA was around -28.4 dBm, implying ~6-dB system margin.

In conclusion, we have proposed a novel loopback scheme for carrier-distributed

WDM-PONs to enhance system tolerance to RB-induced interferometric crosstalk. By using DPSK as the upstream modulation format, the destructive port of the DI used for upstream DPSK demodulation could simultaneously suppress the RB of the optical carrier. Error-free operation of the 10-Gb/s upstream signals is achieved after the transmission of 20-km SMF with less than 0.2-dB power penalties induced by Rayleigh noise.

3.1.3. Application in a long-reach WDM-PON

It has been demonstrated in the last section that the proposed scheme can effectively suppress the carrier RB, enabling a 20-km transmission without ONU gain. For long-reach application, appropriate ONU gain is necessary and in this scenario the effect of signal RB has to be considered. In this part, we will further investigate the feasibility of the proposed scheme in long-reach WDM-PON with ONU gain.

Rayleigh crosstalk is induced by the beating between the upstream signal and the in-band RB noise towards the OLT. The in-band RB noise includes two types of RB: the carrier RB and the signal RB. The carrier RB arises from the CW carrier delivered to the ONU, whereas the signal RB is the back reflection of the upstream signal, which is further modulated at ONU before transmitting to the OLT, along with the upstream signal. It is widely reported that both types of RB induce crosstalk to the upstream signal [13], [15], [20], [21]. Increasing the ONU gain will increase the signal-to-carrier RB ratio, but will decrease the signal-to-signal RB ratio [20]. For this reason, both types of RB need to be considered in optimizing ONU gain if no measure is taken to suppress the Rayleigh noise entering upstream receivers. In this part, we characterize the different weights of two types of RB in a WDM-PON with Rayleigh

noise-suppressed upstream receivers. It is found that the carrier RB is dominant within a reach up to 60 km; thus effective suppression of carrier RB is essential in the design of Rayleigh noise-immune upstream receivers. We then experimentally demonstrate that the proposed scheme can substantially improve the system tolerance to carrier RB by 19 dB. Experimental demonstration of 10-Gb/s upstream signal over 60-km standard single mode fiber (SMF) is achieved with less than 2.5-dB power penalty induced by Rayleigh noise, thanks to the effective suppression of the dominant carrier RB. We also investigate the relation between system margin and ONU gain, based on which the maximum system reach can be predicted.

3.1.3.1. Proposed system architecture and the source of Rayleigh noise

Fig. 3.5 shows the proposed loopback architecture of a WDM-PON. The multi-wavelength optical carriers for upstream transmission are generated by CW lasers at the OLT as the CLS, and then multiplexed by an AWG. After the transmission in a feeder fiber with a length of L_1 , the optical carriers are wavelength routed toward different ONUs, by another AWG at the RN. The length of the distribution fiber (between RN and ONU) is L_2 . At ONU, the CW light is first amplified and then modulated by an optical phase modulator (PM), driven by differentially pre-coded upstream data, before being sent back to the OLT. As both the CLS and the DI are located at CO, their wavelength alignment could be readily achieved by locking the CLS wavelength to the DI. Note that only the destructive port of the DI can be used for upstream DPSK demodulation and carrier RB suppression simultaneously [17], due to

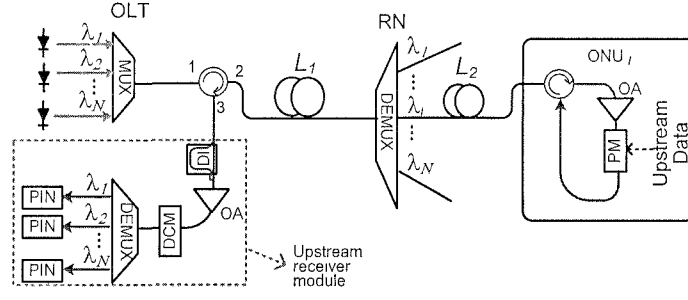


Fig. 3.5 Proposed loopback architecture using DPSK as the upstream modulation format to suppress Rayleigh noise for long-reach WDM-PON. The downstream channels are omitted here for simplicity. OA: optical amplifier, PM: phase modulator, DI: delay-interferometer, DCM: dispersion compensation module, PIN: p-i-n receiver.

its notch filter-like frequency response. The demodulated DPSK signals are pre-amplified before direct detection. Proper dispersion compensation may be required depending on the reach of WDM-PON.

By calculating the power ratio between two types of RB, we can find out their different contributions in the upstream Rayleigh noise. We first calculate the power of carrier RB at port 2 of the OLT optical circulator. The signal RB is generated in both feeder and distribution fiber. The mean intensity of the carrier RB generated in the feeder fiber is given by,

$$P_{CB_1} = \frac{P_C}{R_1} \quad (3.1)$$

where P_C is the power of optical carrier incident to the feeder fiber, and R_1 is the RB-induced return loss of the feeder fiber that is given by [22], [23],

$$R_1 = \frac{2}{S(1 - e^{-2\alpha_p L_1})} \quad (3.2)$$

with S , α_p being the recapture factor, and fiber attenuation coefficient in units of

km⁻¹, respectively. The values of S and α_p are set to be 0.0016 and 0.046, respectively, for the standard SMF used in the experiment. At port 2 of the OLT optical circulator, the mean intensity of the carrier RB generated in the distribution fiber is given by

$$P_{CB_2} = \frac{P_C}{\alpha_1 \cdot \alpha_A} \cdot \frac{1}{R_2} \cdot \frac{1}{\alpha_A \cdot \alpha_1} = \frac{P_C}{(\alpha_1 \cdot \alpha_A)^2 \cdot R_2} \quad (3.3)$$

where α_1 and α_A are the insertion loss of the feeder fiber and the AWG at RN in linear scale, respectively, and R_2 is the RB-induced return loss of the distribution fiber. The insertion loss of AWGs used in this paper is 4 dB, thus the value of α_A is 2.5. Note that linear-scale units are used for the parameters in all the equations of this paper, unless specified otherwise. α_1 and R_2 are given by

$$\alpha_1 = e^{\alpha_p L_1} \quad (3.4)$$

$$R_2 = \frac{2}{S(1 - e^{-2\alpha_p L_2})} \quad (3.5)$$

Similarly, we can calculate the power of signal RB at port 2 of the OLT optical circulator. The mean intensity of the signal RB generated in the feeder fiber is given by

$$P_{SB_1} = \left(\frac{P_C}{\alpha_1 \cdot \alpha_A \cdot \alpha_2} \cdot G_{ONU} \cdot \frac{1}{\alpha_2 \cdot \alpha_A} \right) \cdot \frac{1}{R_1} \cdot \frac{1}{\alpha_A \cdot \alpha_2} \cdot G_{ONU} \cdot \frac{1}{\alpha_2 \cdot \alpha_A \cdot \alpha_1} = \frac{P_C \cdot G_{ONU}^2}{R_1 \cdot \alpha_1^2 \cdot (\alpha_A \cdot \alpha_2)^4} \quad (3.6)$$

with α_2 and G_{ONU} being the insertion loss of the distribution fiber and the ONU gain, respectively. The ONU gain is defined as the power ratio between the output and the input signals at ONU. α_2 is further given by

$$\alpha_2 = e^{\alpha_p L_2} \quad (3.7)$$

The mean intensity of the signal RB generated in the distribution fiber is given by

$$P_{SB_2} = \left(\frac{P_C}{\alpha_1 \cdot \alpha_A \cdot \alpha_2} \cdot G_{ONU} \right) \cdot \frac{1}{R_2} \cdot G_{ONU} \cdot \frac{1}{\alpha_2 \cdot \alpha_A \cdot \alpha_1} = \frac{P_C \cdot G_{ONU}^2}{R_2 \cdot (\alpha_1 \cdot \alpha_A \cdot \alpha_2)^2} \quad (3.8)$$

From Eq. (3.1)-(3.8), the power ratio between the two types of RB at port 2 of the OLT optical circulator can be derived as

$$\frac{P_{CB}}{P_{SB}} = \frac{P_{CB_1} + P_{CB_2}}{P_{SB_1} + P_{SB_2}} = \frac{[(\alpha_1 \cdot \alpha_A)^2 \cdot R_2 + R_1] \cdot \alpha_2^4 \cdot \alpha_A^2}{G_{ONU}^2 \cdot [(\alpha_2 \cdot \alpha_A)^2 \cdot R_1 + R_2]} \quad (3.9)$$

G_{ONU} can be further derived, from the power budget equation, as

$$G_{ONU} = \frac{M \cdot P_{rec} \cdot (\alpha_1 \cdot \alpha_A \cdot \alpha_2)^2 \cdot \alpha_{Cr}}{P_C} \quad (3.10)$$

with M , P_{rec} and α_{Cr} being the system margin, the upstream receiver sensitivity (at BER=10⁻⁹), and the insertion loss from port 2 to 3 of the circulator at OLT, respectively. Note that the upstream receiver sensitivity is measured at the input port of DI. A link margin of 6-8 dB is generally used for future-proof fiber systems [24]. In this part, we use an 8-dB margin in the analysis. For 10-Gb/s DPSK signal, the back-to-back receiver sensitivity P_{rec} is measured to be around -32 dBm. If all the transmission impairments can be eliminated at the upstream receiver module, we can substitute this sensitivity value into Eq. (3.10) to calculate the required ONU gain for different feeder-fiber lengths. Here we assume that the length ratio between the feeder and distribution fiber is 5:1, and the input power to the feeder fiber P_C =3 dBm. Then, by substituting the calculated ONU gain to Eq. (3.9), we can further calculate the power ratio between two types of RB for different feeder-fiber lengths. As shown in Fig.3.6, we can observe that the carrier RB is more than 20-dB larger than the signal RB, implying that carrier RB is the dominant noise entering the upstream receiver module. In practical implementation, the transmission impairments may not be fully eliminated at the upstream receiver module (i.e. there may be residual Rayleigh noise or dispersion.), thus we further calculate the required ONU gain and the power ratio between two types of RB, with additional power penalty of 5 dB (i.e. P_{rec} =-27 dBm) after transmission. The calculated results are also shown in Fig. 3.6. Obviously, the carrier RB is still the dominant noise entering the upstream receiver module in this scenario, even after 60-km transmission. Based on the aforementioned analysis, we

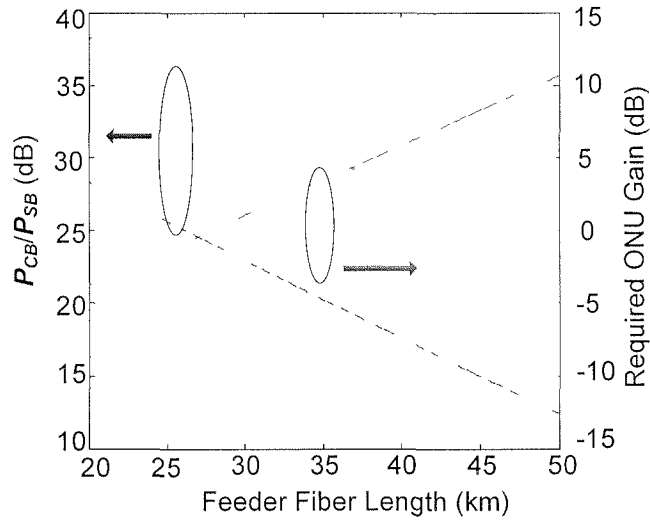


Fig. 3.6 Required ONU gain, and P_{CB}/P_{SB} , for different feeder-fiber lengths.

The upstream receiver sensitivity is set to be -32 dBm for the dashed line, and -27 dBm for the solid line, respectively

conclude that the suppression of carrier RB should be the main consideration in the design of RB-suppressed upstream receiver.

3.1.3.2. Effectiveness of the DI's destructive port on RB suppression and transmission demonstration

We investigated the upstream power penalty as a function of signal-to-crosstalk ratio (SCR) based on the experimental setup in Fig. 3.7, which is similar to that employed in [13]. We first used carrier RB as the crosstalk signal, as in Fig. 3.7(a). Continuous-wave (CW) light at 1553.5 nm with a line width of 100 kHz was generated from a tunable laser diode (TLD) and was split into two paths by an 80/20 coupler. In the upper path, a PM was driven by a 10-Gb/s $2^{31}-1$ PRBS to generate the DPSK signal. Following the PM, a variable optical attenuator (VOA) was used to adjust the signal power to obtain different SCR values. In the lower

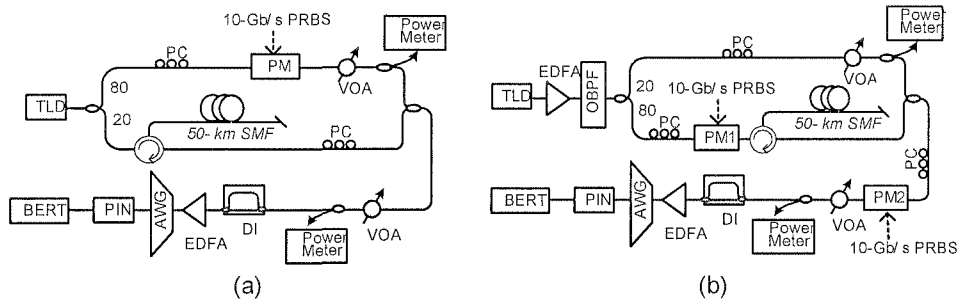


Fig. 3.7 Experimental setup to investigate the effectiveness of the proposed scheme on the suppression of (a) carrier RB, and (b) signal RB.

path, the crosstalk signal was the RB light from a 50-km SMF, with a fixed power of -30 dBm measured after a polarization controller (PC). The PC was used to maximize the beating noise. The DPSK signal and the crosstalk signal were then combined by a 3-dB coupler and fed into the proposed upstream receiver module, which consisted of a 94-ps DI with a measured ER of 22 dB, an EDFA, a 100-GHz AWG (3-dB bandwidth=0.35 nm, insertion loss = 4 dB), and a p-i-n receiver. The measured crosstalk tolerance of the DPSK signal is shown in Fig. 3.8. For comparison, the crosstalk tolerance of the conventional OOK signal was also measured. In this case, the PM was replaced by a Mach–Zehnder modulator (MZM) and the DI was removed from the upstream receiver module. Compared with the conventional scheme using OOK format, the carrier-RB tolerance of the proposed scheme is substantially improved by 19 dB, as shown in Fig. 3.8.

We then used carrier RB as the crosstalk signal, as in Fig. 3.7(b). In the lower path PM1 was used to generate the signal RB, which was further combined with the optical carrier in the upper path. The combined light was then modulated by PM2, which was used to generate the upstream DPSK signal. In the lower path the power of signal RB was fixed at -32 dBm and different SCR values could be obtained by

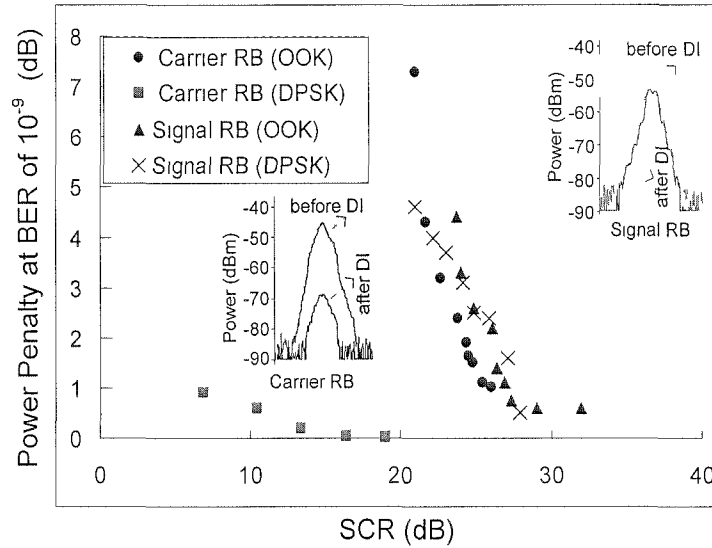


Fig. 3.8 Power penalty as a function of signal-to-crosstalk ratio (SCR). Insets: measured spectra (resolution bandwidth=0.06 nm) of signal (DPSK) RB and carrier RB before and after DI.

adjusting the VOA in the upper path. Again, for comparison, the signal-RB tolerance of the conventional OOK signal was also measured by replacing PM1 and PM2 with two MZMs and removing the DI from the upstream receiver module. The measurement results are also shown in Fig. 3.8. We can find that the signal-RB tolerance is not improved in the proposed scheme. The reason is that the signal RB has a wide spectrum after being modulated twice and thus cannot be effectively suppressed by DI's destructive port. As observed from the spectra (resolution bandwidth=0.06 nm) in the insets of Fig. 3.8, the carrier RB is substantially suppressed by DI's destructive port, whereas the signal-RB only experiences little suppression.

Although the proposed scheme can only suppress the carrier RB, it is sufficient to significantly improve the system's tolerance to Rayleigh noise, due to the aforementioned fact that the carrier RB is the dominant noise.

We then experimentally demonstrated the effectiveness of the proposed loopback scheme based on the architecture shown in Fig. 3.5. At the OLT, CW light at 1553.5 nm from a tunable laser with a power of 3-dBm was fed into a span of 50-km SMF through a circulator (from port 1 to port 2). An AWG (4-dB insertion loss) with a channel spacing of 0.8 nm and a 3-dB bandwidth of 0.6 nm was used at the RN. After transmission through another 10-km SMF (the distribution fiber), the CW light with a power of -13.5 dBm was fed into the ONU, which consisted of a circulator, an EDFA and a PM. The PM was driven by a 10-Gb/s $2^{31}-1$ PRBS to generate the upstream DPSK signal, which was looped back to the OLT through the ONU circulator. A commercially available LiNbO₃ PM was used in this proof-of-concept experiment, but some polarization-insensitive integrated PMs could be more desirable for practical applications [25], [26]. In addition, a semiconductor optical amplifier could also be used as a PM [27]. The upstream receiver module here was the same as in Fig. 3.7, except that a dispersion compensation module (DCM, -666 ps/nm @ 1545 nm) is added to compensate around 2/3 of the accumulated dispersion for the upstream signal. The accumulated dispersion was not fully compensated, as in practical implementation all the upstream channels cannot be simultaneously fully compensated by a common DCM due to the length variation of distribution fibers.

The BER measurement results are shown in Fig. 3.9. Note that the received optical power was measured before the input port of DI, and the ONU gain was fixed at 11 dB for all BER measurements. Compared with the back-to-back cases, around 4.5-dB power penalty (BER= 10^{-9}) is observed for the upstream DPSK signal after 60-km transmission, due to the residual dispersion and the residual Rayleigh noise. To further investigate the power penalty induced by the residual Rayleigh noise, the BER curve after 60-km transmission in dual fibers is also shown in Fig. 3.9.

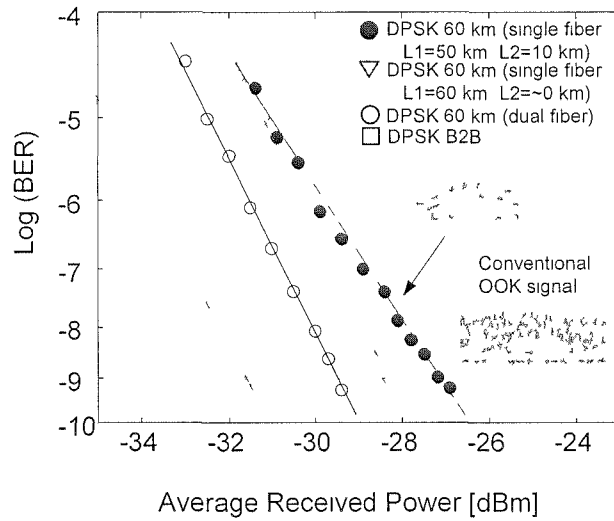


Fig. 3.9 BER measurement results. Insets: upstream eye diagrams in the proposed scheme and in the conventional scheme. Time scale: 20ps/div.

Comparing the single-fiber and dual-fiber curves, less than 2.4-dB Rayleigh noise-induced power penalty is observed, showing the effectiveness of the proposed scheme in Rayleigh noise suppression. Rayleigh noise-induced power penalty will be further decreased when the length of distribution fiber is reduced. As shown in Fig. 3.9, Rayleigh noise-induced power penalty is reduced to 1.2 dB for the extreme case when the total transmission link consists of only feeder fiber ($L_1=60$ km and $L_2=\sim 0$ km). The reason is that the signal RB, which cannot be suppressed by DI's destructive port, is reduced when the distribution fiber is shorter.

We also compared the proposed scheme with that using conventional OOK modulation in upstream. We replaced the PM in Fig. 3.5 with a MZM, removed the DI from OLT, and maintained the same ONU gain. However, in this case the upstream BER could not be measured due to significant degradation by the interferometric crosstalk from Rayleigh noise. In contrast to the wide-open eye diagram of the demodulated upstream DPSK signal, a much degraded eye diagram of the upstream

OOK signal is also shown in the insets of Fig. 3.9.

3.1.3.3. Relation between system margin and ONU Gain

According to the experimental results in Fig. 3.9, the upstream receiver sensitivity (BER=10⁻⁹) is -26.7 dBm when $L_1=50$ km, $L_2=10$ km, and $G_{ONU}=11$ dB. Meanwhile, the measured average received power by the upstream receiver module is -18.7 dBm, implying 8-dB system margin. In practice, the required system margin may vary with different service quality requirements and different external transmission environments. On the other hand, for a given input power to the feeder fiber, system margin is determined by the upstream receiver sensitivity and ONU gain. Next we will investigate the relation between the upstream receiver sensitivity and ONU gain, from which the relation between system margin and ONU gain can also be derived through straightforward calculation.

At the upstream receiver in OLT, the signal-RB beating noise and signal-ASE beating noise are dominant. The optical signal-to-noise ratio (OSNR) before the p-i-n receiver is given by

$$OSNR = \frac{P'_S \cdot G_{OLT}}{(P'_{CB} + P'_{SB}) \cdot G_{OLT} + P_{ASE}} = \frac{1}{\frac{P'_{CB}}{P'_S} + \frac{P'_{SB}}{P'_S} + \frac{1}{P'_S} \cdot \frac{P_{ASE}}{G_{OLT}}} \quad (3.11)$$

where P'_S , P'_{CB} and P'_{SB} are the optical power of the upstream signal, the carrier RB and the signal RB, respectively, before the optical preamplifier at OLT. G_{OLT} and P_{ASE} are the gain of the preamplifier and the power of amplified spontaneous emission (ASE) noise within the passband of an AWG channel, respectively. The ASE noise generated during ONU amplification is neglected, as after transmitting to the upstream

receiver it is significantly smaller than both Rayleigh noise and the ASE noise generated at OLT.

Eq. (3.11) can be rewritten as

$$P_S' = \frac{P_{ASE} / G_{OLT}}{1 / OSNR - P_{SB}' / P_S' - P_{CB}' / P_S'} \quad (3.12)$$

where

$$\frac{P_{ASE}}{G_{OLT}} \approx h\nu n_{sp} \cdot \Delta\nu_{opt} \quad , \quad (G_{OLT} \gg 1) \quad (3.13)$$

with h , ν , n_{sp} , $\Delta\nu_{opt}$ being the Planck constant, the optical frequency, the spontaneous-emission factor ($n_{sp}=2$ in this paper) and the channel bandwidth of the OLT AWG, respectively.

Assume the BER of the upstream signal is 10^{-9} when the optical signal-to-noise ratio equals to a specific value of $OSNR_0$. Then based on Eq. (3.12), the upstream receiver sensitivity (at BER= 10^{-9}) can be expressed as,

$$P_{rec} = \frac{P_{ASE} / G_{OLT}}{1 / OSNR_0 - P_{SB}' / P_S' - P_{CB}' / P_S'} \cdot \alpha_{DI} \quad (3.14)$$

P_{SB}' , P_{CB}' , and P_S' are determined by the following three equations,

$$P_{SB}' = (P_{SB_1} + P_{SB_2}) / \alpha_{DI} \quad (3.15)$$

$$P_{CB}' = (P_{CB_1} + P_{CB_2}) / S_{DI} \quad (3.16)$$

$$P_S' = \frac{P_C \cdot G_{ONU}}{(\alpha_1 \cdot \alpha_A \cdot \alpha_2)^2 \cdot \alpha_{DI}} \quad (3.17)$$

α_{DI} is the insertion loss of DI's destructive port for the upstream signal and signal RB, which was measured to be ~ 4 dB; S_{DI} is the carrier-RB suppression ratio by DI's destructive port, which is defined as the ratio between DI's input power and the output power from DI's destructive port. S_{DI} was measured to be ~ 18 dB in the experiment.

It is easy to understand that S_{DI} will become larger for smaller laser linewidth as well as for larger ER of the DI. Based on the experimental results and Eq. (3.1)-(3.8), and Eq. (3.15)-(3.17), we can derive the value of $OSNR_0$ and can rewrite Eq. (3.14) as,

$$P_{rec} = \frac{k_3}{k_0 - k_1 \cdot G_{ONU} - \frac{k_2}{G_{ONU}}} \quad (3.18)$$

with k_0 , k_1 , k_2 and k_3 being

$$k_0 = 1 / OSNR_0$$

$$k_1 = \frac{1}{(\alpha_2 \cdot \alpha_A)^2 \cdot R_1} + \frac{1}{R_2}$$

$$k_2 = \frac{\alpha_{DI} \cdot \alpha_2^2 \cdot [R_1 + (\alpha_1 \cdot \alpha_A)^2 \cdot R_2]}{S_{DI} \cdot R_1 \cdot R_2}$$

$$k_3 = h\nu n_{sp} \cdot \Delta\nu_{opt} \cdot \alpha_{DI}$$

Then based on Eq. (3.18) we can plot the relation between the upstream receiver sensitivity and ONU gain as in Fig. 3.10. Note that the parameters used in the theoretical calculations are in correspondence with the experimental setup. To confirm the correctness of theoretical analysis described above, different upstream receiver sensitivities corresponding to different ONU gains were measured in experiment and are also shown in Fig. 3.10. Good agreement between the theory and experiment is observed. The theoretical model predicts well the system performance and thus can be

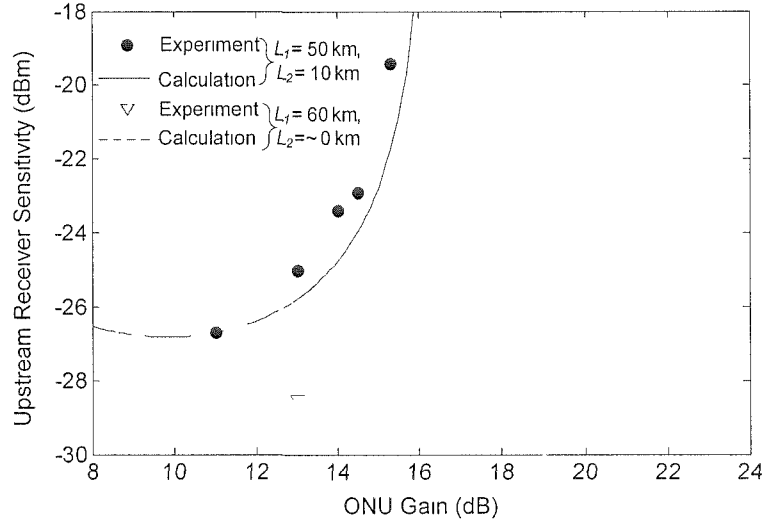


Fig. 3.10 The relation between the upstream receiver sensitivity and ONU gain.

used as a guideline in system design. As an example, based on the aforementioned theoretical model the optimal ONU gain can be derived to maximize the system margin.

Eq. (3.10) can be rewritten as

$$M = \frac{P_c}{(\alpha_1 \cdot \alpha_A \cdot \alpha_2)^2 \cdot \alpha_{c_{ir}}} \cdot \frac{G_{ONU}}{P_{rec}} \quad (3.19)$$

Substituting Eq. (3.18) into Eq. (3.19), we can derive,

$$M = \frac{P_c}{(\alpha_1 \cdot \alpha_A \cdot \alpha_2)^2 \cdot \alpha_{c_{ii}}} \cdot \frac{-k_1 \cdot G_{ONU}^2 + k_0 \cdot G_{ONU} - k_2}{k_3} \quad (3.20)$$

From Eq. (3.20), we can further derive that the maximum system margin can be achieved as

$$M_{Max} = \frac{P_c}{(\alpha_1 \cdot \alpha_A \cdot \alpha_2)^2 \cdot \alpha_{c_{ii}}} \cdot \frac{k_0^2 - 4k_1 \cdot k_2}{4k_1 \cdot k_3} \quad (3.21)$$

when the ONU gain is optimized as

$$G_{ONU_opt} = k_0 / 2k_1 \quad (3.22)$$

Then based on Eq. (3.21) and Eq. (3.22) we can calculate the maximum system margin

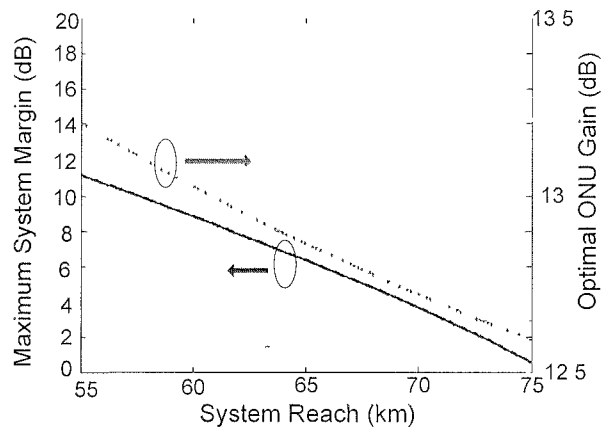


Fig. 3.11 The maximum system margin and the required optimal ONU gain for different system reaches. The length ratio between the feeder and distribution fiber is assumed to be 5:1.

and the required optimal ONU gain for different system reaches as shown in Fig. 3.11. Here we assume that the length ratio between the feeder and distribution fiber is 5:1. We observe that to assure an 8-dB system margin the maximum reach is ~62 km, whereas for a 3-dB system margin the maximum reach can be ~72 km. As the optimal gain is nearly constant for reach ranging from 55 km to 75 km, all ONU's can be set to a fixed gain (e.g. 12.7 dB) to avoid the incurred operation complexity of setting different gains for different ONUs. Note that for the scheme employing conventional OOK in upstream, the optimal ONU gain is a linear function of the reach [20].

3.1.4. Multiple Rayleigh Backscattering

We have investigated the effect of carrier RB and signal RB on system performance. In fact, the RB light will also be back-scattered during transmission in optical fiber, inducing multiple RB. Here we study the effect of second-order RB on the upstream signal, as illustrated in Fig.3.12. The downstream CW carrier will generate the first-order carrier RB (carrier-RB1), which will further generate the second-order

carrier RB (carrier-RB2). Similarly, the upstream signal will generate the first-order signal RB (signal-RB1), which will further generate the second-order signal RB (signal-RB2). The second-order signal RB further includes signal-RB2_(a), generated by the downstream part of signal-RB1, and signal-RB2_(b), generated by the upstream part of signal-RB1.

First, we will explain that the effect of both carrier-RB2 and signal-RB2_(a) is negligible. RB-induced return loss of a fiber will increase as the fiber length increases up to 20 km. For a fiber longer than 20 km the RB-induced return loss is saturated at around 30 dB. For simplicity and also as a conservative estimation, we assume that the RB-induced return loss is 30 dB for any fiber length. Then the power ratio between the upstream signal and carrier-RB2 is always 60 dB, as they share the same transmission path. Similarly, the power ratio between the upstream signal and signal-RB2_(a) is always 60 dB. Thus, the effect of both carrier-RB2 and signal-RB2_(a) is negligible.

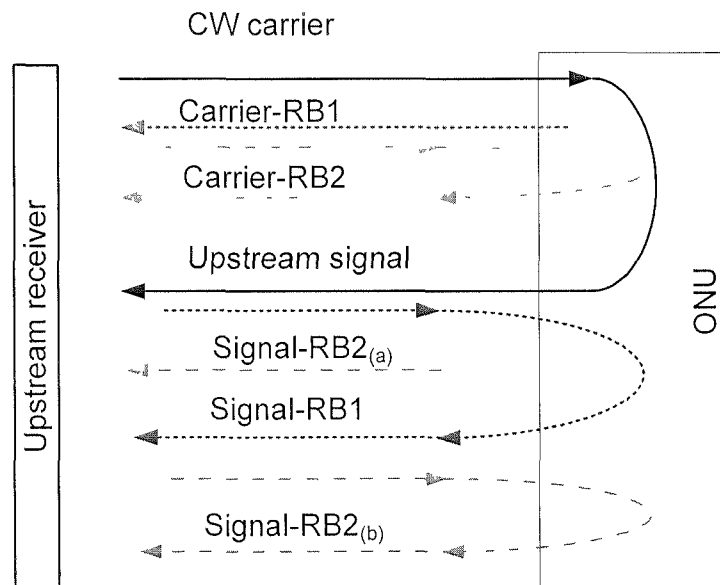


Fig. 3.12 Generation of second-order RB.

As signal-RB2_(b) will be amplified at ONU, it may become comparable with signal-RB1 for large ONU gain. At the upstream receiver, the power ratio between the is the same with that between the upstream signal and signal-RB1, due to the recurrence relation. Based on Eq. (3.6) and Eq.(3.8), the power ratio between signal-RB1 and signal-RB2_(b) can be expressed as,

$$\frac{P_{\text{signal-RB1}}}{P_{\text{signal-RB2}_{(b)}}} = \frac{1}{G_{ONU}} \cdot \frac{(\alpha_A \cdot \alpha_2)^2 \cdot R_1 \cdot R_2}{R_2 + R_1 \cdot (\alpha_A \cdot \alpha_2)^2} \quad (3.23)$$

According to the above equation, we can plot power ratio between signal-RB1 and signal-RB2_(b) as the function of ONU gain, as shown in Fig.3.13.

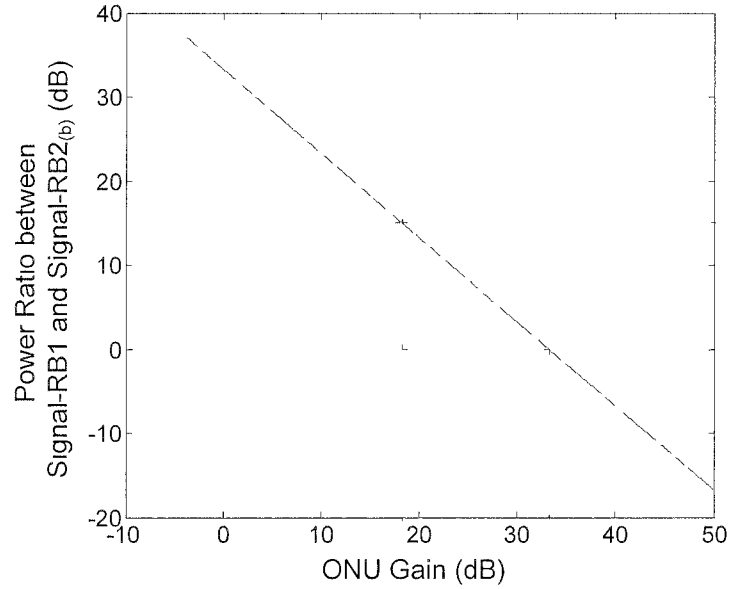


Fig. 3.13 Power ratio between signal-RB1 and signal-RB2_(b) as the function of ONU gain.

We can see that signal-RB2_(b) will be larger than signal-RB1 when the ONU gain is larger than 34 dB. For the ONU gain smaller than 18 dB the power ratio between signal-RB1 and signal-RB2_(b) is larger than 15 dB. In this case the power ratio between the upstream signal and signal-RB2_(b) is larger than 30 dB, and thus signal-RB2_(b) is

negligible. In conclusion, all the second order RBs are negligible for the ONU gain smaller than 18 dB, and for ONU gain larger than 18 dB signal-RB2_(b) will become significant. As the power ratio between the upstream signal and signal-RB1 is smaller than 15 dB for the ONU gain larger than 18 dB, signal-RB1 will induce very large power penalty for the upstream signal as shown in Fig.3.8. Thus, the ONU gain is not likely to be larger than 18 dB if signal-RB1 cannot be effectively suppressed and in this case only considering first-order RB is sufficient.

3.2. Optical phase remodulation with enhanced tolerance to Rayleigh noise

3.2.1. Introduction

Extensive studies have been carried out for Rayleigh noise mitigation in WDM-PON. However, prior reports are mainly for the carrier-distributed scheme, by light source scrambling, spectral broadening of the upstream signal or using specially designed modulation formats. Rayleigh noise mitigation in the remodulation-based WDM-PON is more challenging and only a few approaches have been proposed. In [29], the downstream signal was modulated using frequency-shift keying (FSK) to reduce light coherence, thus reducing the RB effect on upstream channels. However, the residual crosstalk noise still induced a 5-dB penalty at 1 Gb/s. Another scheme utilized downstream 10-Gb/s DPSK and upstream 2.5-Gb/s subcarrier modulation (SCM) to reduce spectral overlap between the reflections and the signals [30]. As a broadband oscillator, with a bandwidth several times larger than the signal bit rate, is needed at each ONU, it is difficult to realize 10-Gb/s symmetric bit-rate that is highly desirable

for future-proof PON systems.

Recently, we have propose a novel remodulation scheme for 10-Gb/s WDM-PON with single feeder fiber by using downstream DPSK with reduced modulation depth (RMD-DPSK) and upstream DPSK with full modulation depth (FMD-DPSK) [31]. The demodulated RMD-DPSK signal from the destructive port of the DI at ONU can maintain a high extinction-ratio (ER), whereas the signal from the DI's constructive port has a very low ER and a reduced phase variation, thus is very suitable as the carrier for upstream phase remodulation. The RB of the downstream RMD-DPSK signal mainly distributes in the low-frequency region, and thus can be suppressed by the notch filter-like destructive port of the DI at OLT, which is simultaneously used to demodulate the upstream DPSK signal. In this section, we further investigate different issues for the proposed scheme in [31]. First, we make a comprehensive comparison between the proposed optical phase remodulation and the conventional optical amplitude remodulation, and conclude that the proposed scheme can alleviate the downstream receiver sensitivity degradation. We then investigate the advantage of using the DI's constructive port output as the upstream carrier. Detailed analysis for the proposed RB suppression scheme will also be given.

3.2.2. System architecture

Fig. 3.14 illustrates the proposed remodulation scheme for a WDM-PON using downstream RMD-DPSK and upstream FMD-DPSK. For each downstream wavelength at the OLT, differentially precoded data is used to drive an optical phase modulator (PM) with a low driving voltage to generate the downstream RMD-DPSK signal. All the downstream wavelengths at the OLT are multiplexed by an AWG. The multiplexed signals are fed into a 20-km SMF. After transmission, the downstream

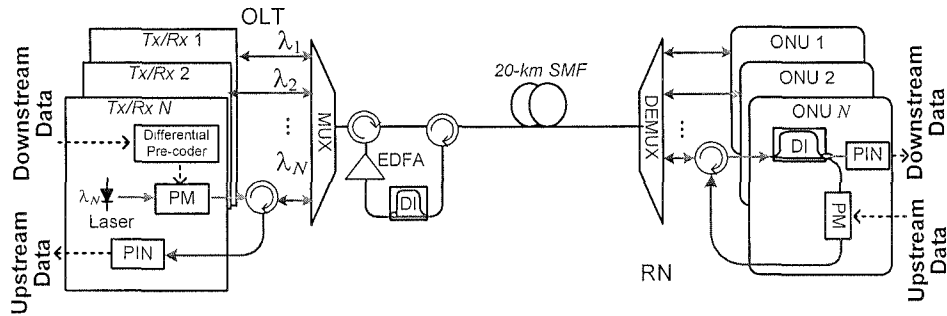


Fig. 3.14 Proposed optical phase remodulation architecture.

signal from the OLT is wavelength routed toward different ONUs, by another AWG at the RN. At the ONU, the downstream RMD-DPSK signal is demodulated from the destructive port of the DI before direct detection, while the light from the constructive port is fed into a PM for upstream data remodulation. The demodulated upstream DPSK signals are pre-amplified by a shared EDFA before direct detection. By using a shared DI and an $N \times N$ cyclic AWG at the RN, the DI at ONU can also be saved [32]

3.2.3. Operation principle

3.2.3.1. A unique feature of phase remodulation when compared with conventional amplitude remodulation

As discussed in chapter 2, the ER of the demodulated RMD-DPSK signal from the destructive port is independent of the phase modulation depth and is always infinite, theoretically. Fig.3.15(a) and (b) depicts the simulated eye diagrams of the demodulated downstream RMD-DPSK signal from DI's destructive port, when the modulation depth of the downstream RMD-DPSK signal is 0.2 and 0.4, respectively.

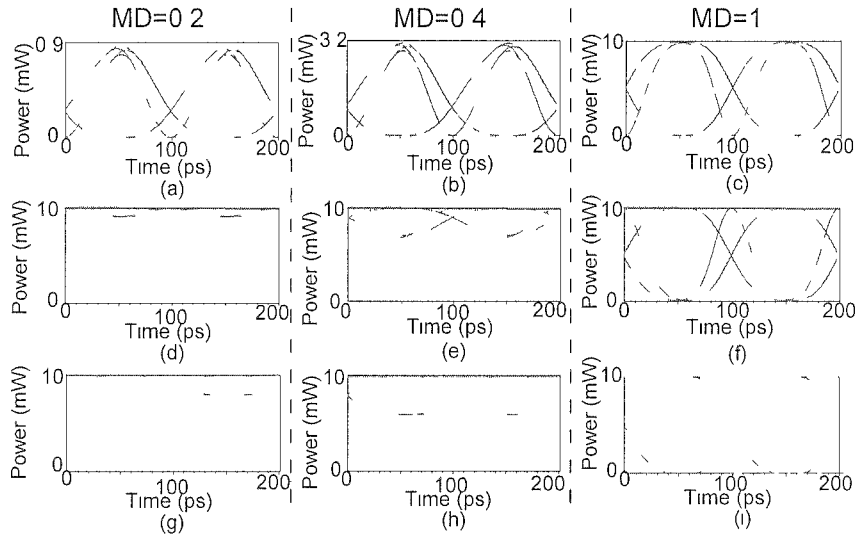


Fig. 3.15 Eye diagrams with different downstream modulation depths: (a)-(c), downstream DPSK signal demodulated from DI's destructive port; (d)-(f), downstream DPSK signal demodulated from DI's constructive port; (g)-(i) downstream OOK signal in conventional optical amplitude remodulation scheme.

Compared with the eye diagram of the demodulated FMD-DPSK signal, shown in Fig.3.15 (c), certain power reduction in the '1' level is observed, whereas the demodulated '0' level is always perfectly null, leading to a theoretically infinite ER. In practice, due to additional noise and device imperfection, the ER cannot be infinite. However it can still maintain a high value for a large range of phase modulation depth. On the contrary, the ER of the output signal from the constructive port is substantially reduced, as in Fig. 3.15(d) and (e), and thus can be used as the carrier for upstream phase remodulation.

One concern is that the insertion loss is larger if the destructive port is used for RMD-DPSK demodulation, due to the reduced '1' level. Here, we investigate the influence of modulation depth on the insertion loss of DI's destructive port for the

downstream RMD-DPSK signal. As shown in Fig. 3.16, the smaller the modulation depth of the downstream RMD-DPSK signal, the larger the insertion loss of the DI's destructive port. As the modulation depth of the downstream RMD-DPSK signal decreases, the “low-frequency” components in its spectrum will increase, as shown in the inset of Fig. 3.16. Thus for the downstream RMD-DPSK signal with a smaller modulation depth, more power will be rejected by the notch filter-like destructive port of the DI, leading to an increased insertion loss. The modulation depth of the downstream RMD-DPSK signal thus should not be too small to assure enough

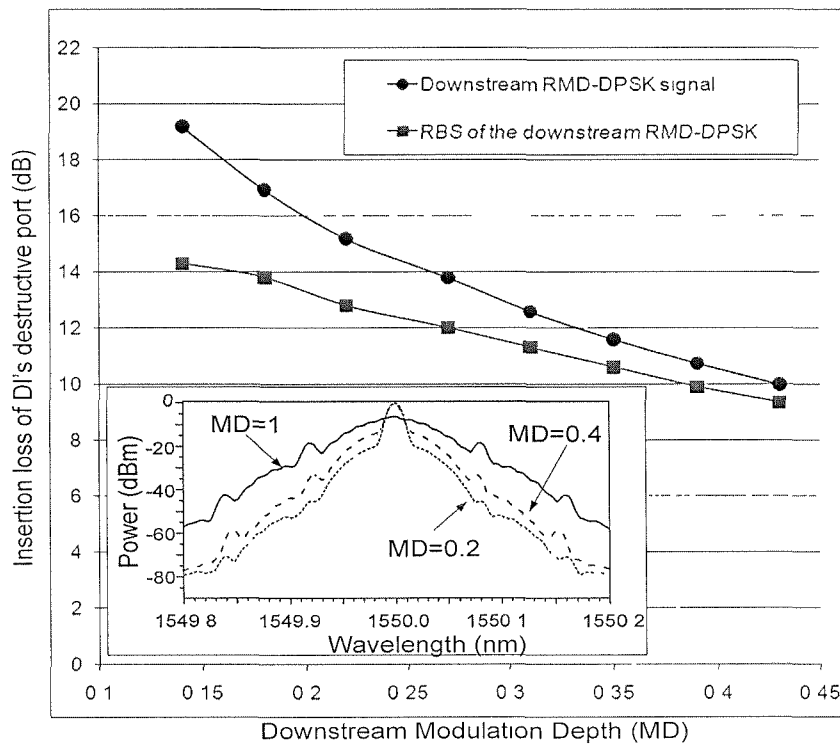


Fig. 3.16 The insertion loss of the DI's destructive port for the downstream RMD-DPSK signal and for its RB, at different downstream modulation depths.

Inset: the simulated spectrum of the downstream RMD-DPSK signal with different modulation depths.

downstream power budget. Nevertheless, the reduced optical power actually appears at the constructive port and will benefit the upstream power budget.

We then investigated the impact of the downstream modulation depth on the receiver sensitivity of both the downstream RMD-DPSK signal and the upstream FMD-DPSK signal through simulation, and the results are reported in Fig. 3.17(a). As the downstream modulation depth decreases, no power penalty is observed for the demodulated downstream RMD-DPSK signal, thanks to its high ER as discussed above. Actually, even a slightly negative power penalty is observed, arising from the RZ-like pulse shape of the demodulated downstream RMD-DPSK signal. For comparison, we also studied the relation between the downstream modulation depth and the receiver sensitivity for the conventional optical amplitude remodulation scheme (downstream RMD-OOK, upstream FMD-OOK). As shown in Fig. 3.17(a), the power penalty of the downstream RMD-OOK signal increases rapidly as the modulation depth of the downstream OOK signal decreases. The power penalty of the downstream RMD-OOK signal is due to the reserved constant optical power that carries no downstream signal, as shown in Fig. 3.15(g) and (h). Both the conventional optical amplitude remodulation and the proposed optical phase remodulation schemes have similar upstream performance when the downstream modulation depth changes, as reported in Fig. 3.17(a) (the open circle and open square). When the downstream modulation depth is 0.4, eye diagrams of the detected upstream signal using the proposed scheme and the conventional amplitude remodulation scheme are shown in Fig. 3.17(b) and Fig. 3.17(d), respectively, with similar eye opening. The downstream modulation depth should be small enough to avoid too much upstream power penalty. In contrast to the conventional optical amplitude remodulation scheme, the advantage of the optical phase remodulation scheme is that there is no downstream power penalty, when the downstream modulation depth is reduced to guarantee the upstream

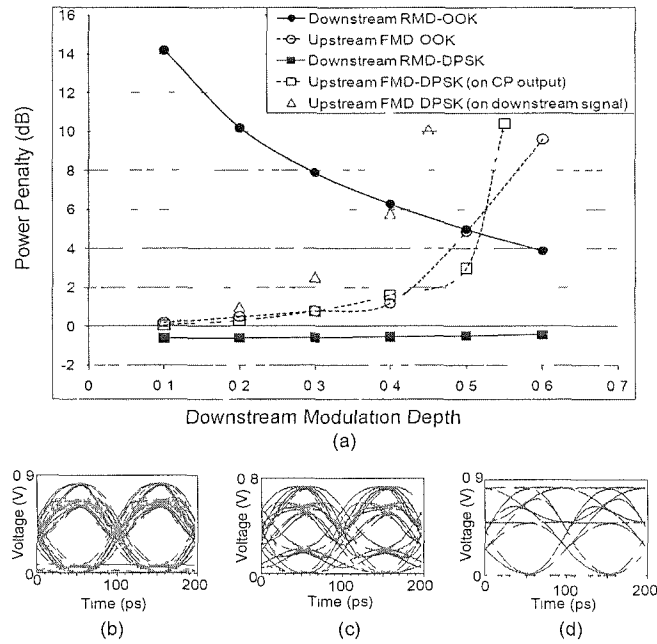


Fig. 3.17 (a) The impact of the downstream modulation depth on the receiver sensitivity of both downstream and upstream signals when using different remodulation schemes. Eye diagrams of the detected upstream FMD-DPSK signal that is remodulated (b) on the DI's constructive port output (c) on part of the downstream RMD-DPSK signal. (d) Eye diagrams of the detected upstream FMD-OOK signal when using the conventional optical amplitude remodulation (downstream RMD-OOK, upstream FMD-OOK). The downstream modulation depth in Fig. 3 (c)-(e) is 0.4

performance (the solid-square in Fig. 3.17(a)).

3.2.3.2.Reduced phase variation by DI's constructive port

Using the DI's constructive port output as the upstream carrier not only avoids the power waste due to the relatively large insertion loss of the destructive port, it also

reduces the phase variation in the upstream carrier by half compared to that when part of the downstream RMD-DPSK signal is used as the upstream carrier. Assume that '0' and ' φ ' are the two symbols of the downstream RMD-DPSK signal, where $0 < \varphi < \pi$, depending on the downstream modulation depth. Each bit of the DI's constructive port output is the summation of two adjacent bits of the downstream RMD-DPSK signal. Thus, if both of the two adjacent bits have the same phase of '0' or ' φ ', their summation from the DI's constructive port will have a phase of '0' or ' φ ', respectively, and if the two adjacent bits have different phase symbols, their summation from the DI's constructive port will have a phase of ' $\varphi/2$ '. From aforementioned analysis, we can derive that there are three possible demodulated phase symbols in the DI's constructive port output, namely '0', ' φ ' and ' $\varphi/2$ '. Interestingly, in the DI's constructive port output the phase symbols of '0' and ' φ ' cannot be adjacent, as the demodulated '0' is from two consecutive '0' in the downstream RMD-DPSK signal, whereas the demodulated ' φ ' is from two consecutive ' φ '. When '0' is adjacent with ' φ ' in the downstream RMD-DPSK signal, a phase symbol of ' $\varphi/2$ ' will be generated in the DI's constructive port output. It means that in the DI's constructive port output, between the phase symbols of '0' and ' φ ' there is at least one phase symbol of ' $\varphi/2$ '. Thus, the maximum phase variation in the upstream carrier is reduced to $\varphi/2$, instead of φ , if using the demodulated signals from DI's constructive port, rather than part of the downstream RMD-OOK signal, as the upstream carrier. Thus, for the upstream FMD-DPSK signal, the reduced phase variation will result in smaller crosstalk from the residual downstream signal as shown in Fig. 3.17(a) (the open triangle and open square). Comparing Fig. 3.17(b) with Fig. 3.17(c), we find that the demodulated upstream FMD-DPSK signal has a wider eye opening when using the DI's constructive port output, instead of the downstream RMD-DPSK signal, as the upstream carrier. RZ-shaped phase modulation with RMD

can be used in downstream to further reduce the remodulation crosstalk [33].

The narrow spectrum from the constructive port of DI at ONU is markedly broadened after phase remodulation by the upstream data with FMD. Thus, the upstream FMD-DPSK can be properly demodulated by the DI's destructive port at OLT, with relatively low filtering loss. On the contrary, as the spectrum of RB towards the OLT consists of more low-frequency components, the RB noise is considerably rejected by the destructive port of the DI at OLT due to its notch filter-like wavelength response. As the downstream modulation depth increases, the spectrum of RB towards the OLT will become wider, thus less RB can be rejected by DI's destructive port. As reported in Fig. 3.16, when the downstream modulation depth increases, the insertion loss of the DI's destructive port for RB reduces. Fig. 3.18 (b)-(d) also show that the RB spectrum passing through the DI's destructive port increases for a larger downstream modulation depth. Thus, the proposed optical phase remodulation scheme is more robust to RB noise when the downstream modulation depth is smaller. One tradeoff in the proposed scheme is that the downstream RMD-DPSK signal is less robust to phase noise due to the reduced symbol distance. Whereas the nonlinear effect induced phase noise may be insignificant considering the relatively low bit rate and short transmission distance in access network, smaller phase noise in laser is necessary for the RMD-DPSK signal [34].

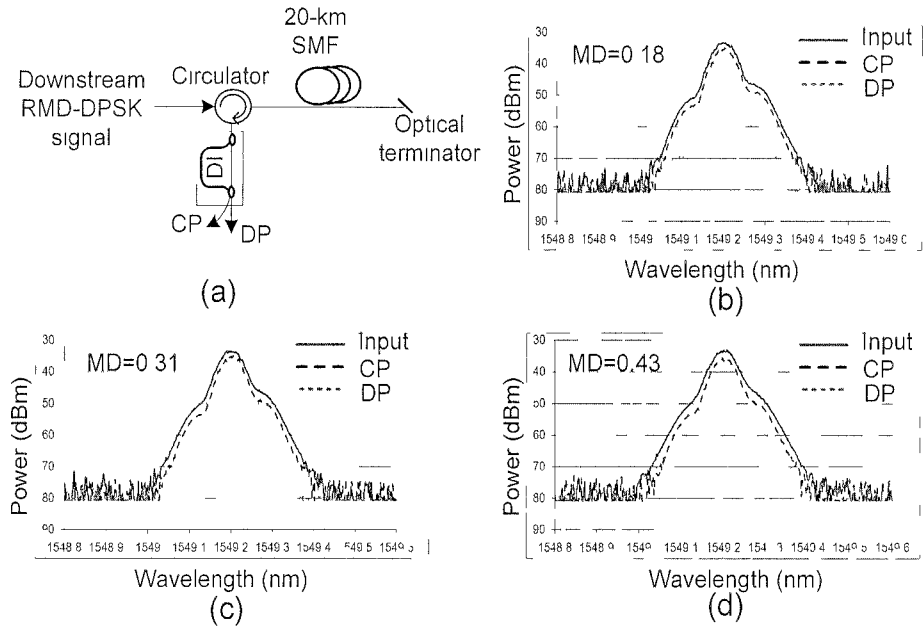


Fig. 3.18 (a) experimental setup used to investigate the effectiveness of DI's two output ports on RB suppression, CP: constructive port, DP: destructive port. (b)-(d), measured spectrum (resolution bandwidth=0.06 nm) of the RB before and after the DI when the downstream modulation depth (MD) is 0.18, 0.31 and 0.43, respectively.

3.2.4. Experimental demonstration

We have experimentally demonstrated the proposed remodulation scheme based on the architecture shown in Fig. 3.14. At the OLT, a CW light source at 1549.2 nm was fed into a PM driven by a 10-Gb/s $2^{31}-1$ PRBS with a modulation depth of 0.22. After power amplification and filtering by a 0.8-nm optical bandpass filter, a 6-dBm RMD-DPSK signal was coupled into a 20-km SMF. At the ONU, the destructive port of a DI with a relative delay of 94 ps was used for downstream RMD-DPSK signal detection. Signal from the constructive port (with 1.4-dB insertion loss) was fed into

another PM, driven by a 10-Gb/s $2^{31}-1$ PRBS with FMD as the upstream data, before being transmitted back to the OLT. At the OLT, the destructive port of another DI with 103-ps relative delay was used for upstream FMD-DPSK signal detection and RB noise suppression. Two DIs with different relative delays were used in the experiment due to component availability. To investigate the enhanced RB tolerance, first the effect from dispersion was isolated, by using a dispersion compensation module (DCM) to fully compensate the dispersion in the 20-km SMF. Fig. 3.19 depicts the eye diagrams of the detected downstream RMD-DPSK and upstream FMD-DPSK signals in both back-to-back (B2B) and transmission cases. The eye of the demodulated DPSK signal from the destructive port of the DI is wide-open, with a measured ER of ~ 9 dB. The eye of the upstream FMD-DPSK signal demodulated by the destructive port of the DI at OLT was also clearly open.

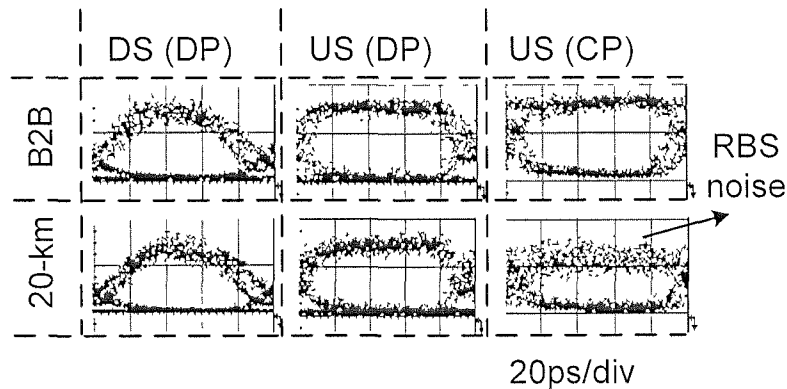


Fig. 3.19 Eye diagrams of the detected downstream RMD-DPSK and upstream FMD-DPSK signals in B2B and transmission cases. B2B: back-to-back, DS: downstream, US: upstream, DP: destructive port of the DI, CP: constructive port.

Although the two output ports of DI are generally equivalent in DPSK signal demodulation, as shown in Fig. 3.15 (c) and Fig. 3.15 (f), using the destructive port of DI to demodulate the upstream DPSK signal is essential to suppress the RB of the

downstream RMD-DPSK signal. As shown in Fig. 3.18 (b)-(d), the RB spectrum can hardly be suppressed by the constructive port of DI. For comparison, the eye of the upstream signal demodulated by the constructive port, which was severely degraded by the RB, was also shown in Fig. 3.19.

We then removed the DCM to investigate the proposed scheme without dispersion compensation. The bit-error-rate (BER) measurement results for both downstream and upstream signals are shown in Fig. 3.20(a). After transmission in 20-km SMF without dispersion compensation, the receiver sensitivity at $\text{BER}=10^{-9}$ for the downstream RMD-DPSK signal is -17.9 dBm, while that for the upstream FMD-DPSK signal is -14.2 dBm. After transmission in 20-km SMF with DCM, less than 0.3-dB power penalty is observed for both downstream RMD-DPSK and upstream FMD-DPSK signals, demonstrating the robustness of the proposed scheme to the RB noise. Without DCM after transmission in 20-km SMF, ~ 4 -dB power penalty, mainly due to dispersion, is observed for the upstream FMD-DPSK signal.

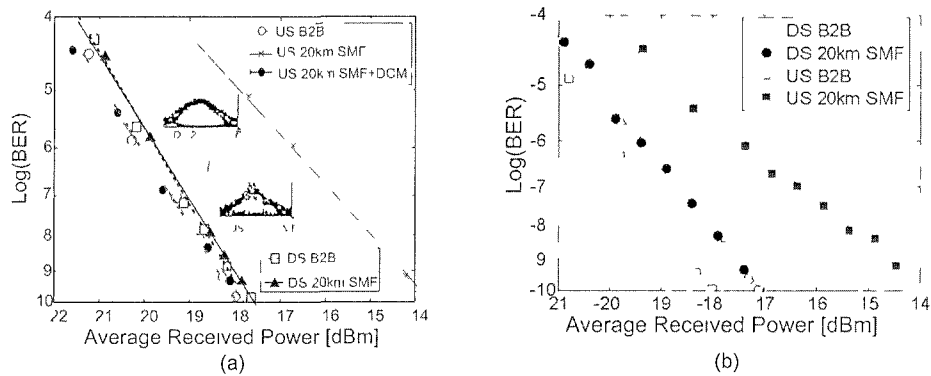


Fig. 3.20 (a) BER measurement results when the downstream modulation depth is 0.22. (b) BER measurement results when the downstream modulation depth is

0.18 and a SOA is used at ONU DS: downstream, US: upstream

Negligible power penalty is observed for the downstream RMD-DPSK signal, thanks to its narrow spectral width. To investigate the power penalty of the downstream RMD-DPSK signal induced by the RMD, we also measured the downstream BER performance when FMD-DPSK signal was used in downstream. In the B2B case, compared with the FMD-DPSK signal, the RMD induces a power penalty of around 2.1 dB instead of a slightly negative power penalty in simulation as reported in Fig. 3.17(a), due to the limited ER of the downstream DI. After 20-km SMF transmission, the sensitivity difference between the RMD-DPSK and FMD-DPSK signal is reduced from 2.1 dB to 1 dB, as the RMD-DPSK signal is more robust to dispersion than the FMD-DPSK signal. Note that the receiver sensitivity will be degraded by more than 9 dB when the modulation depth of the downstream OOK signal is reduced from 1 to 0.22 in the conventional optical amplitude remodulation scheme as shown in Fig. 3.17(a).

In practical implementation, a semiconductor optical amplifier (SOA) can be placed at ONU to improve the system power budget for longer reach. We then experimentally demonstrated the proposed remodulation scheme with a SOA before the DI at ONU. By employing a SOA at ONU to achieve better power budget, the downstream modulation depth could be smaller. The modulation depth of the downstream RMD-DPSK signal was reduced from previous 0.22 to 0.18. A 100-GHz AWG with 4-dB insertion loss and a 3-dB bandwidth of 0.35 nm was used at the OLT. Another AWG with the same specification was used at the RN. The input power to the 20-km SMF was 5 dBm. The received power at the ONU was \sim -3.5 dBm, which was amplified to 2dBm by a SOA, before being fed in to the DI at ONU. The BER measurement results for both downstream and upstream signals are shown in Fig. 3.20(b). After transmission in 20-km SMF without DCM, \sim 3.9-dB power penalty,

mainly due to dispersion, is observed for the upstream FMD-DPSK signal, and negligible power penalty is observed for the downstream RMD-DPSK signal.

3.3. Summary

In this chapter, we confirm that Rayleigh noise can be effectively suppressed in optical domain by leveraging on the notch-filter property of DI's destructive port. To the best of our knowledge, this is the first time that DI's destructive port is proposed to be used as a Rayleigh-noise suppressor.

In the first section, we provide an insight into different design issues for Rayleigh noise mitigation in carrier-distributed WDM-PON. For the first time, we clarify that two types of RB are not comparable in impairing the upstream signal, with carrier RB being the dominant contribution to Rayleigh noise entering the upstream receiver module, within a reach up to 60 km. Then we propose a simple scheme, via in-band optical filtering, to effectively suppress carrier RB in the carrier-distributed WDM-PON, with a demonstrated 19-dB improvement in the tolerance to carrier RB. Error-free transmission of 10-Gb/s upstream signal over 60-km SMF is achieved with less than 2.5-dB power penalty induced by residual Rayleigh noise. The relation between system margin and ONU gain is also comprehensively studied. The theoretical models built in this section predict well the system performance and are expected to serve as a design tool for optimizing the overall performance of a WDM-PON.

In the second section, we apply the technique to a remodulation-based WDM-PON with colorless ONU. We have proposed and experimentally

demonstrated a WDM-PON with single feeder fiber by using downstream RMD-DPSK and upstream FMD-DPSK. Error-free operation of both down- and up-stream signals, at 10-Gb/s/channel, is achieved after the transmission of 20-km SMF without dispersion compensation. The power penalty of the downstream RMD-DPSK signal induced by the modulation depth reduction is effectively reduced compared with the conventional optical amplitude remodulation scheme. The proposed optical phase remodulation scheme is also robust to RB noise, thus bidirectional transmission at the same carrier wavelength over single fiber is achieved with significant simplification in transmission components and reduction in system cost.

The upstream DI in this chapter can also be replaced by a silicon ring resonator to facilitate photonic integration, i.e. integrated OLT module. As discussed in Chapter 2, if a partial-bit DI instead of a one-bit DI is used as the DPSK demodulator, the demodulated signal from the destructive port will be RZ-shaped. The RZ-shaped signal has larger peak power and thus can potentially be more robust to signal RB that is evenly distributed over time. To further increase the reach of WDM, larger ONU gain and hence signal-RB suppression (which are not achieved yet in the proposed schemes) are necessary. In this case the one-bit DI can be replaced by a partial-bit DI at OLT. However, the tradeoff is that the partial-bit DI will induce larger insertion loss for upstream signal and the RZ-shaped signal is less robust to dispersion.

References

- [1] N. J. Frigo, P. P. Iannone, P. D. Magill, T. E. Darcie, M. M. Downs, B. N. Desai, U.

- Koren, T. L. Koch, C. Dragone, H. M. Presby, and G. E. Bodeep, "A wavelength-division multiplexed passive optical network with cost-shared components," *IEEE Photon. Technol. Lett.*, vol. 6, no. 11, pp. 1365–1367, Nov. 1994.
- [2] M. Feuer, M. Thomas, and L. Lunardi, "Backreflection and loss in single-fiber loopback networks," *IEEE Photon. Technol. Lett.*, vol. 12, no. 8, pp. 1106–1108, Aug. 2000.
- [3] T. H. Wood, R. A. Linke, B. L. Kasper, and E. C. Carr, "Observation of coherent Rayleigh noise in single-source bidirectional optical fiber systems," *J. Lightw. Technol.*, vol. 6, no. 2, pp. 346–352, Feb. 1988.
- [4] P. T. Legg, M. Tur, and I. Andonovic, "Solution paths to limit interferometric noise induced performance degradation in ASK/direct detection lightwave networks," *J. Lightw. Technol.*, vol. 14, no. 9, pp. 1943–1953, Sep. 1996.
- [5] P. J. Urban, H. De Waardt, E. Ciaramella, and A. M. J. Koonen, "Reduction of the Influence of Optical Interferometric Crosstalk Noise in a WDM-PON System with a Reflective Semiconductor Optical Amplifier: An Overview," in *Proc. ICTON*, 2010, paper Tu.B1.4.
- [6] T. Monroy, E. Tangdiongga, R. Jonker, and H. de Waardt, "Interferometric crosstalk reduction by phase scrambling," *J. Lightw. Technol.*, vol. 18, no. 5, pp. 637–646, May 2000.
- [7] M. Feuer, M. Thomas, and L. Lunardi, "Backreflection and loss in singlefiber loopback networks," *IEEE Photon. Technol. Lett.*, vol. 12, no. 8, pp. 1106–1108, Aug. 2000.
- [8] Chiuchiarelli, M. Presi, R. Proietti, G. Contestabile, P. Choudhury, L. Giorgi, and E. Ciaramella, "Enhancing resilience to Rayleigh crosstalk by means of line coding and electrical filtering," *IEEE Photon. Technol. Lett.*, vol. 22, no. 2, pp.

85–87, Jan. 15, 2010.

- [9] D. Jorgesen, C. F. Marki, and S. Esener, “Improved high pass filtering for passive optical networks,” *IEEE Photon. Technol. Lett.*, vol. 22, no. 8, pp. 1144–1146, Aug. 2010.
- [10] J. Prat, “Rayleigh Back-scattering reduction by means of Quantized Feedback Equalization in WDM-PONs,” in *Proc. ECOC*, 2010, paper Th.10.B.3.
- [11] P. J. Urban, A. M. J. Koonen, G. D. Khoe, and H. de Waardt, “Interferometric crosstalk reduction in an RSOA-based WDM passive optical network,” *J. Lightw. Technol.*, vol. 27, no. 11, pp. 4943–4953, Nov. 2009.
- [12] T. Yoshida, S. Kimura, H. Kimura, K. Kumozaki, and T. Imai, “A new single-fiber 10-Gb/s optical loopback method using phase modulation for WDM optical access networks,” *J. Lightw. Technol.* Vol. 24, no. 2, pp. 786–796, Feb. 2006.
- [13] C. W. Chow, G. Talli, and P. D. Townsend, “Rayleigh noise reduction in 10-Gb/s DWDM-PONs by wavelength detuning and phase-modulation-induced spectral broadening,” *IEEE Photon. Technol. Lett.*, vol. 19, no. 6, pp. 423–425, Mar. 2007.
- [14] Akanbi et al., “A new scheme for bidirectional WDM-PON using upstream and downstream channels generated by optical carrier suppression and separation technique,” *IEEE Photon. Technol. Lett.*, vol. 8, pp. 340–342, 2006.
- [15] W. Chow, G. Talli, A. D. Ellis, and P. D. Townsend, “Rayleigh noise mitigation in DWDM LR-PONs using carrier suppressed subcarrier- amplitude modulated phase shift keying,” *Opt. Exp.*, vol. 16, no. 3, pp. 1860–1866, Feb. 2008.
- [16] J. Xu, L. K. Chen, C. K. Chan, “Phase-Modulation-Based Loopback Scheme for Rayleigh Noise Suppression in 10-Gb/s Carrier-Distributed WDM-PONs,” *IEEE Photon. Technol. Lett.*, vol. 22, no. 18, pp. 1343–1345, Sep. 2010.
- [17] Peter J. Winzer and Renè-Jean Essiambre, “Advanced Modulation Formats for High-Capacity Optical Transport Networks,” *J. Lightw. Technol.*, vol. 24, no. 12,

pp. 4711-4728, Dec. 2006.

- [18] X. Liu, A. H. Gnauck, X. Wei, J. Y. C. Hsieh, and V. Chien, "Athermal optical demodulator for OC-768 DPSK and RZ-DPSK signals," *IEEE Photon. Technol. Lett.*, vol. 17, no. 12, pp. 2610-2612, Dec. 2005.
- [19] Y. Miyamoto, H. Masuda, A. Hirano, S. Kuwahara, Y. Kisaka, H. Kawakami, M. Tomizawa, Y. Tada, and S. Aozasa, "S-band WDM coherent transmission of 40 x 43-Gbit/s CS-RZ DPSK signals over 400 km DSF using hybrid GS-TDFAs/Raman amplifiers," *Electron. Lett.* 39, 1569-1570 (2002).
- [20] M. Fujiwara, J. Kani, H. Suzuki, and K. Iwatsuki, "Impact of backreflection on upstream transmission in WDM single-fiber loopback access networks," *J. Lightw. Technol.*, vol. 24, no. 2, pp. 740-746, Feb. 2006.
- [21] Cho, K. Y., Y. J. Lee, H. Y. Choi, A. Murakami, A. Agata, Y. Takushima, and Y. C. Chung, "Effects of Reflection in RSOA-based WDM PON utilizing remodulation technique," *J. Lightw. Technol.*, Vol. 27, no. 10, May 2009.
- [22] P. Gysel and R.K. Staubli, "Statistical Properties of Rayleigh Backscattering in Single-Mode Fibers," *J. Lightwave Technol.*, Vol. 8, no. 4, pp. 561-567, Apr. 1990.
- [23] S. K. Liaw, S. L. Tzeng and Y. J. Hung, "Rayleigh backscattering induced power penalty on bidirectional wavelength-reuse fiber systems," *Opt. Commun.*, Vol. 188, no. 1-4, pp. 63-67, Feb. 2001.
- [24] G. Keiser, *Optical Fiber Communications*, 3rd ed. New York: McGraw-Hill, 2000.
- [25] F. Y. Gardes, K. L. Tsakmakidis, D. Thomson, G. T. Reed, G. Z. Mashanovich, and O. Hess, "Micrometer size polarization independent depletion-type photonic modulator in Silicon On Insulator," *Opt. Exp.*, vol. 15, no. 9, pp. 5879- 5884, Apr. 2007.
- [26] J. Zhang, T. Y. Liow, G. Q. Lo, and D. L. Kwong, "10Gbps monolithic silicon

- FTTH transceiver without laser diode for a new PON configuration,” *Opt. Express* 18(5), 5135–5141 (2010).
- [27] S. P. Jung, Y. Takushima, and Y. C. Chung, “Transmission of 1.25-Gb/s PSK signal generated by using RSOA in 110-km coherent WDM PON,” *Opt. Express* 18, 14871–14877 (2010).
- [28] D. Derickson, *Fiber Optic Test and Measurement*. Englewood Cliffs, NJ: Prentice-Hall, 1998.
- [29] J. Prat et al., “Full-Duplex Single Fiber Transmission Using FSK Downstream and IM Remote Upstream Modulations for Fiber-to-the-Home,” *IEEE Photon. Technol. Lett.* 17, 702-704 (2005).
- [30] A. Chowdhury et al., “Rayleigh Backscattering Noise-Eliminated 115-km Long-Reach Bidirectional Centralized WDM-PON With 10-Gb/s DPSK Downstream and Remodulated 2.5-Gb/s OCS-SCM Upstream Signal,” *IEEE Photon. Technol. Lett.* 20, 2081-2083 (2008).
- [31] J. Xu, L.K. Chen, “Optical Phase Remodulation for 10-Gb/s WDM-PON with Enhanced Tolerance to Rayleigh Noise,” *IEEE/OSA Optical Fiber Communication Conference / National Fiber Optic Engineers Conference, OFC/NFOEC 2010*, Paper OThG3, San Diego, California, USA, 2010.
- [32] X. F. Cheng, Y. K. Yeo, Z. W. Xu, Y. X. Wang, “A Novel Hybrid WDM/TDM-PON using Downlink DPSK and Uplink Remodulated OOK Signals Based on a Shared DI,” *ECOC 2009*, 20-24 September, 2009, Vienna, Austria.
- [33] J. Xu, L.K. Chen, C.K. Chan, “High Extinction Ratio Phase Re-modulation for 10-Gb/s WDM-PON with Enhanced Tolerance to Rayleigh Noise,” *International Conference on Optical Internet, COIN 2010*, Paper P1061, Korea, Jeju, Jul. 2010.
- [34] Y. Atzmon, M. Nazarathy, “Laser phase noise in coherent and differential optical transmission revisited in the polar domain,” *J. Lightw. Technol.*, vol. 27, no. 1, pp.

19–29, Jan. 2009.

Chapter 4 Rayleigh Noise

Suppression in Electrical Domain

4.1. Offset Manchester coding for Rayleigh noise

suppression in carrier-distributed WDM-PONs

4.1.1. Introduction

In the last chapter, we have demonstrated that the intrinsic Rayleigh noise in CLS-based WDM-PON can be effectively suppressed in optical domain. Recently, the electrical high-pass filter (HPF) based approach also attracts some research attention [1]-[3]. In this approach only 8B10B coding or electronic equalization is required, thus resulting in only minor modifications to the PON structure.

In this part, we propose an offset-Manchester coding (OMC) to suppress Rayleigh noise more effectively in the carrier-distributed WDM-PON and to simultaneously realize upstream differential detection, via a postdetection HPF. Compared with prior schemes using 8B10B coding or electronic equalization [1, 2], albeit Manchester coding requires larger bandwidth it enables much easier clock extraction. The unique self-clocking property of Manchester coding together with differential detection enables burst-mode upstream detection [9], which is desirable in hybrid WDM/TDM-PONs. Although 8B10B coding has been widely used in industry,

the Manchester encoder, an exclusive OR (XOR) gate, is simpler than the 8B10B encoder. Unlike the 8B10B coding, no decoder is needed at the receiver side for Manchester signal. In addition, by further using OMC that is generated by offsetting data and clock signal before the XOR gate, the cutoff frequency of the HPF used to remove Rayleigh noise can be much higher than that using 8B10B coding or electronic equalization [1], [4], leading to more effective Rayleigh noise suppression and much relaxed requirement for the seed laser linewidth. The proposed scheme is also simpler than the prior scheme employing differential Manchester coding and self-homodyne coherent detection [5].

4.1.2. System architecture and operation principle

Fig. 4.1 illustrates the proposed loopback architecture. After the transmission in a 50-km standard SMF, the optical carriers from the OLT are wavelength routed toward different ONUs, by an AWG at the RN. At the ONU, the CW light is modulated by a reflective modulator driven by upstream data with OMC, before being sent back to the OLT. The received upstream signals are pre-amplified by a shared EDFA before direct detection. A postdetection HPF is used to suppress Rayleigh noise and to simultaneously realize upstream differential detection.

For the signal with conventional Manchester coding (MC), the low frequency components are significantly suppressed. Thus the MC-signal can pass through a properly designed HPF without compromising the signal quality. To further reduce low frequency components, we propose an OMC by temporally offsetting the data and

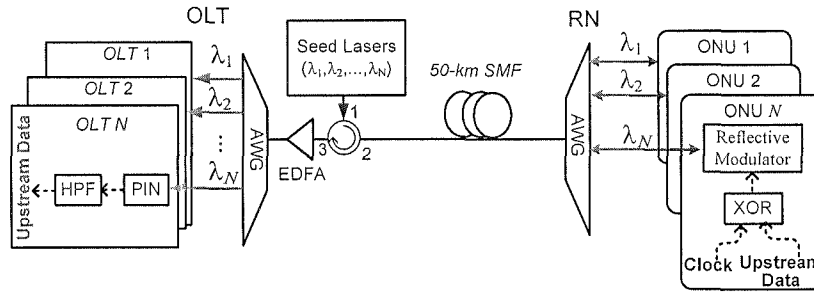


Fig. 4.1 Proposed loopback architecture using Manchester coding and postdetection electrical high-pass filter in upstream to suppress Rayleigh noise.

The downstream channels are omitted here for simplicity.

clock signal properly before the XOR gate. Thus for the OMC-signal, the cutoff frequency of the HPF can be higher. Note that in the previous schemes using 8B10B coding (bit rate: 1.25 Gb/s) or electronic equalization (bit rate: 2.5 Gb/s), the cutoff frequency of the HPF is as low as 10 MHz [1, 2], whereas in this paper the cutoff frequency of the HPF is substantially increased to 164 MHz. The HPF also serves as a simple passive differentiator for the differential detection of the upstream Manchester encoded signal [6], with a fixed optimal threshold at zero level that is highly desirable for burst-mode detection. As the optical spectra of both the RB and the upstream OMC-signal have strong low-frequency components, after detection the beating noise mainly distributes at the low frequency region and can be substantially suppressed by an electrical HPF. The 3-dB spectral width of the beating noise is roughly the double of the linewidth of the seed laser [2]. Thanks to the much higher cutoff frequency of the HPF in the proposed scheme, more beating noise can be removed. In addition, less expensive seed lasers with a relatively wider linewidth can be used.

4.1.3. Experimental demonstration

We first investigated the upstream power penalty as a function of signal-to-crosstalk ratio (SCR) based on the experimental setup in Fig. 4.2, which is similar to that employed in [6]. CW light at 1553.5 nm from a tunable laser diode (TLD) was split into two paths by a 3-dB coupler. In the upper path, Manchester data were first generated by the logic XOR operation of a non-return-to-zero (NRZ) 2.5-Gb/s 2^{31} -1 PRBS and a 2.5-GHz clock via a commercial XOR chip, and then used to drive a Mach–Zehnder modulator (MZM). The MC-signal was generated when the NRZ PRBS and the clock signal were well aligned, whereas the OMC-signal was generated when the NRZ PRBS and the clock signal were temporally offset by 74 ps. Following the MZM, a variable optical attenuator (VOA) was used to adjust the signal power to obtain different SCR values. In the lower path, the crosstalk signal was the RB light from a 50-km SMF, with a fixed power of -33.4 dBm measured after a polarization controller (PC). The PC was used to maximize the beating noise. The Manchester encoded signal and the crosstalk signal were then combined by a 3-dB coupler and fed into the upstream receiver, which consisted of an EDFA, a 100-GHz AWG (3-dB bandwidth=0.6 nm, insertion loss = 4 dB), and a p-i-n receiver, followed by an

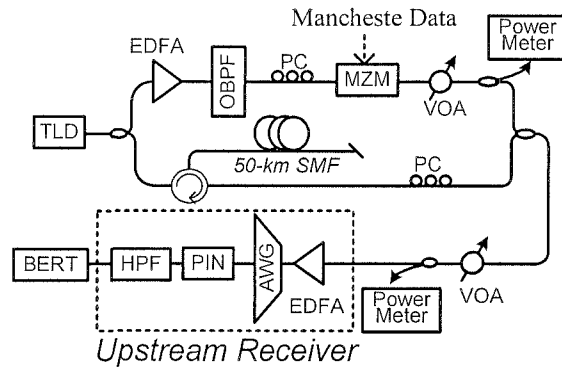


Fig. 4.2 Experimental setup to investigate the Rayleigh-noise tolerance.

electrical HPF with a 3-dB lower cutoff frequency of 164 MHz and a 1-dB upper cutoff frequency of 3 GHz. For comparison, the crosstalk tolerance of the NRZ signal was also investigated. In this case, the MZM was directly driven by the same NRZ 2.5-Gb/s $2^{31}-1$ PRBS and the HPF was removed from the upstream receiver. Without removing the HPF, the detected eye diagram of the NRZ signal was completely closed due to baseline wandering.

Three conclusions can be derived from Fig. 4.3, which depicts the eye diagrams at different SCR levels. First, the OMC-signal always has a wider eye opening than the MC-signal, as it has fewer low frequency components and is more robust to high pass filtering. Second, both the OMC-signal and the MC-signal are more resistant to the Rayleigh noise than the NRZ signal, as the majority of beating noise is suppressed by the HPF. Thirdly, in contrast to the NRZ signal for which the optimal threshold level decreases as the SCR decreases, the optimal threshold level of the Manchester signals is always fixed at zero level as the SCR decreases. The reason is that differential detection of the Manchester signal is simultaneously realized via the HPF that is used to suppress the beating noise.

The measured upstream power penalty ($\text{BER}=10^{-9}$) at different SCR levels is shown in Fig. 4.4. In all BER measurements, the decision threshold level was fixed at zero level, which was an optimal threshold for all the three signals when there was no crosstalk. For a 2-dB power penalty at 2.5 Gb/s, by using OMC or MC the SCR can be reduced by 7 dB than using NRZ PRBS. Note that in the prior scheme using 8B10B coding [6], the SCR value for a 2-dB power penalty can only be reduced by 5 dB than using NRZ PRBS at 1.25 Gb/s.

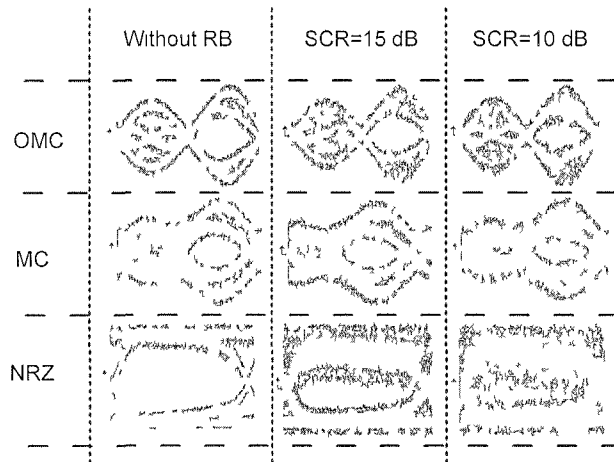


Fig. 4.3 Eye diagrams of the OMC-signal, the MC-signal and the NRZ signal at 2.5-Gb/s with different SCR values. Time scale: 100ps/div

We then experimentally demonstrated the proposed loopback scheme based on the architecture shown in Fig. 4.1. At the OLT, CW light at 1553.5 nm from a TLD with a power of 3 dBm was fed into a span of 50-km SMF through a circulator (from port 1 to port 2). An AWG (4-dB insertion loss) with a channel spacing of 0.8 nm and a 3-dB bandwidth of 0.6 nm was used at the RN. The input CW power to the ONU was -11.5 dBm. At the ONU, the reflective modulator consisted of a circulator, an EDFA and a Mach-Zehnder modulator (MZM). In practical implementation, the reflective modulator could be a reflective semiconductor optical amplifier (RSOA) or an effective electro absorption modulator integrated with a SOA [8]. The upstream receiver here was the same as in Fig. 4.2, and was connected to the port 3 of the circulator at OLT.

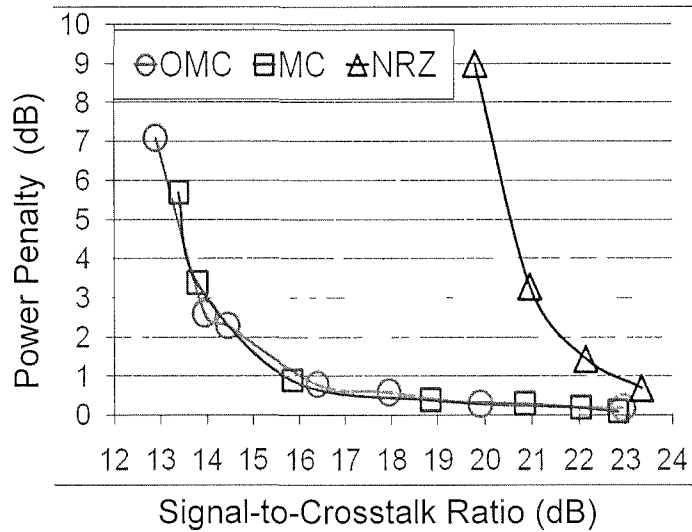


Fig. 4.4 The upstream power penalty (BER=10⁻⁹) as a function of SCR.

The BER measurement results are shown in Fig. 4.5. The ONU gain, defined as the power ratio between the output and the input signals at ONU, was fixed at 11.8 dB for all BER measurements shown in Fig. 4.5. We first investigated the dispersion tolerance of the upstream signals. Compared with the back-to-back cases, after transmission in 50-km dual feeder fibers (SMF), less than 0.6-dB dispersion-induced power penalty (at BER=10⁻⁹) is observed for both the OMC-signal and the MC-signal. Compared with dual-fiber transmission, around 4-dB power penalty is observed for both signals when single feeder fiber is used, due to residual Rayleigh noise. We also obtained that the Rayleigh noise induced power penalty could be further reduced to around 1 dB, when the ONU gain was increased to 15.6 dB. The receiver sensitivity of the OMC-signal is improved by around 2 dB compared with that of the MC-signal as shown in Fig. 4.5.

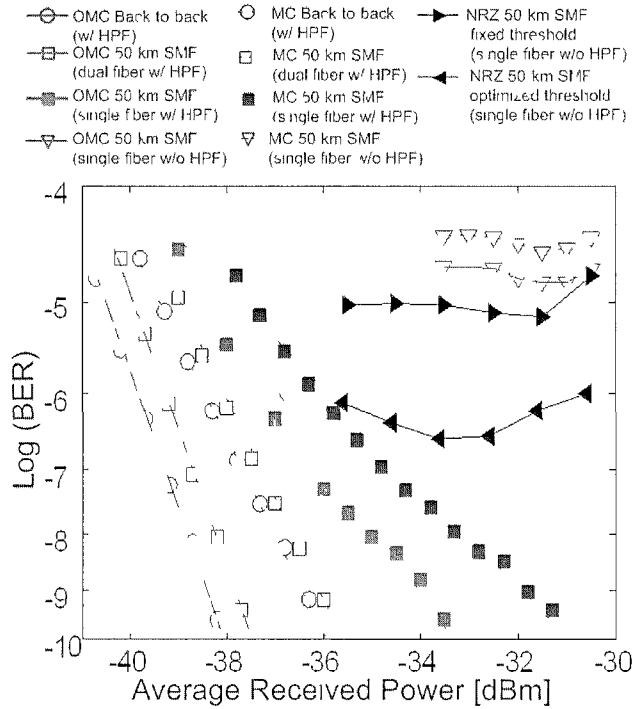


Fig. 4.5 BER measurement results.

Without the HPF, both signals show an error floor between 10^{-4} ~ 10^{-5} . Similarly, for NRZ signal, error floors at $\sim 10^{-5}$ and $\sim 10^{-7}$ are observed for the fixed and the optimized decision thresholds, respectively. In all BER measurements for both the OMC-signal and the MC-signal, the decision threshold level was always fixed at zero level, without dynamic threshold optimization. Note that dynamic threshold optimization is challenging in practical implementation.

If the conventional NRZ signal is used in the upstream, the upstream receiver sensitivity will be degraded when the ONU gain is larger than 12.5 dB [7]. We also investigated the impact of ONU gain on the upstream receiver sensitivity in the proposed scheme. The measurement result is shown in Fig. 4.6. It is worthwhile to note that no degradation in the upstream receiver sensitivity is observed for an ONU gain up to ~ 16 dB, implying that the proposed scheme is also robust to signal RB as first reported in [9].

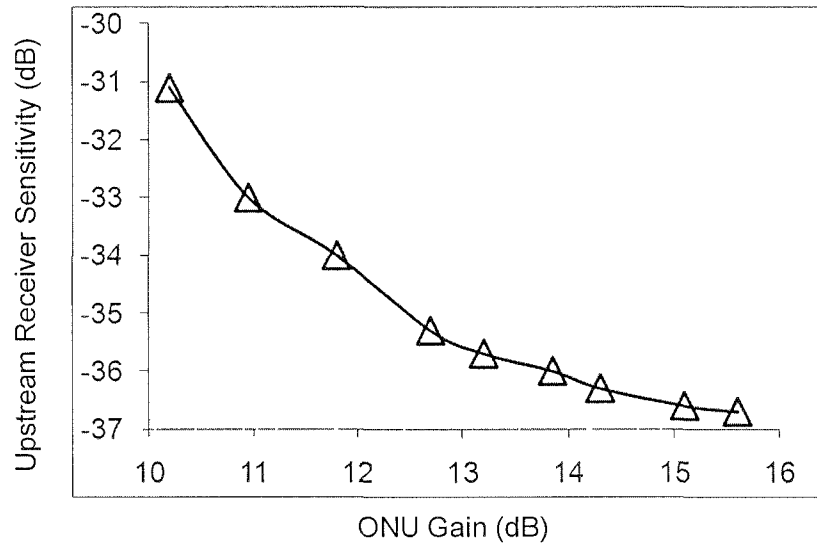


Fig. 4.6 The impact of ONU gain on the upstream receiver sensitivity (at BER= 10^{-9}).

4.2. A novel chirp-free optical Manchester signal

transmitter

4.2.1. Introduction

Manchester coding, in which the original symbols are encoded by the transition directions (“rise” or “fall”) at the center of each bit, enables easy clock extraction at the expense of bandwidth doubling. It has been widely used in copper-based Ethernet 10BASE-T. The unique self-clocking property together with differential detection also makes Manchester coding a promising candidate for high-speed optical burst mode transmission links [8], [9]. In addition, as the Manchester code has negligible low-frequency spectral components, it can also be used in optical access network to reduce the re-modulation crosstalk [12], and to suppress Rayleigh noise as discussed in last section.

Manchester coding can be realized in electrical domain via an exclusive OR (XOR) gate or a multiplying mixer. The obtained electrical Manchester signal can be used to drive an electro-optical modulator, operating in the linear transfer region, to generate the optical Manchester signal. However, the modulator requires a driver amplifier with a bandwidth twice as large as that for the NRZ signal generation at the same bit rate. A dual parallel Mach-Zehnder modulator (MZM) has been used to realize Manchester coding directly in optical domain, eliminating high-speed electronic processing at the expense of more complicated modulator structure [13]. A more elegant approach has been proposed by using a single dual-drive MZM to implement high-speed Manchester coding directly in optical domain [14]. However, as the two driving signals (data signal and clock, respectively) are not complementary, the generated optical Manchester signal cannot be chirp-free and is thus vulnerable to chromatic dispersion during transmission, especially in the differential detection case.

In this section, we propose a novel chirp-free optical Manchester signal transmitter that consists of a conventional chirp-free single-drive MZM together with a passive electronic power combiner. The driving signal is obtained simply by adding the original NRZ data and the synchronized clock signal via the power combiner. The chirp-free optical Manchester signal can be generated by leveraging on the inherent sinusoidal transfer curve of a MZM. As integrated MZMs have been demonstrated for using at ONU [15], the proposed scheme has potential application in broadband (i.e. above 10Gb/s) Rayleigh noise-resilient WDM-PON by taking advantage of the technique discussed in last section.

4.2.2. Operation principle

Fig. 4.7(a) illustrates the proposed optical Manchester signal transmitter. The combination of the original raised-cosine shaped NRZ data and the synchronized clock signal is used as the driving signal as shown in Fig. 4.8. The marks in the original NRZ data plus the clock signal result in the mark-level oscillation between $\sim V_\pi$ and $\sim 2V_\pi$ in the combined signal, while the spaces in the NRZ data plus the clock signal result in the space-level oscillation between around 0 and V_π in the combined signal. Within a bit period T , the mark-level oscillation will experience the swing from the peak voltage $\sim 2V_\pi$ to the valley voltage $\sim V_\pi$, corresponding to a “fall” transition at the center of a bit in the MZM output; similarly, the space-level oscillation will experience the swing

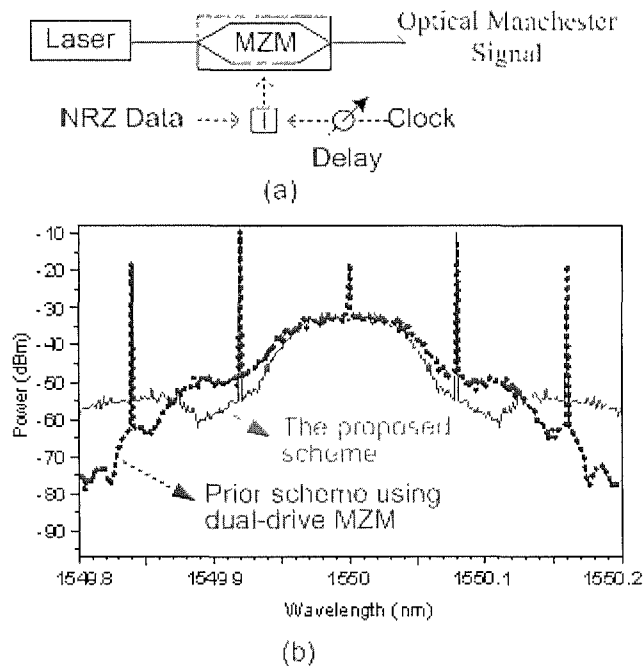


Fig. 4.7 (a) Proposed optical Manchester signal transmitter. (b) simulated spectrum of the optical Manchester signal.

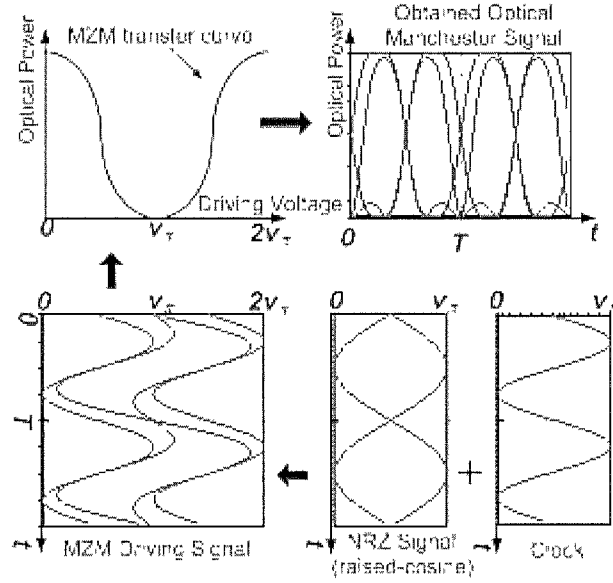


Fig. 4.8. Operation principle of the proposed optical Manchester signal transmitter.

from the peak voltage $\sim V_\pi$ to the valley voltage ~ 0 , corresponding to a “rise” transition at the center of a bit in the MZM output. Thus, the original NRZ data are now encoded by the transition directions (“rise” or “fall”) at the center of each bit in the MZM output, realizing the Manchester coding directly in optical domain. The simulated spectrum of the optical Manchester signal is shown by the solid line in Fig. 4.7(b). For comparison, we also show the simulated spectrum of the optical Manchester signal, generated by a dual-drive MZM [14], as the dashed line in Fig. 4.7(b). The dashed spectrum is wider due to the inherent chirp in the scheme using a dual-drive MZM.

4.2.3. Experimental demonstration

We have experimentally demonstrated the proposed optical Manchester signal transmitter based on the setup shown in Fig. 4.7(a). CW light at 1550 nm was fed into a MZM driven by the combination of a 5-Gb/s $2^{31}-1$ PRBS and a 5-Gb/s sinusoidal

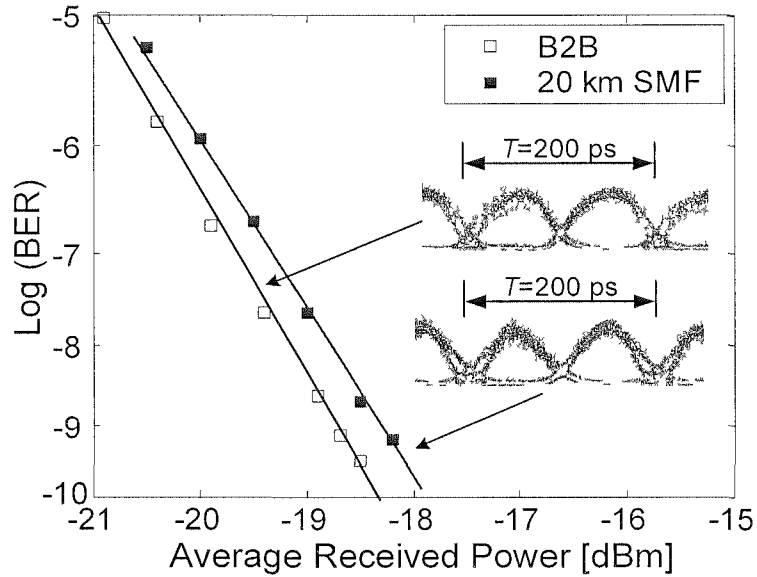


Fig. 4.9: BER measurements. Inset: eye diagram of the detected optical Manchester signal by a 10-Gb/s p-i-n receiver.

clock signal. It is worth mentioning that the bandwidth of the driving signal generated by a passive power combiner is reduced by half [16], [17], compared with that of the driving signal generated by an XOR gate or a multiplying mixer. Thus, the bandwidth of the MZM and driving circuit is also reduced in the proposed scheme. To compare the dispersion tolerance between the proposed scheme and the prior scheme using dual-drive MZM [14], the obtained optical Manchester signal from the MZM output was transmitted through a span of 20-km standard SMF with a dispersion coefficient of 17 ps/nm/km, before being detected by a 10-Gb/s p-i-n receiver. The BER measurement results are shown in Fig. 4.9. Compared with the BER curve of the B2B Manchester signal, around 0.4-dB power penalty at BER of 10^{-9} is observed after 20-km transmission in SMF. It should be noted that for the 5-Gb/s Manchester signal generated by a dual-drive MZM, the reported power penalty is 1.5 dB after 20-km transmission in SMF [12]

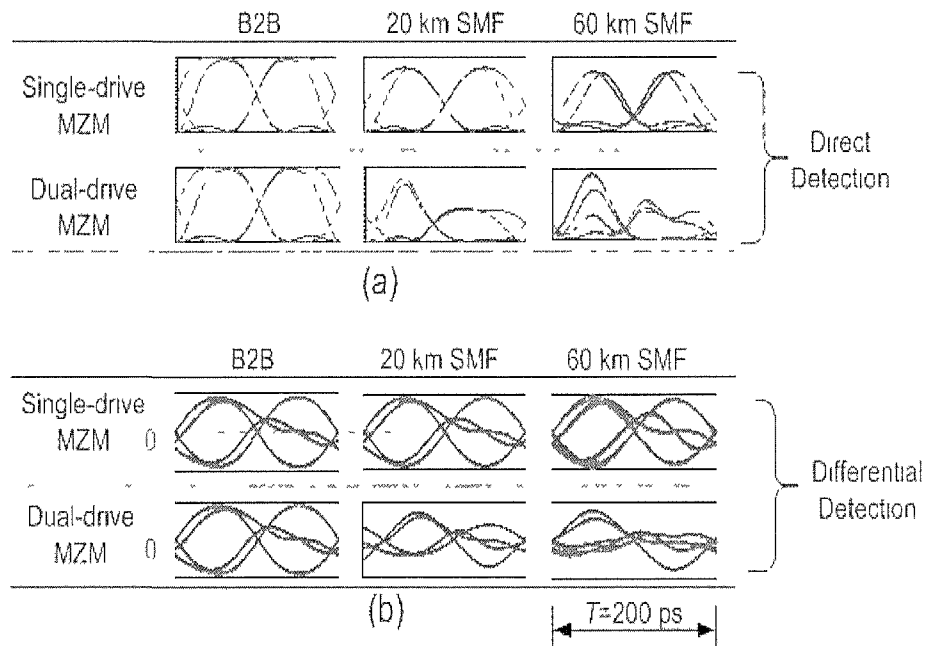


Fig. 4.10 Dispersion tolerance comparison between the proposed scheme and the prior scheme using dual-drive MZM, (a) direct detection, (b) differential detection [14].

4.2.4. Enhanced dispersion tolerance

The dispersion tolerance of both schemes was also investigated through simulation, as show in Fig. 4.10. The proposed scheme is more robust to dispersion than the scheme using a dual-drive MZM, for both direct detection and differential detection cases. As the dispersion accumulates, the optimal decision threshold always rests on the “0” level for the proposed scheme using differential detection as show in Fig. 4.10(b). In contrast, for the scheme using a dual-drive MZM, the optimal decision threshold in differential detection drifts away quickly as the dispersion accumulates.

We then investigated the dispersion tolerance in both schemes when the bit rate was increased from 5 Gb/s to 10 Gb/s through simulation, as show in Fig. 4.11 and Fig.

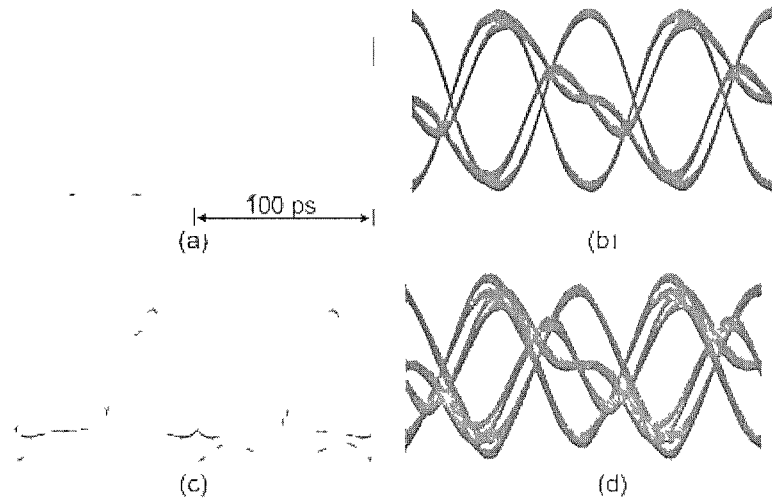


Fig. 4.11 Eye diagrams of the detected 10-Gb/s optical Manchester signal generated by the proposed scheme, (a) back to back, direct detection; (b) back to back, differential detection; (c) after the transmission in 20-km SMF, direct detection; (d) after the transmission in 20-km SMF, differential detection;

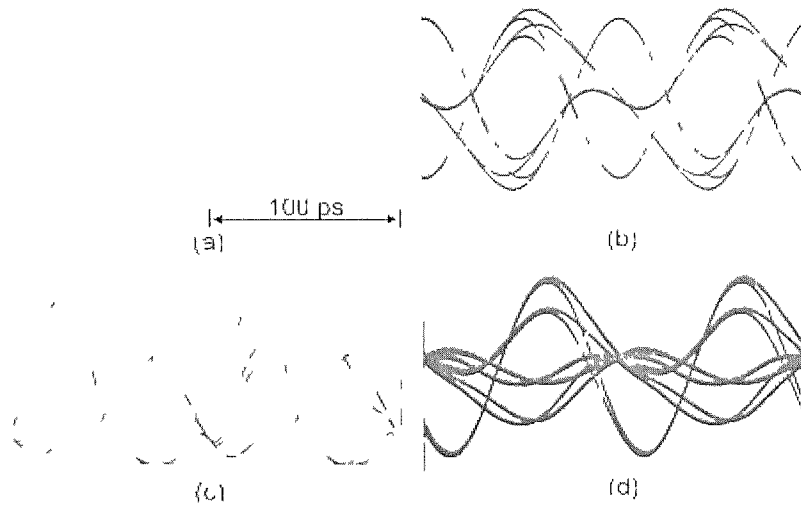


Fig. 4.12: Eye diagrams of the detected 10-Gb/s optical Manchester signal generated by the prior dual-drive MZM based scheme, (a) back to back, direct detection; (b) back to back, differential detection; (c) after the transmission in 20-km SMF, direct detection; (d) after the transmission in 20-km SMF, differential detection;

4.12, respectively. Similarly, the proposed scheme is proved to be more robust to dispersion than the scheme using a dual-drive MZM, in both direct detection and differential detection cases.

4.3. Summary

In this chapter, we propose a novel offset Manchester coding to simultaneously achieve Rayleigh noise suppression and upstream differential detection for WDM-PONs. Error-free transmission of 2.5-Gb/s upstream signals in 50-km SMF is demonstrated, with a 7-dB enhanced tolerance to Rayleigh noise. The transmission distance can be further increased using a higher ONU gain. The unique self-clocking property of Manchester coding together with differential detection facilitates new designs of future hybrid WDM/TDM-PONs, in which burst-mode upstream detection and the resistance to reflection crosstalk are essential.

We also have proposed and experimentally demonstrated a novel chirp-free optical Manchester signal transmitter with enhanced tolerance to dispersion, which can be potentially used as the upstream modulator in the aforementioned WDM-PON with enhanced tolerance to Rayleigh noise. By using a single-drive MZM together with a passive power combiner, Manchester coding is realized directly in optical domain, thus eliminating high-speed electronic processing without increasing the complexity of the modulator structure. For the 5-Gb/s Manchester signal generated by the proposed scheme, after transmitting in 20-km SMF, the dispersion induced power penalty is reduced to 0.4 dB, from 1.5 dB in the previous scheme using a dual-drive MZM. Simulation results for the eye diagrams of the 10-Gb/s systems are also given. The proposed scheme eliminates the conventional bandwidth doubling issue in optical

Manchester signal generation and will potentially find application in high-speed optical burst mode transmission links.

References

- [1] A. Chiuchiarelli et al., "Enhancing Resilience to Rayleigh Crosstalk by Means of Line Coding and Electrical Filtering," *IEEE Photon. Technol. Lett.* 22, 85-87 (2010).
- [2] J. Prat, "Rayleigh Back-scattering reduction by means of Quantized Feedback Equalization in WDM-PONs," *ECOC*, Th.10.B.3, 2010.
- [3] D. Jorgesen et al., "Improved High Pass Filtering for Passive Optical Networks," *IEEE Photon. Technol. Lett.* 22, 1144-1146 (2010).
- [4] O. Akanbi et al., "A new scheme for bidirectional WDM-PON using upstream and downstream channels generated by optical carrier suppression and separation technique", *IEEE Photon. Technol. Lett.*, vol. 8, pp. 340 2006.
- [5] S. P. Jung et al., "Demonstration of RSOA-based WDM PON Employing Self-Homodyne Receiver with High Reflection Tolerance," *OFC/NFOEC*, JWA69 (2009).
- [6] Y. Yamada et al., "High-Level Fluctuation Tolerant Optical Receiver for Optical Packet Switch and WDM Cross-Connect," *J. Lightwave Technol.* 16, 2220- (1998)
- [7] M. Fujiwara, J. Kani, H. Suzuki, and K. Iwatsuki, "Impact of backreflection on upstream transmission in WDM single-fiber loopback access networks," *J. Lightw. Technol.*, vol. 24, no. 2, pp. 740–746, Feb. 2006.
- [8] N. Dupuis et al., "10 Gbit/s Semi-Insulating Buried Heterostructure Loss-less Reflective Amplified Modulator for Wavelength Agnostic Networks,"

OFC/NFOEC, OThC2 (2008).

- [9] Y. Yamada et al., "High-Level Fluctuation Tolerant Optical Receiver for Optical Packet Switch and WDM Cross-Connect," *J. Lightwave Technol.* 16, 2220- (1998)
- [10] H. Nishilawa, et.al, "Design of a 10-Gb/s Burst-Mode Optical Packet Receiver Module and Its Demonstration in a WDM Optical Switching Network," *J. Lightwave Technol.* 20, 1078- (2002).
- [11] Y. Yamada, et.al, "10-Gb/s differential receiver for large optical power fluctuation", *Electron. Lett.*, vol. 33, no. 19, pp. 1642 - 1964, 1997.
- [12] B. K. Kim, et. al, "Optical access network scheme with downstream Manchester coding and upstream NRZ remodulation," *IEE, Electron. Lett.* , vol 42, no. 8, April, pp. 484-485, 2006.
- [13] X. Tian, et.al, "A multi-format transmitter using a single dual-parallel Mach-Zehnder modulator," *ECOC 2006, Paper We3. P. 84.*
- [14] J. Zhang, et.al, "Method for high-speed Manchester encoded optical signal generation," *OFC 2004, Paper MF76.*
- [15] J. Zhang, T. Y. Liow, G. Q. Lo, and D. L. Kwong, "10Gbps monolithic silicon FTTH transceiver without laser diode for a new PON configuration," *Opt. Express* 18(5), 5135-5141 (2010).
- [16] A. Sano et al., "20 Gbit/s chirped RZ transmitter with simplified configuration using electro-absorption modulator," *IEE, Electron. Lett.*, 36, 1858-1860 (2000).
- [17] H. Kim, "An ASE-injected FP-LD-based return-to-zero transmitter for long-reach WDM-PONs," *OFC 2010, paper OWG6.*

Chapter 5 Multicast Transmission in WDM-PON

5.1. Introduction to broadcast/multicast Overlay

With more diverse multimedia and data services available for broadband access, the access network has to be flexible enough to cope with various data or video delivery such as broadcast/multicast services, in addition to the point-to-point (unicast) traffic. Broadcast/multicast is an efficient way to provide information accessibility to a large number of users. In the wavelength plan for ITU-T TDM-PON standard, the downstream band between 1550 and 1560 nm is assigned to broadcast-video. Broadcast can be easily realized in TDM-PON as it employs power-splitting at the RN. Whereas it is more challenging for WDM-PON, due to the dedicated connection between the OLT and the ONU. To realize more flexible network functions, several studies have been carried out to deliver simultaneously point-to-point data and broadcast/multicast data to subscribers [1]-[6].

Multicast is more attractive, compared to broadcast, as it allows selective control of the connection for each subscriber individually. There are two key issues to transmit both point-to-point and multicast data simultaneously in WDM-PON: (1) how to multiplex the point-to-point and multicast traffic and (2) how to enable/disable the multicast traffic flexibly. An additional wavelength together with a specially designed arrayed waveguide grating (AWG) could be used to realize the broadcast

capability in WDM-PONs [1], but it will increase system complexity and cost. Subcarrier multiplexing could be employed to superimpose the multicast data on the point-to-point data and less than 1.5 Gb/s was demonstrated [2]-[4]. However, broadband modulators and oscillators, with bandwidth several times larger than the signal bit rate, are needed at the OLT and/or ONU sides. Recently, two schemes were proposed to superimpose a 10-Gb/s multicast data stream on conventional 10-Gb/s downstream point-to-point data [5], [6]. The multicast control is achieved, respectively, by adjusting the extinction ratio of the downstream point-to-point NRZ data [10], or switching the modulation format of the downstream point-to-point data between non-return-to-zero-on-off-keying (NRZ-OOK) and inverse-return-to-zero-on-off-keying (IRZ-OOK) [6]. However, when the multicast service is disabled, as the upstream transmission is realized by remodulating part of the downstream non-return-to-zero (NRZ) signal with a high extinction ratio (ER), it results in a limited upstream bit rate. Less than 2.5 Gb/s is demonstrated. With the surge of peer-to-peer applications, symmetric bit rates in both upstream and downstream signals are highly desirable for future-proof PON systems. In this chapter, two multicast overlay schemes that can solve all these challenging issues are proposed and experimentally demonstrated. Before introducing those two multicast overlay schemes, we will first introduce two broadcast schemes, as broadcast is the foundation of multicast.

5.2. Hybrid- OTDM-based broadcast overlay

5.2.1. Introduction

In this section, we propose a novel WDM-PON architecture to simultaneously deliver

both downstream unicast data and broadcast data to subscribers based on hybrid optical time-division multiplexing (OTDM). The point-to-point data encoded in OOK format and the multicast data encoded in DPSK format are time-interleaved at the OLT to form a hybrid OTDM signal, with no optical time demultiplexing is required before direct detection [7]. Part of downstream DPSK signal is remodulated by upstream data, thus the ONU is colorless and only centralized multi-wavelength pulse source at the OLT is required. The multi-wavelength pulse source can be generated by a laser array followed by a common pulse caver, i.e. an electroabsorption modulator (EAM). A supercontinuum broadband light source shared by all subscribers may be a cost-effective alternative for this centralized pulse source [8].

5.2.2. System architecture

Fig. 5.1 shows the proposed WDM-PON architecture with hybrid-OTDM based broadcast overlay. At the OLT, light from the multi-wavelength pulse source, generated by a laser array followed by a common pulse caver, is divided into two parts. One part is fed in to an intensity modulator (IM) driven by the broadcast data, while the other part is wavelength-demultiplexed by an arrayed waveguide grating or its equivalent such that each channel can be phase-modulated by the downstream point-to-point data. The delay line before each phase modulator (PM) should have a proper length, such that after wavelength-multiplexing and combination with the point-to-point signals the point-to-point signals and the broadcast signals are interleaved in time. The timing alignment between the pulse caver and data modulator is adjusted in electrical domain, using a timing alignment monitoring module together with a feedback control circuit. We have proposed a scheme for such a timing alignment monitoring, which will be discussed in the next section. The combined

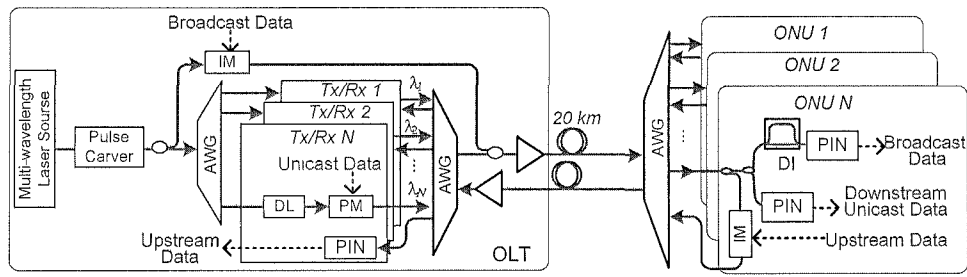


Fig. 5.1 The proposed WDM-PON architecture with hybrid-OTDM based broadcast overlay.

signals are first amplified and then fed into the feed fiber. At an ONU, a portion of the received downstream signal power is tapped off for reception while the remaining is fed into an optical IM for upstream data remodulation. By direct detection the RZ-OOK signal can be simply detected, as the adjacent RZ-DPSK bit with constant power will only cause certain extinction ratio degradation for its detection. Similarly, when the hybrid OTDM is passed through the DI, the RZ-DPSK signal can be directly detected, with limited detection noise caused by the residual RZ-ASK signal [6].

5.2.3. Experimental demonstration

We have conducted a proof-of-concept experiment to demonstrate one channel of the proposed WDM-PON based on the architecture shown in Fig. 5.1. At the OLT, the optical pulse train (wavelength 1548 nm, FWHM ~ 1.5 ps, repetition rate 10.61 GHz) generated by a semiconductor mode-locked laser diode (MLLD) was first split into two parts before being modulated by a 10-Gb/s $2^{31}-1$ PRBS via an optical phase modulator and an intensity modulator, respectively, to generate the RZ-DPSK and RZ-OOK tributaries. The choice of pulsewidth can be much broader, as far as the pulses have no overlap after interleaving [6]. A tunable optical delay line (DL) was inserted to assure that the optical 10.61-Gb/s RZ-DPSK pulses (downstream unicast

signals) are properly interleaved with the 10.61-Gb/s RZ-OOK (broadcast signals) signal pulses to form a 21.22-Gb/s hybrid OTDM signal. A tunable optical attenuator was also used, to keep the two tributaries having the same power. The hybrid OTDM signal was then amplified to around 4 dBm and coupled into a 20-km dispersion-shifted fiber to emulate the transmission link with dispersion compensation. An optical bandpass filter (OBF) with a 3-dB bandwidth of ~ 0.8 nm was used after the EDFA to emulate one channel of a 100-GHz AWG and to suppress the ASE noise. At the ONU, a part of the received downstream signal power was fed into an optical IM, driven by a properly delayed 10-Gb/s $2^{31}-1$ PRBS as the upstream data, before being transmitted back to the OLT, via another piece of 20-km dispersion-shifted fiber. Fig. 5.2 shows eye diagrams of the downstream point-to-point data, multicast data and upstream data detected by receivers with the bandwidth of 50 GHz (for comparison) or 10 GHz (for real detection). By using 10-GHz receivers, all the detected signals show

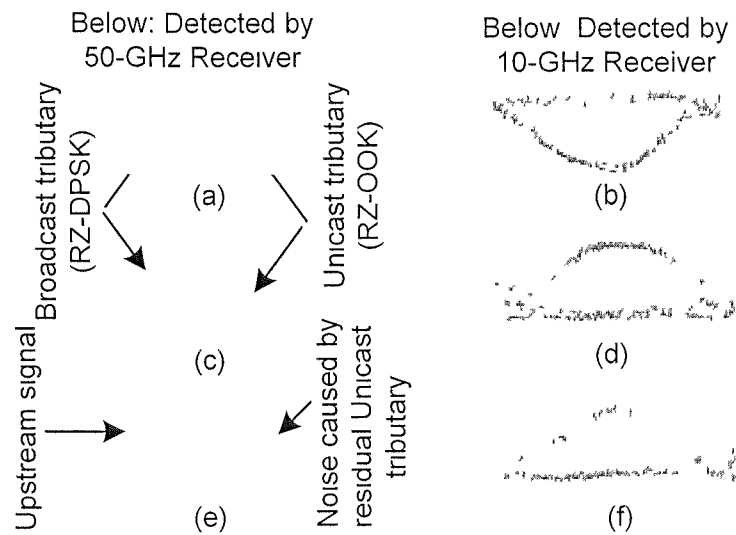


Fig. 5.2 Eye diagrams of (a), (b) before DI (for downstream unicast signal detection); (c), (d) after DI (for broadcast signal detection); (e),(f) the detected upstream signal. Time scale: 20 ps/div.

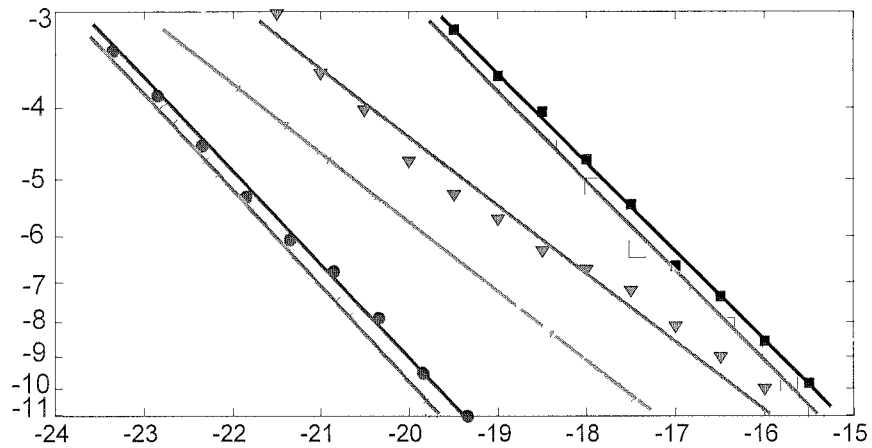


Fig. 5.3 BER curves for downstream unicast signal, broadcast signal and upstream signal.

clearly open eyes. The BER measurement results are shown in Fig. 5.3. After 20-km transmission, for the downstream unicast and broadcast signals, negligible power penalty is observed. For the upstream signals, around 1-dB power penalty, mainly due to the remodulation caused waveform degradation, is observed.

In conclusion, we propose a novel WDM-PON architecture with centralized light source and hybrid OTDM-based broadcast overlay. Experimental demonstration of downstream unicast signals, broadcast signals, and upstream signals, all at 10 Gb/s, are achieved with the power penalties less than 1 dB for all signals after 20-km transmission with dispersion compensation. The required timing alignment monitoring module at OLT will be discussed in the next section.

5.2.4. Delay-interferometer based timing alignment

monitoring for RZ-transmitters

5.2.4.1. Introduction

Return-to-zero (RZ) format is used in the aforementioned hybrid OTDM-based broadcast transmission in WDM-PON. It is also the preferred data format for long-haul high bit-rate WDM transmission systems [9]. In such RZ systems RZ-DPSK and RZ-OOK are two dominant modulation formats, for which correct timing between pulse carving and data modulation must be maintained. Timing drift of 2~5 ps was observed when the temperature of the 1-m-long optical fiber between the pulse carver and data modulator was changed by 50°C, which may cause a power penalty of around 1 dB for an optically preamplified receiver in 40-Gb/s systems [10]. Thus an automatic alignment is necessary to compensate the timing drift between pulse carving and data modulation, due to temperature variation and device aging. On the other hand, as such timing drift process is rather slow, it is possible to realize automatic alignment using cost-effective low-speed components.

Alignment monitoring is essential to realize the desired automatic timing alignment between pulse carving and data modulation. For RZ-DPSK systems, the timing-misalignment induced polarization variation in a polarization-maintaining fiber has been utilized as indicators for modulation alignment monitoring [10]. However this scheme is polarization sensitive and has a limited monitoring power dynamic range (MPDR) of 0.2 dB. MPDR is the ratio between the two detected monitoring signal powers that correspond to the maximum and minimum timing misalignment. With a larger MPDR, a higher monitoring resolution can be attained.

Another scheme utilizes an off-center optical filter to capture the frequency chirp due to the timing-misalignment, and the MPDR has been improved to 3.35 dB [11]. To further enhance the MPDR, an optical frequency discriminator and a microwave detector centered at half the data rate are used to monitor the spectrum broadening induced by timing misalignment [12], and an MPDR of 17 dB is achieved. However, a broadband photodetector capable of retrieving the data waveform is required. For RZ-OOK systems, it has been proposed to monitor the modulation alignment status by detecting the microwave power spectrum of the signal [13]. Similar with [12], a broadband photodetector is also required. Another scheme that is based on the chirping characteristic of the EAM may not be applicable to other chirp-free modulators [14].

In this part, we describe and experimentally demonstrate a simple modulation alignment monitoring scheme applicable to both RZ-DPSK and RZ-OOK systems using a delay-interferometer (DI) with properly designed delay. Not relying on any high speed components, the scheme needs only an athermal DI and one or two optical power meters. It is applicable to any kinds of intensity modulator, and differential monitoring can further enhance the MPDR for RZ-DPSK systems. Because of the periodic wavelength response of the DI [15], the proposed scheme has potential for multichannel operation. As athermal DI has been commercially available [16], [17], the proposed scheme becomes more practical.

5.2.4.2. Operation principle

The operation principle is illustrated as follows. For simplicity, square waveform with a duty cycle of 50% is adopted for the obtained RZ pulse train. Zero rise- and fall-time are used for both phase and amplitude modulation for the clarity of illustration. The

obtained RZ-DPSK (or RZ-OOK) signals are fed into a DI with 0.75-bit relative delay between the two arms. For such relative delay, the overlapped portions between the RZ-DPSK (or RZ-OOK) signals on different arms of the DI will be within half pulse width, as illustrated in Fig. 5.4. When the pulse carver and data modulator are well aligned, the overlapped portions of the signals in the two arms may carry different signals (i.e. different phases for RZ-DPSK signals and different amplitudes for RZ-OOK signals). In contrast, when the pulse carver and data modulator have half-bit misalignment, the overlapped portions must carry the same signal. Such difference will induce power variation through interference at the output ports of the DI and thus can be utilized as indicators for modulation alignment monitoring.

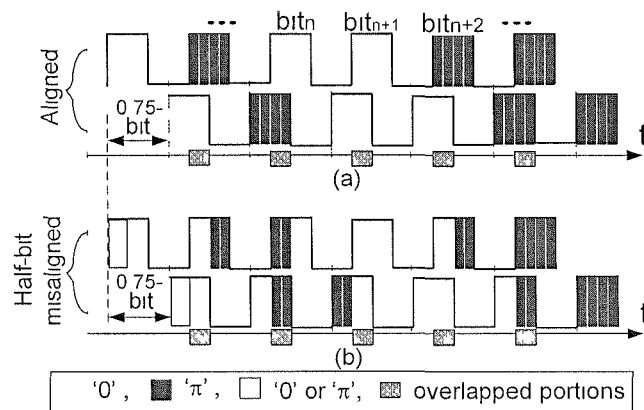


Fig. 5.4 RZ-DPSK signals in the two arms of the DI before combining by the output 3-dB coupler for (a) aligned and (b) half-bit misaligned cases.

The question now is how to determine the optimal relative delay between two arms of the DI to maximize the MPDR for both constructive port (CP) and destructive port (DP). Under the aforementioned assumption of square waveform and instantaneous data transition, it is found, through simple calculation, that the optimal relative delay should be $\tau/2$ or $T-\tau/2$, where τ is the pulse width and T is the bit period.

Furthermore, for RZ-DPSK signals shown in Fig. 5.4, the signal symbols ‘0’ and ‘ π ’ are assumed to be equally probable. For the aligned case, DI’s both ports have the same average power, due to the fact that the overlapped portions generate complementary output at each port of the DI via constructive or destructive interference. Thus, if differential monitoring (DM) (using the power difference between the two output ports of the DI for alignment monitoring) is used, theoretically, the MPDR can reach infinity as the minimum monitoring power is 0. It should be noted such differential monitoring is quite different from the well-known balanced detection for DPSK demodulation, where strict timing alignment between two photo-detectors is required. Since the drift of the timing between pulse carver and data modulator occurs on the time scale of tens of minutes [14], the implementation of such differential monitoring requires neither broadband photodetectors nor precise timing alignment between the two optical power meters.

For practical systems with non-square pulse waveform and non-zero rise/fall-time for data modulation, simulation using OptSim™ is conducted to find the optimal relative delay for 10-Gb/s RZ-DPSK and RZ-OOK signals with duty cycle of 50%. In the simulation, all the parameters (say rise- and fall-time) are set according to the specifications of the devices used in the following experiment. The simulation result is shown in Fig. 5.5. We can conclude that the destructive port has larger MPDR than the constructive port for both RZ-DPSK and RZ-OOK systems, thus the destructive port should be used for single port monitoring. DM can further enhance the MPDR from less than 2 dB to ~14 dB for RZ-DPSK signals.

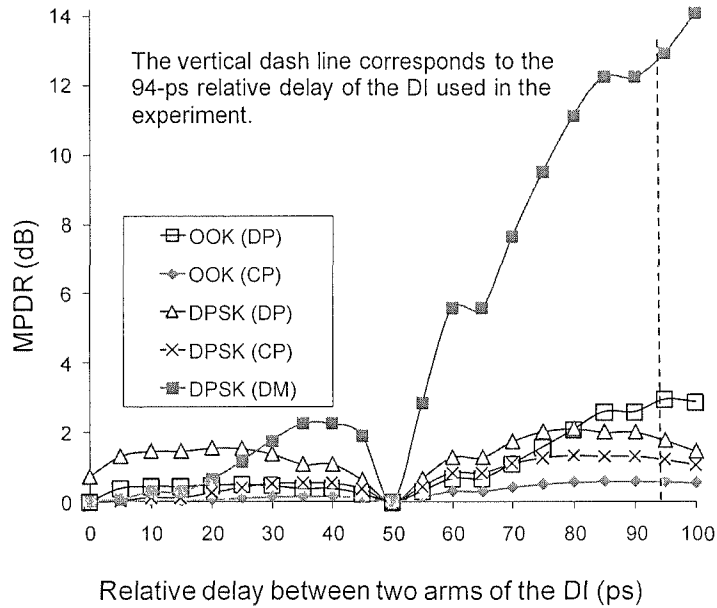


Fig. 5.5: MPDR versus the delay of DI. The duty cycle of the RZ pulse train in simulation was 50%. DP: destructive port, CP: constructive port, DM: differential monitoring.

5.2.4.3. Experimental demonstration

Fig. 5.6 shows the experimental setup used to investigate the proposed scheme. A CW light at 1549 nm was carved into a 10-Gb/s pulse train with a pulse width of 50 ps and rise-time of ~ 15 ps via a Mach-Zehnder intensity modulator (MZM), driven by a 10-GHz sinusoidal clock signal. The pulse train was then modulated with a 10-Gb/s $2^{31}-1$ Pseudorandom binary sequence (PRBS) using a LiNbO₃ phase modulator (PM) or MZM to generate the RZ-DPSK or RZ-OOK signal. A tunable electrical delay was used to provide different timing misalignments between the pulse carver and data modulator. At the output of the PM or MZM, a portion of optical power was tapped off and fed into a DI with ~ 94 -ps relative delay for alignment monitoring. The inset in Fig. 5.6 shows the eye diagrams of the detected RZ-DPSK signals from each port of the DI

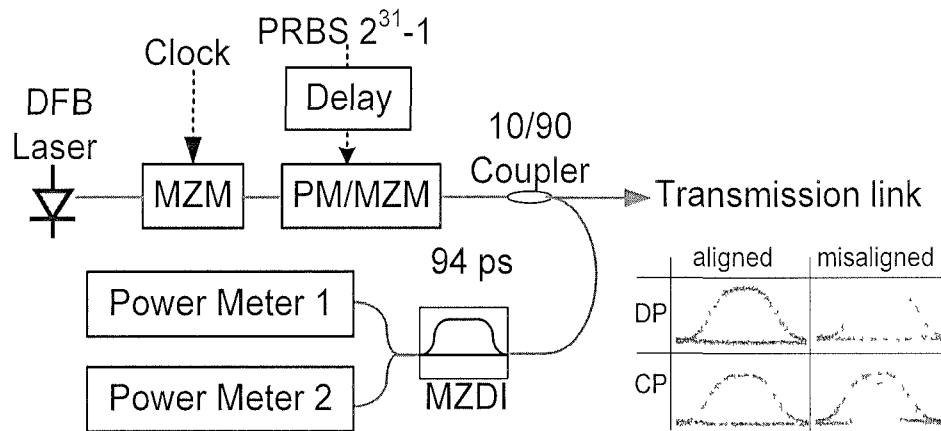


Fig.5.6 Experimental setup. Inset: Eye diagrams of the detected RZ-DPSK signals from each port of the DI when the pulse carver and data modulator are well aligned or have half-bit misalignment. Time scale: 20ps/div. DP: destructive port, CP: constructive port.

when the pulse carver and data modulator are well aligned or have half-bit misalignment. When they are aligned, the constructive port and the destructive port should have nearly the same output monitoring power (assume '0' and ' π ' are equally probable), since their output signals are complementary. As the timing misalignment increases, for the destructive port, the output monitoring power will decrease due to the dip in the middle of the eye diagram. At the same time the output monitoring power will increase for the constructive port from the principle of conservation of energy. The experimental results on MPDR are shown in Fig. 5.7.

When differential monitoring is used for the RZ-DPSK signal, the power difference between the DI's two output ports monotonously increases as the absolute value of the timing misalignment increases. Thus, the timing misalignment of the RZ-DPSK signal can be confined by stepwise dithering the timing alignment and minimizing the power

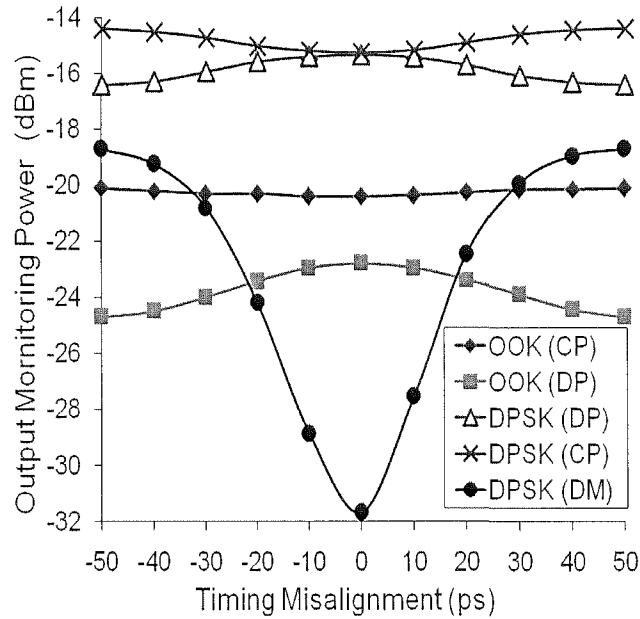


Fig.5.7 Experimental results of output monitoring power for different timing misalignments using a 94-ps DI.

difference between the DI's two output ports through a feedback circuit. On the other hand, when single-port monitoring is used for RZ-DPSK/RZ-OOK signals, the DI's output monitoring power, from the destructive port, monotonously decreases as the absolute value of the timing misalignment increases. Thus, the timing misalignment can be confined by stepwise tuning the timing alignment and maximizing DI's output monitoring power through a feedback circuit. For RZ-DPSK (RZ-OOK) signals, the MPDR of ~ 1.2 dB (~ 2 dB) and ~ 0.9 dB (~ 0.3 dB) are observed for the destructive port and the constructive port, respectively. Compared with the points intersected by the dash line (~ 94 -ps delay) in Fig. 5.5, these experimental results are slightly smaller than those in the simulation, due to the limited accuracy in the simulation parameter value selection based on our devices. Overall, the experimental and simulation results agree well. When differential monitoring is used, the MPDR for RZ-DPSK systems is effectively improved to 13 dB, which also agrees well with the simulation result of

12.9 dB. The differential monitoring case has better agreement between the experimental and simulation results, compared to the single-port cases, as some common errors in the two ports are rejected by differential monitoring.

For the proposed scheme, we also investigated its tolerance to temperature-induced frequency offset of the 94-ps DI through simulation. For the athermal DI in [16], the temperature-induced frequency offset is $\leq \pm 0.5$ GHz over the range of $[0, 70^\circ\text{C}]$. Within such a small frequency offset, only 0.33-dB MPDR degradation is observed when the RZ-OOK signal is monitored by DI's destructive port, whereas the MPDR degradation is less than 0.1dB for the other four cases. In addition, when differential monitoring is used for the RZ-DPSK signal, within such a small frequency offset, the power difference between DI's two output ports still monotonously increases as the absolute value of the timing misalignment increases. Thus, the timing misalignment of the RZ-DPSK signal can be confined by stepwise dithering of the timing alignment and minimizing the power difference between DI's two output ports through a feedback circuit. Similarly, when the destructive port is used for single-port monitoring, the timing misalignment can be minimized by maximizing the DI's output monitoring as in the aforementioned discussion.

For RZ-DPSK signals, the power difference between the two output ports of the DI decreases as the timing misalignment is reduced, as shown in Fig. 5.7. With no timing misalignment, the power difference is nearly vanished. Thus, differential monitoring can significantly enhance the MPDR for RZ-DPSK signals. For RZ-OOK signals, although the power difference between the two output ports of the DI also

decreases as the timing misalignment reduces, the minimum value of the power difference is not very small and cannot effectively enhance the MPDR by DM. Thus, differential monitoring is only applicable to RZ-DPSK signals.

We then investigated the feasibility of the proposed scheme for RZ signals with a duty cycle of 33% through simulation. Raised-cosine pulse was assumed in the simulation. We also studied the relationship between MPDR and the delay of DI as shown in Fig. 5.8. When the destructive port is used for single-port monitoring, the MPDR for the RZ-OOK signal is around 3.6 dB with an optimal delay of ~ 95 ps, whereas the MPDR for the RZ-DPSK signal is around 2.4 dB with an optimal delay of ~ 86 ps. The MPDR for the RZ-DPSK signal is significantly enhanced to ~ 34 dB by

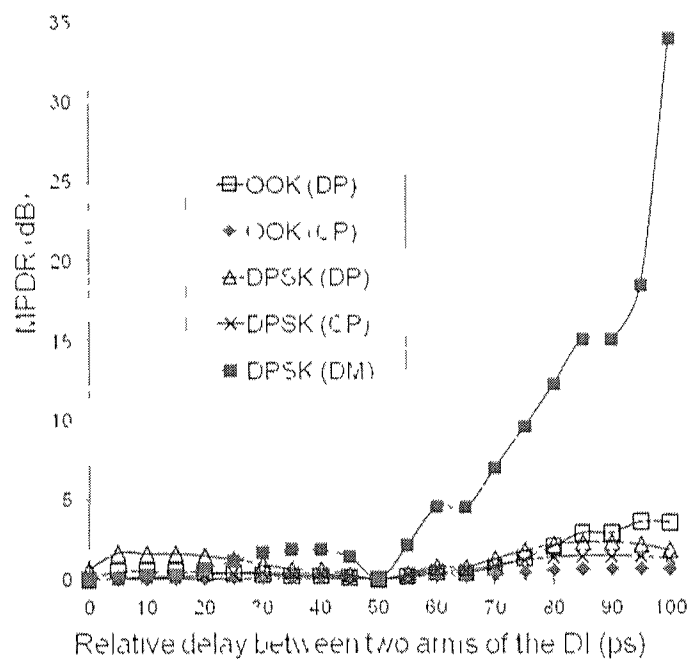


Fig 5.8 MPDR vs. the delay of DI The duty cycle of the RZ pulse train in simulation was 33%. DP: destructive port, CP: constructive port, DM: differential monitoring.

differential monitoring, with an optimal delay of 100 ps.

5.2.4.4. Discussions

The mixing between the data signal and the clock for RZ signal generation could also be done in the electrical domain to save the modulator used as the pulse cover. The AND operation between the data signal and the clock can generate RZ-shaped driving signal to drive a single MZM for the generation of RZ-OOK signal [18]. RZ-DPSK signal could also be generated by a single MZM with specially designed driver electronics [19]. In both schemes, timing misalignment between the data signal and the clock signal will degrade the obtained RZ-OOK/ RZ-DPSK signals. The proposed monitoring scheme can also be applied to these single-modulator schemes. We investigated the relationship between MPDR and the delay of DI through simulation, as shown in Fig. 5.9. When the destructive port is used for single-port monitoring, the MPDR for the 10-Gb/s RZ-OOK signal is around 2.8 dB with an optimal delay of ~95 ps, whereas the MPDR for the 10-Gb/s RZ-DPSK signal is around 4 dB with an optimal delay of ~75 ps. The MPDR for the 10-Gb/s RZ-DPSK signal is enhanced to ~8.5 dB by differential monitoring, with an optimal delay of 100 ps. It is noteworthy that for these single-modulator schemes, even without using the proposed monitoring scheme the timing-misalignment-induced power variation in the MZM output still has a 1.6-dB and a 0.12-dB MPDR for the 10-Gb/s RZ-DPSK and RZ-OOK signal, respectively. By using the proposed monitoring scheme, the MPDR can be improved by 6.9 dB and 2.68 dB for the RZ-DPSK signal and the RZ-OOK signal, respectively.

In conclusion, we have proposed and demonstrated a simple scheme for monitoring the alignment status between the data and the clock signal for the

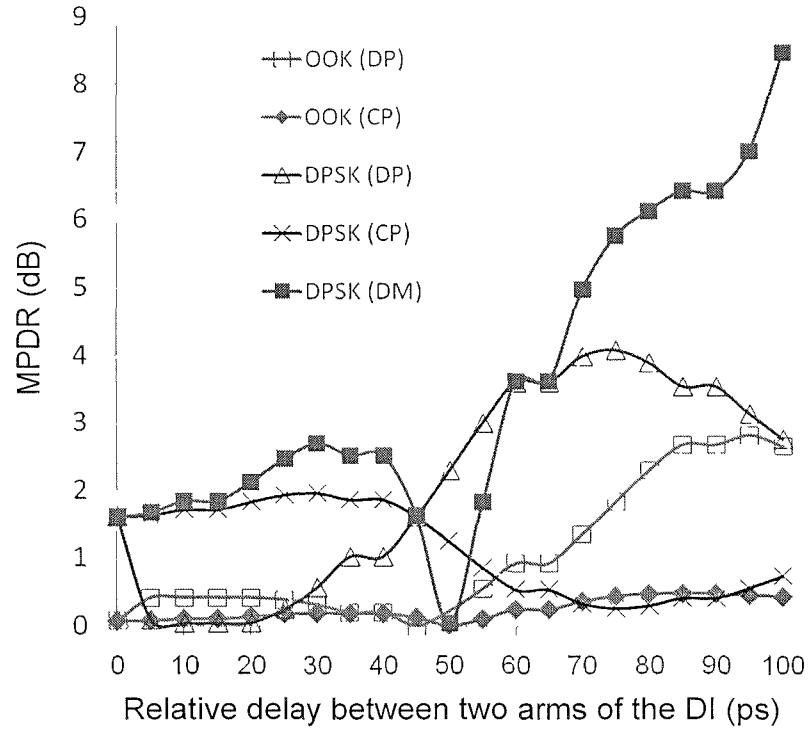


Fig. 5.9 MPDR versus the delay of DI when the RZ-DPSK/ RZ-OOK signals are generated by single modulator. DP: destructive port, CP: constructive port, DM: differential monitoring.

generation of RZ-DPSK and RZ-OOK signals. Not relying on any high-speed components, the proposed scheme needs only an athermal delay-interferometer and one or two optical power meters. The scheme also has potential for multichannel operation, because of the periodic wavelength response of the DI. The proposed scheme is first applied to the transmitter configuration using cascaded data modulator and pulse carver. For 10-Gb/s RZ-DPSK signals with a duty cycle of 50% and 33%, by differential monitoring, the MPDR was significantly improved to ~13 dB and ~34 dB, respectively. For 10-Gb/s RZ-OOK signals, the MPDR of ~2 dB and ~3.6 dB were obtained for the duty cycle of 50% and 33%, respectively. The proposed scheme is also applicable to the single-modulator transmitter configuration, in which the data

signal and the clock are mixed in the electrical domain. The MPDR for the 10-Gb/s RZ-DPSK and RZ-OOK signals is enhanced to 8.5 and 2.8 dB, respectively, by using the proposed scheme.

5.3. Broadcast transmission using time-interleaved phase remodulation

5.3.1. Introduction

In this section, we propose a novel time-interleaved phase remodulation scheme to multiplex the broadcast traffic with the conventional bidirectional unicast traffics in a WDM-PON. The broadcast data encoded in DPSK format is superimposed onto all downstream unicast data channels that are also encoded in DPSK format. At ONU, the unicast and broadcast data can be simultaneously obtained from the destructive port of a half-bit-delay DI. By properly reducing the modulation depth of the broadcast and unicast DPSK signals at OLT, optical carrier can be recovered from the constructive port of the DI at ONU and used as the source for upstream transmission, without compromising the downstream extinction ratio (ER) [20]. Additional light sources as in [21], [22] are not needed in the proposed scheme.

5.3.2. System architecture and operation principles

Fig. 5.10 shows the proposed WDM-PON architecture with symmetric unicast bit rates and broadcast overlay. For each downstream wavelength at the OLT, differentially precoded data is used to drive an optical PM to generate the downstream unicast DPSK signal. All downstream wavelengths at the

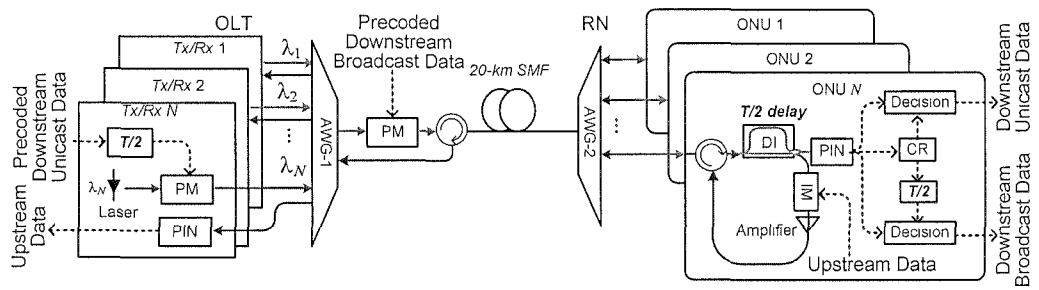


Fig. 5.10 Proposed WDM-PON architecture with symmetric bit rates and broadcast overlay. CR: clock recovery.

OLT are multiplexed by an AWG before feeding into a shared optical PM, which is driven by the precoded broadcast data. The broadcast and unicast DPSK signals with the same bit rate are temporally offset by $T/2$, with T being the bit period. At an ONU, the downstream broadcast and unicast DPSK signals are demodulated simultaneously by the destructive port of a DI with half-bit delay, before direct detection by a single photo-detector with two decision modules. Light from the DI's constructive port is fed into an optical intensity modulator (IM) for upstream data re-modulation. Compared with the ONU structure in [23], one receiver module and two power splitters for the separation of the downstream signals and the upstream source can be saved in the proposed scheme, leading to cost-effective and simplified implementation of ONU. Athermal DIs, with C+L band coverage by a single device, are commercially available and can be used at ONU.

As a half-bit-delay DI, rather than a conventional one-bit-delay DI, is used at ONU, the demodulated DPSK signal is determined by the phase difference between the leading half of a bit in the downstream unicast (or broadcast) DPSK signal and the trailing half of its previous bit. As for the leading half and the trailing half within one bit in the DPSK signal, at DI's destructive port, destructive interference always occurs.

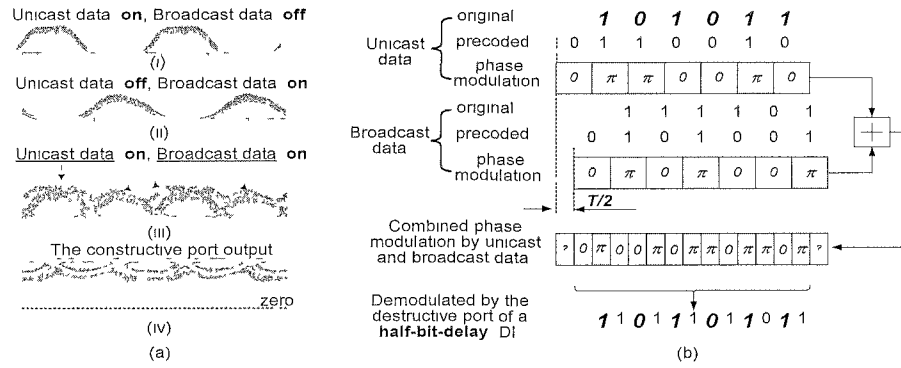


Fig. 5.11 (a) Eye diagrams of (i) the detected downstream unicast data when the broadcast signal is off, (ii) the detected broadcast data when the unicast signal is off, (iii) the detected downstream unicast and broadcast data, (iv) the constructive port output with optical power in each bit. Time scale: 50 ps/div. (b) Operation principles of time-interleaved phase remodulation.

Thus RZ-shaped eye diagram can be obtained when the destructive port a half-bit-delay DI is used to demodulated the downstream unicast or broadcast DPSK signal, as shown in Fig. 5.11(a)(i) and Fig. 5.11(a)(ii). The unicast and broadcast signals have slightly different waveforms as the two phase modulators have different modulation bandwidths.

By temporally offsetting the broadcast and unicast data by $T/2$, the phase difference between the leading half of a bit in the downstream unicast DPSK signal and the trailing half of its previous bit will not be altered by the broadcast PM, as they will experience the same phase change induced by the phase modulation of the broadcast data. Thus correct demodulation of the unicast DPSK signal via the destructive port of a half-bit-delay DI can be obtained as long as the broadcast and unicast data are temporally offset by $T/2$, as shown in Fig. 5.11(b). Likewise, correct demodulation of the broadcast DPSK signal can be obtained simultaneously. At the

DI's destructive port, the demodulated broadcast and unicast DPSK signals are interleaved, as shown in Fig. 5.11(a)(iii) and Fig. 5.11(b). To facilitate the carrier recovery from the DI's constructive port for upstream remodulation, both the broadcast and unicast DPSK signals are with reduced modulation depth (RMD). The output from the constructive port is Inverse-RZ shaped with optical power in each bit as shown in Fig. 5.11(a)(iv), and can be readily re-modulated by the upstream data [24]. For RMD modulation, the " π " phase in Fig. 5.11(b) is changed to a smaller value, leading to a "1" bit with smaller level after demodulation. The operation principle of the time-interleaved phase remodulation is still applicable.

5.3.3. Experimental demonstration

We have experimentally demonstrated the proposed scheme based on the architecture shown in Fig. 5.10. At the OLT, CW light at 1552.7 nm was coupled into a PM driven by a 5-Gb/s $2^{31}-1$ PRBS with a driving voltage of $\sim 0.4 V_{\pi}$. The obtained RMD-DPSK signals were fed into another PM also driven by a 5-Gb/s PRBS with a driving voltage of $\sim 0.4 V_{\pi}$ as the pre-coded broadcast data. Then through a circulator, the phase remodulated signal with an average power of 5 dBm was coupled into a 20-km SMF. After propagating through a 100-GHz AWG (insertion loss= 4 dB, 3-dB bandwidth= 0.6 nm) at the RN and a circulator, -3.6-dBm optical power was fed into a 94-ps DI at ONU. The destructive port of the DI was used to simultaneously demodulate the downstream unicast and broadcast RMD-DPSK signals. The output power from the DI's destructive port was -13.9 dBm. The demodulated unicast and broadcast RMD-DPSK signals could attain a high ER [24]. After demodulation, the interleaved RZ-shaped unicast and broadcast signals were detected by a 10-Gb/s p-i-n receiver followed by a 12.5-GHz bit-error-rate (BER) tester. The clock delay of the BER tester

was manually adjusted correspondingly when measuring the BERs of the unicast and broadcast RMD-DPSK signals, to emulate the two decision modules of the receiver shown in Fig. 5.10. Optical power of -6.3-dBm from the constructive port was fed into an intensity modulator (IM), driven by a 5-Gb/s $2^{31}-1$ PRBS as the upstream data. The upstream signal with a power of -15 dBm from the IM was amplified to 5 dBm, and then transmitted back to the OLT. The amplification increased the power ratio of the upstream signal to the Rayleigh backscattered signal. The BER measurement results for downstream and upstream signals are shown in Fig. 5.12(a) and Fig. 5.12(b), respectively. After 20-km transmission in SMF, around 1-dB power penalty is observed for the unicast and broadcast signals, due to dispersion. The insets in Fig. 5.12(a) show the wide-open eye diagrams of the downstream unicast and broadcast signals. In the back-to-back case, compared with that using CW light as the upstream source, around 2-dB power penalty (at $\text{BER}=10^{-9}$) is observed for the upstream signal modulated on the DI's constructive port output, as shown in Fig. 5.12(b). After 20-km transmission in SMF, around 1.5 dB power penalty is observed for the upstream signal due to dispersion and Rayleigh backscattering. To investigate the tolerance to

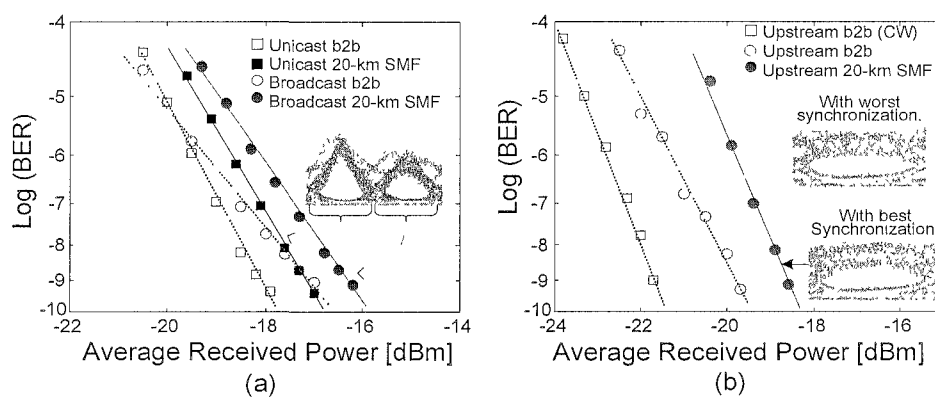


Fig. 5.12 BER results of (a) the downstream unicast and broadcast signals. (b) the upstream signal. Inset: the corresponding eye diagrams for different cases. Time scale: 50ps/div.

remodulation timing misalignment we have deliberately adjusted the remodulation synchronization through an electronic delay within one bit period. Only less than 0.9-dB power penalty was observed. The eye diagram corresponding to the worst remodulation synchronization is shown in the inset of Fig. 5.12(b), with only slight distortion compared with the eye with optimal re-modulation synchronization.

5.4.A delay-based multicast control scheme for

WDM-PONs with 10-Gb/s symmetric two-way traffics

5.4.1. Introduction

As discussed in the beginning of this chapter, Multicast is more attractive, compared to broadcast, as it allows selective control of the connection for each subscriber individually. Recently, we proposed a novel scheme to realize 10-Gb/s symmetric uplink and downlink bit rates and 10-Gb/s multicast overlay with simple centralized control for multicast service [25]. The multicast data, encoded in DPSK format, are superimposed on all point-to-point data channels, modulated in IRZ format. By adjusting the synchronization of the DPSK/IRZ orthogonal modulation, simple and flexible multicast control could be realized. It should be noted that such synchronization control is also required in [4]-[6]. Compared with prior schemes [2], [4]-[6], additional ER adjustment or modulation format switching is not required when the multicast service is switched from one operation mode (enabled/disabled) to the other, thus reducing system complexity and cost. The upstream transmission can be

realized by remodulating part of the downstream IRZ signal which carries optical power in each bit. In this section, we further investigate different issues for the proposed scheme. First, the effects and tradeoff for different ERs of the IRZ signal are studied. It is shown that the error floor of the multicast disabled data is enhanced from previous 10^{-7} to higher than 10^{-4} when the ER of the downstream IRZ signal is increased from 4.5 dB to 6 dB. The effect of timing misalignment on downstream orthogonal modulation and upstream re-modulation is quantitatively analyzed. We also investigate the applicability of the scheme for systems with different downstream and multicast data rates.

5.4.2. Proposed system architecture and multicast control

Fig. 5.13 shows the proposed WDM-PON architecture with symmetric bit rates and multicast overlay. For each downstream wavelength at the OLT, IRZ-shaped data signal is first generated, via a logic NAND gate, and is used to drive an optical IM to generate the downstream point-to-point IRZ signal. All the downstream wavelengths at the OLT are multiplexed by an AWG. The multiplexed signals are first amplified by a shared EDFA and then fed into an optical PM, which is driven by the pre-coded multicast data. Through this orthogonal modulation, the multicast DPSK data are superimposed on all point-to-point data channels in IRZ format. As at least half of a bit period in each downstream point-to-point IRZ bit is in high-power state, it can readily enable the orthogonal modulation. At the ONU, the received downstream signal power is divided into three portions by two 3-dB optical power splitters. One quarter of the received downstream signal power is fed into a photodiode for the direct detection of the downstream point-to-point IRZ data. Another quarter is demodulated by a delay interferometer (DI) before the direct detection of the multicast DPSK data. The remaining power is fed into an optical IM for upstream data remodulation. The

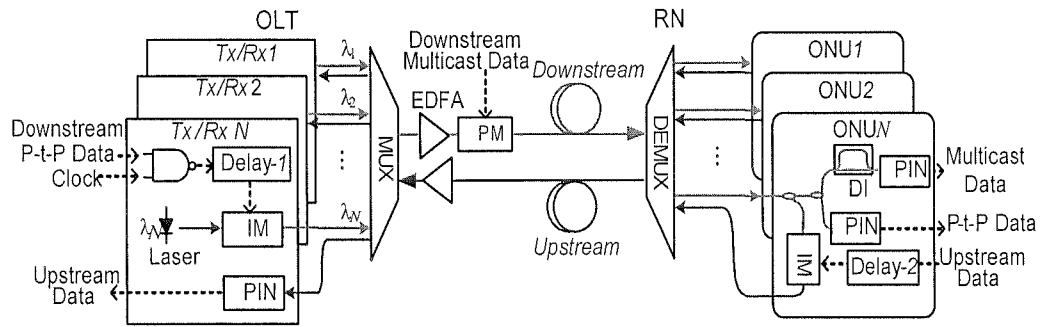


Fig. 5.13 The proposed WDM-PON architecture with symmetric bit-rates and multicast overlay. Tx/R: transceiver, P-t-P Data: point-to-point data, IM: intensity modulator, OLT: optical line terminal, EDFA: Erbium Doped Fiber Amplifier, DI: delay interferometer, PIN: p-i-n photodetector, PM: phase modulator, RN: remote node, ONU: optical network unit.

high-power portion in each bit of the downstream point-to-point IRZ data also facilitates the upstream data remodulation. Proper synchronization between the downstream and upstream data is needed to assure that the upstream data can be imprinted on the high-power portion of each bit in the downstream IRZ data during remodulation.

By properly aligning the IRZ data temporally through an electronic delay circuit (Delay-1) such that the multicast DPSK data rest in the middle of two adjacent IRZ pulses at the PM, the multicast DPSK data can be properly demodulated and detected at ONUs. In contrast, if the DPSK bits coincide with the IRZ data dips, the multicast DPSK will suffer from excessive intensity fluctuation and cannot be properly demodulated at the ONU. Thus, multicast control can be achieved by centralized electrical delay adjustment of the downstream IRZ signal.

5.4.3. Experimental demonstration

We have performed a proof-of-concept experiment for the proposed delay-based multicast overlay scheme based on the architecture shown in Fig. 5.13. At the OLT, the IRZ-shaped data signal was first generated by the logic NAND operation of a NRZ 10-Gb/s $2^{31}-1$ PRBS and a 10-GHz clock, via a commercial NAND gate. A continuous-wave light source at 1547.8 nm was then modulated with an IM driven by the obtained IRZ-shaped data. The resultant output with a dark pulse width of 55 ps was amplified by an EDFA. An optical bandpass filter with a 3-dB bandwidth of ~ 0.8 nm and an insertion loss of 2.1 dB was used to suppress the ASE noise. After power amplification and filtering, the IRZ signals with an ER of ~ 4.5 dB were fed into a PM driven by a 10-Gb/s PRBS as the pre-coded multicast data. Then the orthogonally modulated signal (DPSK/IRZ) with an average power of 5 dBm was coupled into a 20-km dispersion-shifted fiber to emulate the dispersion-compensated transmission between the OLT and the RN. At the ONU, one quarter of the received downstream signal power was fed into a p-i-n photodiode for IRZ detection. Another quarter was demodulated by a DI with a relative delay of 94.3 ps for DPSK detection. The remaining power was fed into an optical IM, driven by a properly aligned 10-Gb/s $2^{31}-1$ PRBS as the upstream data, before being transmitted back to the OLT via another piece of 20-km dispersion-shifted fiber. A commercially available LiNbO_3 IM was used in this experiment. For practical implementation it can be replaced by an electro-absorption modulator integrated with semiconductor optical amplifiers (SOA-EA-SOA) for 10-Gb/s polarization-insensitive operation [26].

To enable multicast, the synchronization of the DPSK/IRZ orthogonal modulation was carefully adjusted via a commercially available digital phase shifter (Delay-1) at OLT as shown in Fig. 5.13, such that each bit of the DPSK data could be

superimposed right in the middle of two adjacent IRZ pulses, as denoted by ‘A’ in Fig. 5.14(a), in which the longest period of high intensity level resides. The DPSK data was detected at the ONU, showing a clear eye diagram as depicted in Fig. 5.14(c)(i). The uplink data was measured, with the eye-diagram shown in Fig. 5.14(b). To show the effect of timing misalignment on multicast control using electronic delay circuit (Delay-1), the eye diagrams for different timing misalignments are depicted in Fig. 5.14(c)(i)-(vi), and the increasing degradation by the increasing timing misalignment is shown clearly. When the synchronization of the DPSK was detuned by 50 ps, corresponding to the period ‘B’ in Fig. 5.14(a), the superimposed DPSK multicast data could not be detected correctly at the ONU. Its degraded eye diagram is depicted in Fig. 5.14(c)(vi). The BER measurement results for both downlink and uplink signals are shown as the solid lines in Fig. 5.15 and Fig. 5.16, respectively.

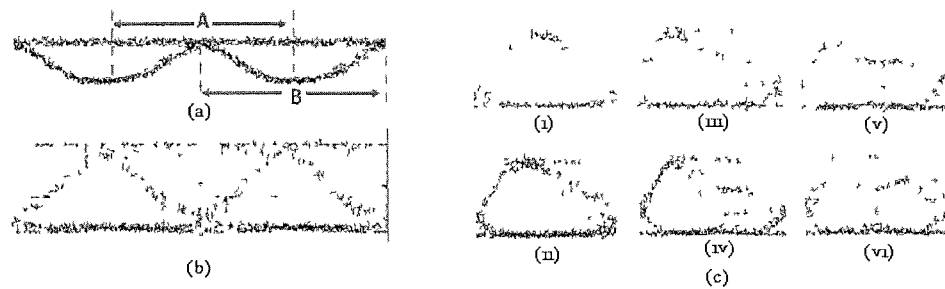


Fig. 5.14 Eye diagrams of (a) the detected 10-Gb/s downstream point-to-point data in IRZ format, (b) the detected upstream data with proper delay at the Delay-2, (c) (i) – (vi) the 10-Gb/s demodulated DPSK multicast signal with timing misalignment adjusted from 0 to 50 ps with a 10-ps step. Time scale: 20 ps/div.

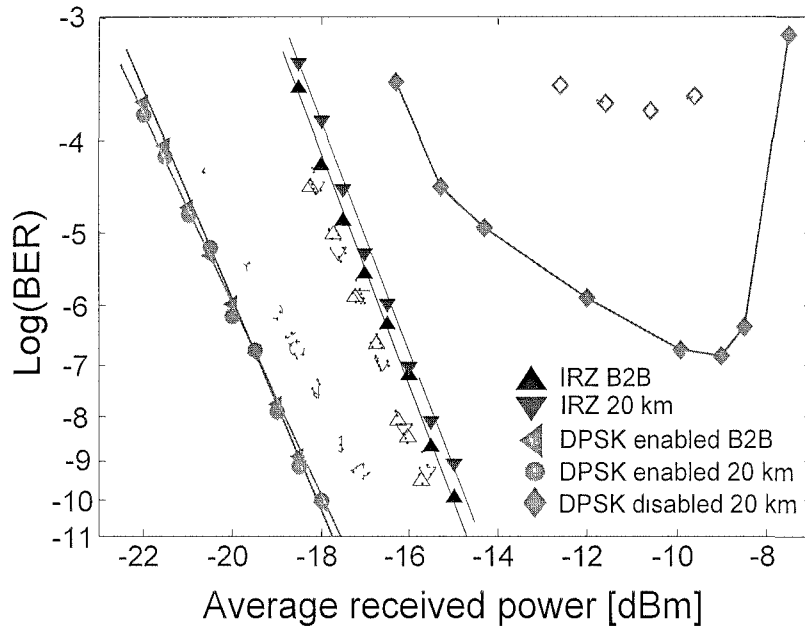


Fig. 5.15 BER measurements of downstream IRZ point-to-point signals and multicast DPSK signals with multicast enabled (0-ps time misalignment) and disabled (50-ps time misalignment) cases. The solid and dashed lines correspond to the cases that the ERs of the IRZ signal are ~ 4.5 dB and ~ 6 dB, respectively.

The performance of the downstream point-to-point signal, the downstream multicast signal, and the upstream signal depends on the ER of the IRZ signal. We then adjusted the ER of the IRZ signal to 6 dB for BER measurements to investigate the tradeoff for different ER's. The corresponding results for all the three types of data are depicted by the dashed lines in Fig. 5.15 and Fig 5.16.

For both ER values, negligible power penalty is observed after 20-km transmission for the downstream point-to-point and multicast enabled signals. For the upstream signal, less than 0.5-dB power penalty at the BER of 10^{-9} , mainly due to the degraded waveform, is shown. When multicast is disabled, the multicast DPSK signal

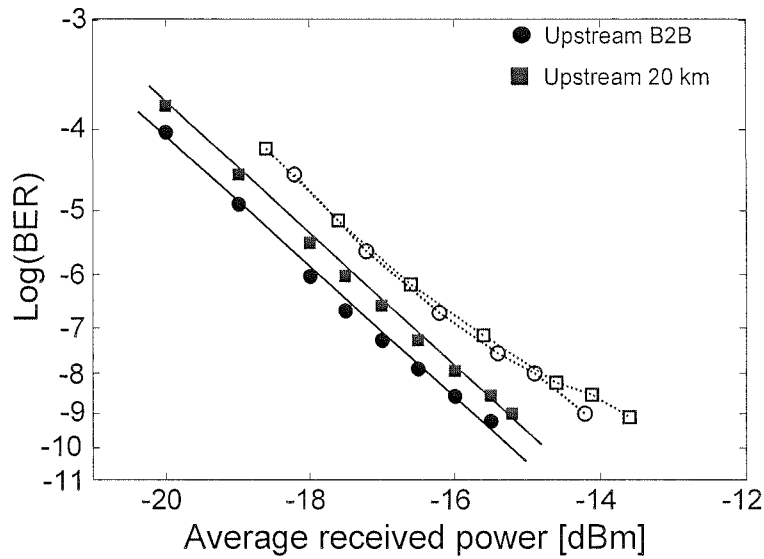


Fig. 5.16 BER measurements of upstream signals. The solid and dashed lines correspond to the cases that the ERs of the IRZ signal are ~ 4.5 dB and ~ 6 dB, respectively.

exhibits an error floor. The error floor is enhanced from 10^{-7} to higher than 10^{-4} when the ER of the downstream IRZ signal is increased from 4.5 dB to 6 dB. Thus the multicast disabled signal can be suppressed more effectively. However, the trade-off is that the upstream signal has an error floor below 10^{-9} when the ER of the IRZ signal is 6 dB. For the upstream BER, if more stringent BER (better than the conventional 10^{-9}) is required, the ER of the IRZ signal should be limited to a lower value.

To quantitatively analyze the effectiveness of the proposed multicast control scheme to suppress the multicast disabled signal, we also measured the power penalty of the multicast DPSK signals at the BER of 10^{-9} , for different timing misalignments as depicted in Fig. 5.17. In the multicast enabled case, Fig. 5.17 shows that the multicast data can tolerate up to ± 20 -ps time misalignment for less than 1-dB power penalty, for both ER values. When the time misalignment is larger than ± 20 -ps, the corresponding power penalty of the multicast DPSK signals increases sharply,

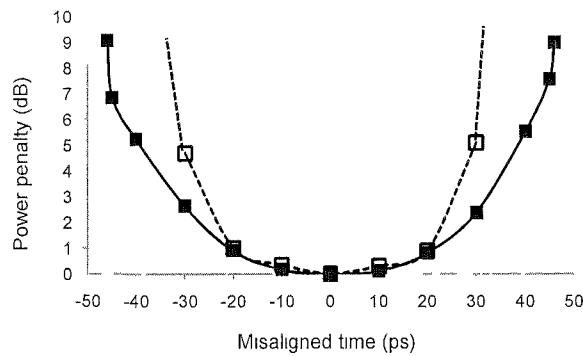


Fig. 5.17 Power penalty of multicast signal versus misaligned time between the downstream IRZ signals and the multicast DPSK signals. The solid and dashed lines correspond to the cases that the ERs of the IRZ signal are ~ 4.5 dB and ~ 6 dB, respectively.

especially for the case with a larger ER, thus the multicast DPSK signals can be effectively disabled via increasing the timing misalignment.

It should be noted that the uplink performance was measured under the best remodulation synchronization such that each bit of the upstream data could be superimposed right in the middle of two adjacent IRZ pulses as denoted by ‘A’ in Fig. 5.14(a). The remodulation synchronization was realized via carefully adjusting a digital phase shifter (Delay-2) at ONU as shown in Fig. 5.13. For practical implementation, the recovered clock from the downstream point-to-point data could be used for remodulation synchronization. To investigate the tolerance to re-modulation misalignment we had deliberately adjusted the re-modulation synchronization through the Delay-2. We measured the power penalty of the upstream signals at the BER of 10^{-9} , for different timing misalignments as shown in Fig. 5.18. For less than 1-dB power penalty, the upstream data can tolerate up to ± 20 -ps

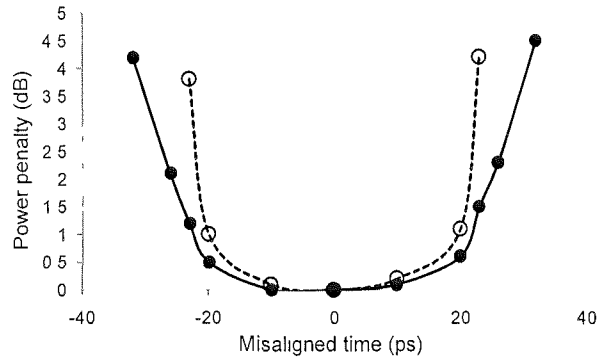


Fig. 5.18 Power penalty of upstream signal versus misaligned time between the downstream IRZ signals and the upstream signals. The solid and dashed lines correspond to the cases that the ERs of the IRZ signal are ~ 4.5 dB and ~ 6 dB, respectively.

re-modulation misalignment when the ER of the IRZ signal is ~ 6 dB, and can further tolerate up to ± 23 -ps re-modulation misalignment when the ER is ~ 4.5 dB.

In the demonstration, the signal power fed into the transmission link was 5 dBm after the PM. For both ER values of 4.5 and 6 dB, the receiver sensitivity at the BER of 10^{-9} for the downstream IRZ signals was higher than -15 dBm, and for the downstream multicast enabled DPSK signals was higher than -17 dBm, while that for the upstream NRZ signals was higher than -13.8 dBm. The loss caused by the transmission link and the optical demultiplexing at the remote node was around 10 dB, and the insertion loss of a 3-dB optical power splitter or a DI (when the destructive port of the DI is used) was around 3.5 dB. Thus, the received powers for the IRZ and DPSK detection were -12 dBm and -15.5 dBm, respectively, implying around 3-dB and 1.5-dB system margin for the downstream point-to-point and multicast enabled signals, respectively. Via an IM (~ 6 -dB insertion loss), a portion of the downstream light (at -8.5 dBm) was re-modulated by upstream data. The optical power arrived at the OLT was around

-24.5 dBm without amplification. An EDFA with a gain of around 20 dB was used as the upstream pre-amplifier at the OLT, thus around 3-dB system margin could be obtained for each upstream channel. Standard EDFAs can support more than 23-dBm saturation output power. They can satisfy the requirement of the two shared EDFAs at the OLT for 32 channels, to have an output power of 5-dBm/ch for the downstream signals or to have a 20-dB small signal gain for the upstream signals. In the analysis of power margin, we assume the insertion loss of one AWG is 6 dB, based on our current available device (with a channel spacing of 0.8 nm and a 3-dB bandwidth of 0.35 nm). This is a conservative estimate, as the AWG with an insertion loss of 3 dB or less is commercially available. By using the integrated SOA-EA-SOA module as the upstream modulator [26], the upstream power budget can be further improved and the upstream EDFA can possibly be eliminated.

5.4.4. Discussions

As the DPSK multicast data are imposed on the IRZ point-to-point signal and the upstream NRZ signal, the channel bandwidth of the AWGs used at the OLT and the RN should be wide enough. Otherwise improper optical filtering will cause phase-to-amplitude conversion, corrupting the IRZ signal and the upstream NRZ signal. AWGs with flat-top passband are preferred to alleviate this degradation. We also investigated such narrow filtering effect via simulation. The relationship between the power penalty (at BER= 10^{-9}) by optical filtering and the AWG channel bandwidth is shown in Fig. 5.19. For all the three types of data, less than 0.5-dB power penalty is observed when the AWG bandwidth is larger than 0.5 nm.

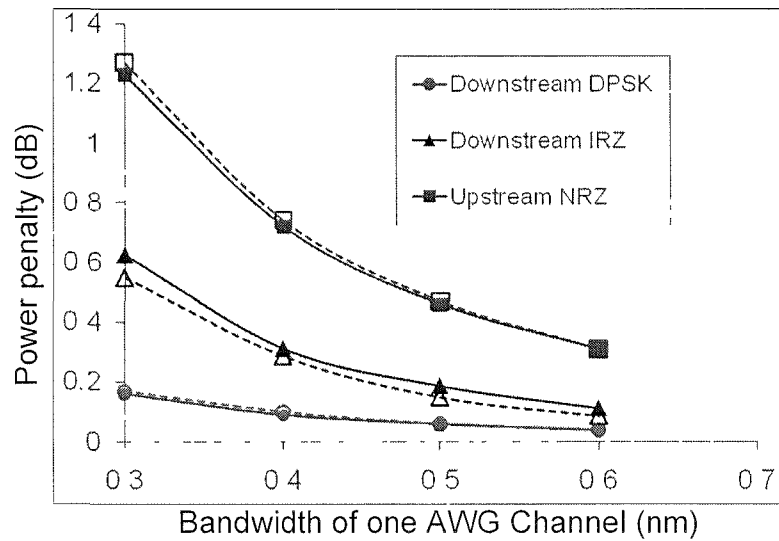


Fig. 5.19 Power penalty (at BER= 10^{-9}) versus the 3-dB channel bandwidth of AWGs used at the OLT and the RN. The solid and dashed lines correspond to the cases that the ERs of the IRZ signal are ~ 4.5 dB and ~ 6 dB, respectively.

The dispersion-shifted fiber was used in the experiment, whereas standard SMF together with a broadband dispersion compensation module (DCM) can be used as the feeder fiber for practical deployment. As the length of the distribution fiber (between the RN and the ONU) may vary in a range of several kilometers, it is necessary to investigate the dispersion compensation tolerance of the proposed scheme, which was studied through simulation. The 3-dB channel bandwidth and insertion loss of AWGs used in the simulation were set to be 0.44 nm and 3 dB, respectively, according to a commercially available AWG. As shown in Fig. 5.20, for both ER values of 4.5 and 6 dB, the power penalty (at BER= 10^{-9}) induced by 51-ps/nm (corresponding to ~ 3 -km SSMF) residual dispersion in the distribution fiber is less than 0.83 dB and 0.19 dB for the downstream IRZ signal and the upstream NRZ signal, respectively. The downstream multicast DPSK signal is more robust to dispersion, and the power

penalty induced by 85-ps/nm residual dispersion in the distribution fiber is less than 0.06 dB (not shown in Fig. 5.20) for both ER values.

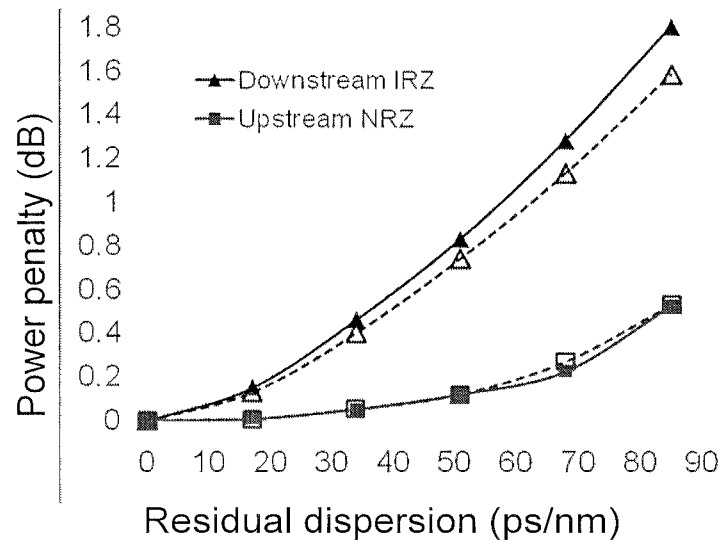


Fig. 5.20. Power penalty (at BER= 10^{-9}) versus residual dispersion in the distribution fiber. The solid and dashed lines correspond to the cases that the ERs of the IRZ signal are ~ 4.5 dB and ~ 6 dB, respectively.

We have demonstrated the effectiveness of the proposed multicast control scheme in the case when both multicast and downstream point-to-point data are 10 Gb/s. We should point out that when the bit rate of the multicast data is lower than that of the downstream point-to-point data, the proposed multicast control scheme may not function properly. We first investigated the feasibility of the proposed multicast control scheme by simulation for 5-Gb/s multicast data, which are superimposed on the 10-Gb/s downstream point-to-point data. In the simulation, the ER of the 10-Gb/s downstream point-to-point data was set at a higher value of 10 dB, which shall provide a stronger suppression for the multicast disabled signals. The optical eye diagrams of

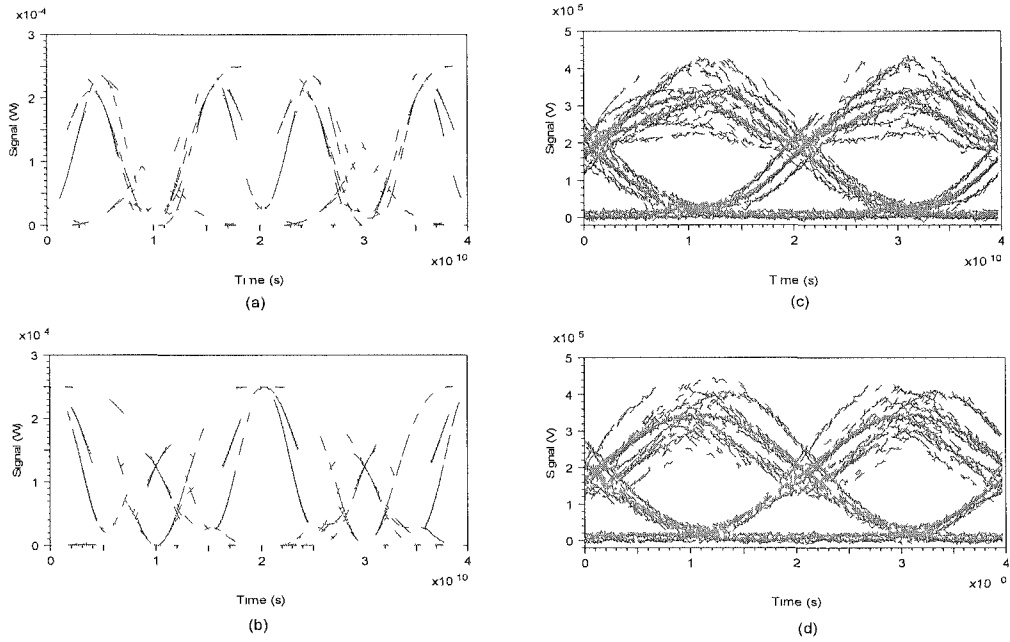


Fig. 5.21. (a) Optical eye diagram of the detected 5-Gb/s multicast data with timing misalignment of 50 ps. (b) Optical eye diagram of the detected 5-Gb/s multicast data with timing misalignment of 0 ps. (c) Detected electrical eye diagram of the 5-Gb/s multicast data with 50-ps timing misalignment using a 4-GHz receiver. (d) Detected electrical eye diagram of the 5-Gb/s multicast data with 0-ps timing misalignment using a 4-GHz receiver.

the 5-Gb/s multicast data for timing misalignment of 50 ps and 0 ps are shown in Fig. 5.21(a) and Fig. 5.21(b), respectively. The 50-ps timing misalignment corresponds to the multicast disabled case. In this case, the 5-Gb/s DPSK bits coincide with the 10-Gb/s IRZ data dips, leading to large intensity fluctuation in the optical eye diagram of the detected 5-Gb/s multicast data. Nevertheless, such intensity fluctuation is significantly suppressed in the detected electrical eye diagram of the 5-Gb/s multicast data, as shown in Fig. 5.21(c), due to the low-pass filtering effect of the electronic filter used in the receiver. In the simulation, a 4-GHz electronic filter was used in the

receiver. Compared to the electrical eye diagram with 0-ps timing misalignment in Fig. 5.21(d), which corresponds to the multicast enabled case, no obvious degradation is observed for the multicast disabled mode. The electrical eye diagram of the multicast disabled case is even a little more open than that of the multicast enabled case. It is different from the previous case when both the multicast and the downstream point-to-point data are with the same data rate of 10 Gb/s, for which obvious degradation is observed for the multicast disabled data. The proposed scheme is not applicable to this case with 10-Gb/s downstream point-to-point data and 5-Gb/s multicast data, as the multicast data cannot be effectively disabled even when the IRZ signal has a higher ER value of 10 dB.

We then further investigated the feasibility of the proposed multicast control scheme for 2.5-Gb/s multicast overlay. Prior to the 10-Gb/s systems, 2.5-Gb/s systems are widely used. In the simulation, the ER of the 10-Gb/s downstream point-to-point data was also 10 dB and a 2-GHz electronic filter was used in the receiver. The BER measurement results for the 2.5-Gb/s multicast data with timing misalignment of 50 ps and 0 ps were shown in Fig. 5.22. At the BER of 10^{-9} , compared with the multicast data with 0-ps timing misalignment, a negative power penalty of around 0.4-dB was observed for the multicast data with 50-ps timing misalignment. It is consistent with the previous case of 5-Gb/s multicast overlay in that the multicast disabled mode has slightly better performance than the multicast enabled mode and the multicast data cannot be disabled through timing misalignment adjustment.

As discussed above, the proposed multicast control scheme may not function properly when the bit rate of the multicast data is lower than that of the downstream point-to-point data. In a real system deployment, it will be a limiting factor for the

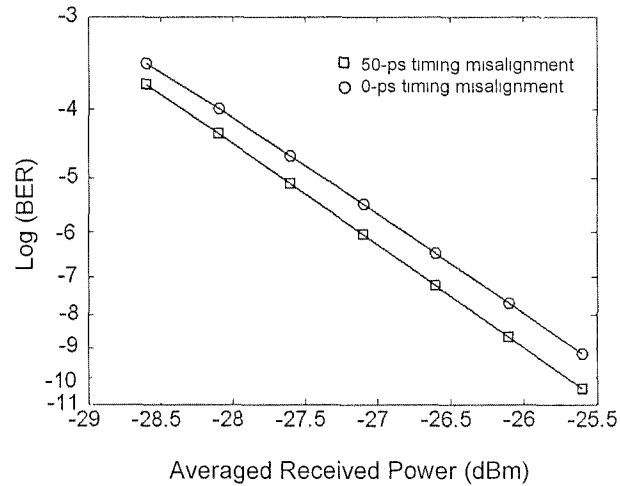


Fig. 5.22. BER measurements of the 2.5-Gb/s multicast data for timing misalignment of 50 ps and 0 ps. The ER of the 10-Gb/s downstream point-to-point data is 10 dB.

proposed scheme if the multicast bit rate is lower than the point-to-point bit rate at the initial stage of the deployment.

In conclusion, we propose a novel WDM-PON architecture to provide symmetric bit rates and multicast overlay based on DPSK/IRZ orthogonal modulation and synchronization control. Simple and flexible multicast control could be realized at the OLT. Experimental demonstration of downstream point-to-point signals, downstream multicast signals, and upstream signals, all at 10 Gb/s, are achieved with power penalties less than 0.5 dB for all signals after 20-km dispersion-shifted fiber. The error floor of the multicast disabled data is enhanced from 10^{-7} to higher than 10^{-4} when the ER of the downstream IRZ signal is increased from 4.5 dB to 6 dB. The effect of timing misalignment on downstream orthogonal modulation and upstream re-modulation is quantitatively analyzed. For less than 1-dB power penalty, both the multicast enabled data and the upstream data can tolerate 20-ps or above timing

misalignment.

5.5.A wavelength detuning-based multicast control scheme

5.5.1. Introduction

A delay based multicast control scheme is demonstrated in last section, with a shortcoming that the multicast traffic could not be effectively disabled when its bit rate was lower than that of the downstream data. In this section we propose a further simplified multicast control scheme that is also applicable for the multicast traffic with a bit rate lower than that of the downstream data.

In the proposed scheme, the multicast data encoded in DPSK format is superimposed onto all downstream unicast channels modulated in IRZ format. The multicast data can be effectively disabled by slightly detuning the laser wavelength at OLT, which has negligible effect on the unicast data. The proposed scheme differs from all the previous schemes in that, the multicast control is realized via the inherent wavelength management of WDM systems, rather than any other additional adjustment of signal's extinction ratio, synchronization, modulation formats, etc.

5.5.2. System architecture and multicast control

Fig. 5.23 shows the proposed architecture. At OLT, the IRZ-shaped electrical signal is

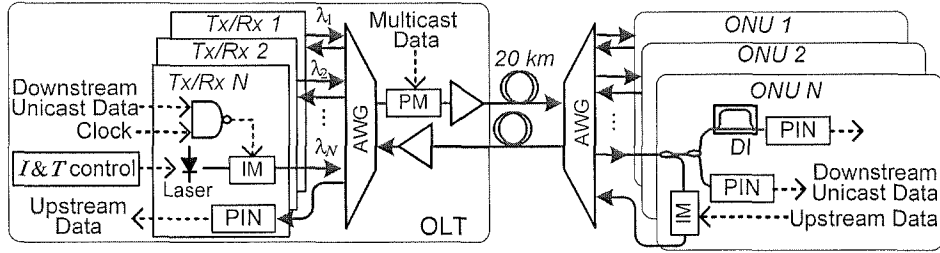


Fig. 5.23 Proposed WDM-PON architecture with wavelength tuning-based multicast control. I&T control: driving current and temperature control of the DFB Laser.

first generated via an electronic logic NAND gate before driving an IM to generate the downstream unicast IRZ signal. The multiplexed downstream unicast signals are then modulated by a shared PM which is driven by the precoded multicast data. As at least half of each bit in the downstream IRZ signal bit is in ‘1’ level, it can greatly facilitate the orthogonal modulation as well as upstream remodulation [23]. The unicast data and the multicast data could be bit-synchronized by using a common clock signal at OLT. At each ONU, a DI is employed to properly demodulate the multicast data. Identical DI can be employed for all ONUs to keep them colorless by setting each of the downstream unicast wavelength to coincide with one of the periodic frequency response peaks or dips of the DI, depending on whether the constructive or destructive port of the DI is used for DPSK demodulation. Wavelength offset between optical source and DI will result in degradation in DPSK demodulation [27]. Hence, the multicast data can be disabled by properly detuning the respective downstream unicast laser wavelength by 0.02 nm (a quarter of a free spectral range of the DI), which can be easily realized by slightly adjusting the driving current of the respective downstream laser at the OLT. As the range of wavelength detuning is less than 0.02 nm that is much smaller than the channel spacing of AWG, it has negligible effect on the unicast data which is intensity-encoded.

5.5.3. Experimental demonstration

We have experimentally demonstrated the proposed scheme based on the architecture shown in Fig. 5.23. At OLT, continuous-wave light at 1549.485 nm from a temperature-controlled distributed feedback laser was IRZ modulated by an IM with a 10-Gb/s $2^{31}-1$ PRBS. The resultant output with an ER of ~ 4 dB was fed into a PM driven by a 10-Gb/s $2^{31}-1$ PRBS as the multicast data. After power amplification, the orthogonally modulated signal with an average power of 5 dBm was coupled into a 20-km dispersion-shifted fiber to emulate the dispersion-compensated transmission between OLT and the RN. A 100-GHz AWG with a 3-dB bandwidth of ~ 0.6 nm and an insertion loss of ~ 4 dB was used at RN. At the ONU, one quarter of the received downstream signal power was fed into a photodiode for IRZ detection as downstream unicast data. Another quarter was demodulated by a 94.3-ps DI for DPSK detection as the multicast data. The remaining half of the power was fed into an IM, driven by a 10-Gb/s $2^{31}-1$ PRBS as the upstream data, before transmitting back to the OLT via another piece of 20-km dispersion-shifted fiber.

When the multicast was enabled, the driving current of the DFB laser should be carefully adjusted, such that its center wavelength could coincide with a frequency response dip of the DI, as the destructive port was used for DPSK demodulation. With the optimal driving current of 59.2 mA, the superimposed DPSK multicast data was successfully detected at the ONU, with a clear eye diagram as shown in the inset of Fig. 5.24. To quantitatively show the effect of wavelength tuning on multicast control via laser driving current adjustment, we also measured the power penalty of

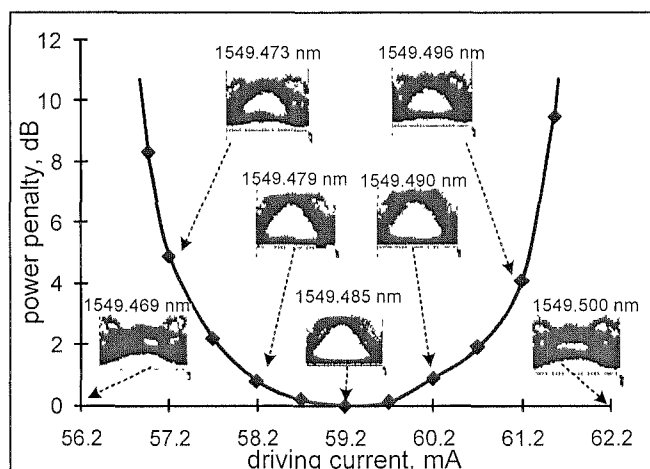


Fig. 5.24 Power penalty versus laser driving current and wavelength tuning for multicast control

the multicast DPSK signals, for different driving current as depicted in Fig. 5.24. The eye diagrams for different laser driving current are depicted in the insets, and the increasing degradation by the wavelength detuning is shown clearly. No performance degradation was observed for the unicast signals during wavelength tuning, and the output power variation of the downlink EDFA was within 0.1 dB. The BER

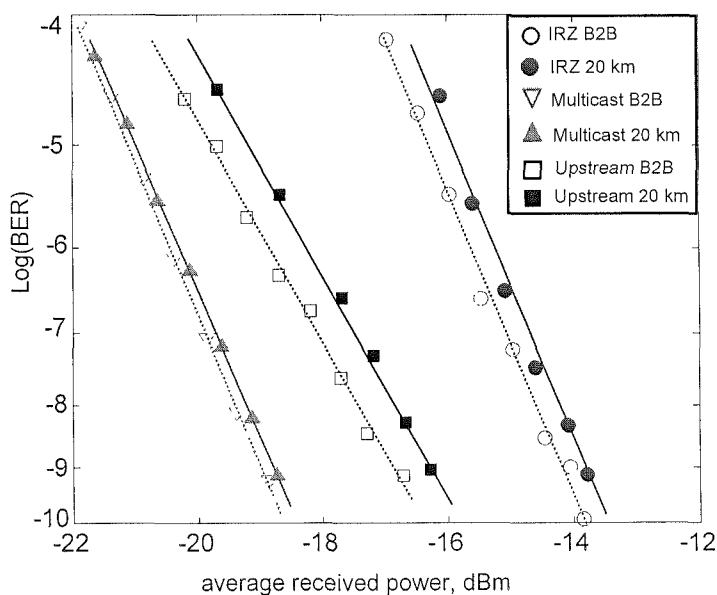


Fig. 5.25 BER measurements. B2B: back-to-back.

measurement results are shown in Fig. 5.25. After 20-km transmission, for the downstream unicast and multicast enabled signals, negligible power penalty compared to back-to-back case was observed. For the upstream signals, less than 0.7-dB power penalty was observed.

5.6. Summary

On the one hand, broadcast/multicast is an efficient way to provide information accessibility to a large number of users. On the other hand, its implementation in WDM-PON is challenging due to the dedicated connection between OLT and each ONU. In this chapter, we deal with the issue of broadcast/multicast transmission in WDM-PON.

We first propose to multiplex the downstream unicast and broadcast signals via hybrid OTDM. The hybrid OTDM signals have a unique feature that no optical time demultiplexing is required to separate the two TDM channels before direct detection. Note that in OTDM system, demultiplexing is typically more challenging than multiplexing. In this scheme, RZ-transmitters are needed to generate different TDM channels at OLT, which bring about the synchronization issue between the data and clock signal. Thus, we also describe and experimentally demonstrate a simple modulation alignment monitoring scheme applicable to both RZ-DPSK and RZ-OOK systems using a DI with properly designed delay. The main shortcoming of this hybrid OTDM-based scheme is that the parallel configuration for the generation of hybrid OTDM signals is complicated, with an optical delay line being needed for each wavelength to assure that the two TDM channels can be time-interleaved. This problem is solved in the second broadcast scheme, based on time-interleaved phase

remodulation. In this scheme, error-free transmission of 5-Gb/s bidirectional unicast data and 5-Gb/s broadcast data is experimentally demonstrated at the same carrier wavelength over a 20-km SMF.

Compared to broadcast service, multicast service can offer exclusive service to premium subscribers, thus generating more revenue. In this chapter we also propose and demonstrate two schemes for multicast transmission in WDM-PON. In the first scheme, we superimpose a DPSK-modulated multicast signal on a point-to-point downstream IRZ-modulated signal. By adjusting the synchronization of the DPSK and the IRZ modulation on the downstream carrier, simple and flexible multicast control could be realized. We have successfully demonstrated the proposed scheme for three different traffics, namely 10-Gb/s IRZ downstream point-to-point data, 10-Gb/s DPSK downstream multicast data, and 10-Gb/s OOK upstream re-modulated data, respectively. An error floor of 10^{-4} is observed for the multicast data when it is intended to be disabled. The effect of timing misalignment on the downstream DPSK/IRZ orthogonal modulation and the upstream re-modulation is analyzed. We also investigate the feasibility of the proposed multicast control scheme for 2.5-Gb/s and 5-Gb/s multicast overlay. For 10-Gb/s downstream point-to-point data, the 2.5-Gb/s or 5-Gb/s DPSK overlay cannot work in multicast mode. This problem is solved in the second wavelength detuning-based multicast control scheme. The second scheme is also simpler than the delay-based scheme since it is realized via the inherent wavelength management of WDM systems. In this scheme, the multicast and unicast data are also encoded in DPSK and IRZ formats, respectively, which is the same as in the delay-based scheme. The multicast data is disabled by slightly detuning the laser wavelength at OLT, which has negligible effect on the unicast data but will induce degradation in the DPSK signal's demodulation by an athermal DI at ONU. In this

scheme, experimental demonstration of downstream unicast and multicast signals, as well as upstream signals, all at 10 Gb/s, are also achieved with the power penalties less than 0.7 dB for all signals after 20-km transmission with dispersion compensation.

References

- [1] T. Luk, J. Goodchild, and R. Habel, "WDM PON RF/Video Broadcast Overlay," US Patent 20100021164, Jan. 2010.
- [2] M. Khanal, C. J. Chae, and R. S. Tucker, "Selective broadcasting of digital video signals over a WDM passive optical network," *IEEE Photon. Technol. Lett.*, 17, 1992–1994 (2005).
- [3] Y. Tian, Q. J. Chang, and Y. K. Su, "A WDM passive optical network enabling multicasting with color-free ONUs," *Opt. Exp.*, 16, 10434-10439 (2008).
- [4] Q. J. Chang, J. M. Gao, Q. Li, and Y. K. Su, "Simultaneous transmission of point-to-point data and selective delivery of video services in a WDM-PON using ASK/SCM modulation format," OFC/NFOEC2008, OWH2 (2008).
- [5] Y. Zhang, N. Deng, C.K. Chan, and L.K. Chen, "A multicast WDM-PON architecture using DPSK/NRZ orthogonal modulation," *IEEE Photon. Technol. Lett.*, 20, 1479-1481 (2008).
- [6] N. Deng, C.K. Chan, L.K. Chen, C.L. Lin, "A WDM passive optical network with centralized light sources and multicast overlay," *IEEE Photon. Technol. Lett.*, 20, 114-116 (2008).
- [7] N. Deng et al, "Optical Time Division Multiplexing of RZ-ASK and RZ-DPSK Signals and Their Detection without Optical Demultiplexing," ECOC 2006, Th3.5.6 (2006).
- [8] B. Zhang "A Simple High-Speed WDM PON Utilizing a Centralized

- Supercontinuum Broadband Light Source for Colorless ONUs,” OFC/NFOEC 2006, OTuC6 (2006).
- [9] I. P. Kaminow, T. Li, *Opt. Fiber Telecomm. IVB*, pp.166-167.
- [10] Hoon Kim, C. R. Doerr, R. Pafchek, L. W. Stulz, and P. Bernasconi, “Alignment monitoring of the pulse carver and data modulator for RZ-DPSK systems,” *IEEE Photon. Technol. Lett.*, vol. 15, no. 11, pp. 1594 – 1596, Nov. 2003.
- [11] Guo-Wei Lu, Yuen-Ching Ku, Lian-Kuan Chen, and Chun-Kit Chan, “A Novel Technique for Pulse-Carver and Data Alignment Monitoring in RZ-DPSK Systems Using Off-Center Optical Filtering,” *IEEE Photon. Technol. Lett.*, vol. 17, no. 3, pp. 711-713, Mar. 2005.
- [12] K.T. Tsai, G.-W. Lu, L.-K. Chen, and W.I. Way, “Alignment Monitoring Technique for Pulse Carver and Data Modulator in RZ-DPSK Systems Using an Optical Frequency Discriminator,” *IEEE Photon. Technol. Lett.*, vol. 18, no. 10, pp. 1119-1121, May. 2006.
- [13] J.H. Sinsky, “High-Speed Data and Pulse-Carver Alignment in Dual Mach–Zehnder Modulator Optical Transmitters Using Microwave Signal Processing,” *J. Lightw. Technol.*, vol. 21, no. 2, pp. 412- 423, Feb. 2003.
- [14] Inuk Kang, Linn Mollenauer, Benjamin Greene, and Andrew Grant, “A Novel Method for Synchronizing the Pulse Carver and Electroabsorption Data Modulator for Ultralong-Haul DWDM Transmission,” *IEEE Photon. Technol. Lett.*, vol. 14, no. 9, pp. 1357–1359, Sep. 2008.
- [15] D. O. Caplan, M. L. Stevens, and J. J. Carney, “High-sensitivity multi-channel single-interferometer DPSK receiver,” *Opt. Exp.*, vol. 14, no. 23, pp. 10984-10989, Nov. 2006.
- [16] http://www.optoplex.com/download/Athermal_DPSK_Demodulator_ECO

- [17] http://www.optoplex.com/download/DPSK_Demodulator.pdf
- [18] Y. Kao, A. Leven, Y. Baeyens, Y. Chen, D. Grosz, F. Bannon, W. Fang, A. Kung, D. Maywar, T. Lakoba, A. Agarwal, S. Banerjee, T. Wood, "10Gb/s Soliton Generation for ULH Transmission Using A Wideband GaAs pHemt Amplifier," in Proc. OFC 2003, Paper FF6.
- [19] Xiang Liu and Yuan-Hua Kao, "Generation of RZ-DPSK Using a Single MACH-ZEHNDER Modulator and Novel Driver Electronics," in Proc. ECOC 2004, Paper We3.4.2.
- [20] J. Xu et al., "A New Remodulation Scheme for WDM-PONs With Enhanced Tolerance to Chromatic Dispersion and Remodulation Misalignment," *Photon. Technol. Lett.*, vol. 22, no. 7, pp. 456 - 458, 2010.
- [21] E.S. Son et al., "Bidirectional WDM passive optical network for simultaneous transmission of data and digital broadcast video service", *J. Lightwave Technol.*, Vol.21, No.8, 1723-1727, 2003.
- [22] Z.X. Liu et al., "A WDM-PON Optical Multicast Overlay Scheme Using Inverse-RZ-Duobinary Signal," OFC/NFOEC2010, OThG5 (2010).
- [23] J. Xu et al., "A Delay-based Multicast Overlay Scheme for WDM Passive Optical Networks with 10-Gb/s Symmetric Two-way Traffic," *J. Lightwave Technol.*, vol. 28, no. 18, pp.2660-2666, Sep. 2010.
- [24] J. Xu et al., "A New Remodulation Scheme for WDM-PONs With Enhanced Tolerance to Chromatic Dispersion and Remodulation Misalignment," *Photon. Technol. Lett.*, vol. 22, no. 7, pp. 456 - 458, 2010.
- [25] J. Xu, Y. Zhang, L.K. Chen, and C.K. Chan, "A WDM-PON with 10-Gb/s Symmetric Bit-Rates and Multicast Overlay with Delay-based Multicast Control," OFC/NFOEC2009, NME5 (2009).

- [26] J. Nakagawa and K. Shimizu, "Next-generation Optical Access Systems," Mitsubishi Electric ADVANCE, vol. 114, pp. 23-25, Jun. 2006.
- [27] H. Kim et al., "Robustness to Laser Frequency Offset in Direct-Detection DPSK and DQPSK Systems," J. Lightw. Technol., vol. 21, no. 9, pp. 1887-1891, 2003.

Chapter 6 Conclusion

6.1. Summary of the thesis

This thesis aims to tackle two challenging issues in WDM-PON: Rayleigh noise suppression and multicast transmission. In this thesis, we have proposed and demonstrated several novel techniques, including optical phase remodulation, offset-Manchester coding, time-interleaved phase remodulation, and wavelength detuning-based multicast control.

Following an introduction to the basic concept and recent research thrust on CLS-based WDM-PON in Chapter 2, two novel remodulation schemes are proposed and experimentally demonstrated. They have enhanced tolerance to wavelength offset or to chromatic dispersion and remodulation misalignment, albeit both schemes are vulnerable to the intrinsic Rayleigh noise.

In Chapter 3, we propose to use DI's destructive port as a Rayleigh noise suppresser. The carrier RB can be considerably rejected by the notch filter-like destructive port of the delay-interferometer (DI) at the optical line terminal (OLT), which is used simultaneously to demodulate the upstream DPSK signal. As no deliberate spectral up-shifting is required in this scheme, neither additional modulator nor complicated modulation/demodulation circuit is needed at ONU/OLT. In terms of the optical notch filter used to suppress the RB light, the standard DI used in the proposed scheme is also more favorable than the non-standard filters that are either specially designed ultra-narrow notch filters or wavelength-detuned arrayed

waveguide gratings (AWG) in the prior schemes. Theoretical models related to Rayleigh noise suppression are also built in this work. These models correctly predict that carrier RB suppression should be the primary target in the design of Rayleigh noise-resilient upstream receiver module in a WDM-PON with a reach up to 60 km. They can also predict well the system performance and are expected to serve as a design tool for optimizing the overall performance of a WDM-PON. DI's destructive port can also be used as a Rayleigh noise suppresser in the remodulation-based WDM-POM, as long as the spectrum of the downstream signal has a significant amount of low-frequency components. We propose and demonstrate a novel phase remodulation scheme with enhanced tolerance to Rayleigh noise.

In Chapter 4 we propose a novel offset Manchester coding for electrical-domain Rayleigh-noise suppression with relaxed linewidth requirement for seed lasers. We also propose a simple chirp-free optical Manchester signal transmitter which eliminates the conventional bandwidth doubling issue in optical Manchester signal generation.

In Chapter 5, we first introduce two TDM-based broadcast schemes. In one scheme the downstream unicast and broadcast signals are multiplexed via hybrid OTDM that requires no optical time demultiplexing. The other scheme is based on time-interleaved phase remodulation, with simplified structure in both transmitter and receiver. Then we realize multicast transmission via orthogonal modulation and flexible multicast control. The multicast control can be realized either by synchronization adjustment between the DPSK and the IRZ modulation on the downstream carrier, or by tuning the wavelength offset between optical source and DI. For both schemes, over one wavelength channel we have successfully demonstrated

30-Gb/s transmission of three different traffics, namely 10-Gb/s IRZ downstream point-to-point data, 10-Gb/s DPSK downstream multicast data, and 10-Gb/s OOK upstream re-modulated data, respectively, in a WDM-PON. The wavelength detuning-based multicast control is simpler since it is realized via the inherent wavelength management of WDM systems, rather than any other additional adjustment of signal's extinction ratio, synchronization, modulation formats, and others.

6.2.Suggestion on future work

As demonstrated in Chapter 3, the upstream DPSK signal is robust to Rayleigh noise as the DPSK demodulator (DI's destructive) can act as an effective Rayleigh noise suppressor. In this scheme, the phase modulator, located in customer's side, is an essential, cost-sensitive component. Photonic integration is one possible solution to lower the cost of external phase modulator [1], [2]. We may cooperate with device/component-related research groups to develop cost-effective integrated ONU module, based on which a long-reach, Rayleigh noise-resilient WDM-PON can be realized. RSOA can also be used a cost-effective phase modulator, as demonstrated in [3]. In that demonstration, coherent detection is necessary to enable long reach transmission in a WDM-PON with single feeder fiber and single distribution fiber. Based on the proposed schemes in Chapter 3, long reach transmission in a WDM-PON is possible even without using any coherent technology. We can further investigate the system performance when using RSOA as a phase modulator in the proposed schemes in Chapter 3.

Time-interleaved phase remodulation in Chapter 5 is realized via two cascaded

phase modulator. It can also be realized via one phase modulator that is driven by the combination of two time-interleaved data with the same bit rate. Note that the combination is realized via a passive combiner, and thus the combined signal has the same bandwidth with each of the original input data to the combiner. When using the combined signal to drive a RSOA (used as a phase modulator), it can potentially double the operation bandwidth of a RSOA.

As discussed in Chapter 4, Rayleigh noise induced crosstalk can also be suppressed in electrical domain with minor modifications to the conventional PON structure. However, the improvement in Rayleigh noise tolerance is around 10-dB less than that using the optical-domain schemes. Thus, for Rayleigh noise suppression the electrical-domain scheme still leaves much room for improvement. In addition, electronic signal processing is also a promising approach to meet PON's increasing demand on reach, loss budget and migration flexibility. A case in point is the emerging research interest in OFDM-PON and coherent-PON. Possibly we can pay more attention to the application of electronic signal processing in access network.

References

- [1] F. Y. Gardes, K. L. Tsakmakidis, D. Thomson, G. T. Reed, G. Z. Mashanovich , and O. Hess, "Micrometer size polarization independent depletion-type photonic modulator in Silicon On Insulator," *Opt. Exp.*, vol. 15, no. 9, pp. 5879- 5884, Apr. 2007.
- [2] J. Zhang, T. Y. Liow, G. Q. Lo, and D. L. Kwong, "10Gbps monolithic silicon FTTH transceiver without laser diode for a new PON configuration," *Opt. Express* 18(5), 5135–5141 (2010).

- [3] S. P. Jung, Y. Takushima, and Y. C. Chung, "Transmission of 1.25-Gb/s PSK signal generated by using RSOA in 110-km coherent WDM PON," *Opt. Express* 18, 14871–14877 (2010).

Appendix:

A. List of abbreviations

3D TV: three dimension television

AON: active optical network

APON: ATM PON

ASE: amplified spontaneous emission

AWG: arrayed waveguide grating

B2B: back-to-back

BER: bit error rate

BPON: Broadband PON

CD: chromatic dispersion

ch: channel

CIR: committed information rate

CLS: centralized light source

CO: central office

CW: continuous-wave

DBA: dynamic bandwidth allocation

DCM: dispersion compensation module

DFB: distributed fiber bragg

DI: delay-interferometer

DL: delay line

DM: differential monitoring

DPSK: differential phase-shift keying

DS: downstream

DSF: dispersion-shifted fiber

DSL: digital subscriber line

EAM: electroabsorption modulator

EDFA: erbium-doped fiber amplifier

EPON: Ethernet PON

ER: extinction ratio

FMD: full modulation depth

FP-LD: Fabry-Perot laser diode

FSK: frequency-shift keying

FTTC: fiber to the curb

FTTH: fiber to the home

FTTP: fiber to the premises

GPON: Gigabit PON

HDTV: high-definition television

HPF: high-pass filter

IM: intensity modulator

IPTV: Internet protocol TV

IRZ: inverse-return-to-zero

MC: Manchester coding

MLLD: mode-locked laser diode

MPDR: monitoring power dynamic range

MZM: Mach-Zehnder modulator

NGA: generation access network

NRZ: non-return-to-zero

OBF: optical bandpass filter

OLT: optical line terminal

OMC: offset-Manchester coding

ONU: optical network units

OOK: on-off keying

OTDM: optical time-division multiplexing

PC: polarization controller

PLC: planar lightwave circuit

PM: phase modulator

PON: passive optical network

PRBS: pseudorandom binary sequence

PtMP: point-to-multipoint

PtP: point-to-point

RB: Rayleigh Backscattering

RMD: reduced modulation depth

RMD-DPSK: DPSK signal with reduced modulation depth

RN: remote node

RoI: return on investment

RSOA: reflective semiconductor optical amplifier

RZ: return-to-zero

SMF: single mode fiber

SOA: semiconductor optical amplifier

TDMA: time-division multiple access

TDM-PON: time-division-multiplexed passive optical network

TEC: thermo-electric coolers

TLD: tunable laser diode

US: upstream

VOA: variable optical attenuator

VoD: video-on-demand

WDM-PON: wavelength-division-multiplexed passive optical network

B. List of publications

JOURNALS:

1. Z.X. Liu, Y. Qiu, **J. Xu** and C. K. Chan, "An Optical Multicast Overlay Scheme for a WDM PON using Inverse-RZ-Duobinary Signals," *IEEE Photonics Technology Letters*, vol. 23, no. 4, pp. 257-259, Feb. 2011.
2. W. Jia, **J. Xu**, Z.X. Liu, K.H. Tse and C. K. Chan, "Generation and Transmission of 10-Gb/s RZ-DPSK Signals using a Directly Modulated Chirp Managed Laser," *IEEE Photonics Technology Letters*, vol. 23, no. 3, pp. 173-175, Feb. 2011.
3. **J. Xu**, L.K. Chen and C.K. Chan, "Phase Modulation Based Loopback Scheme for Rayleigh Noise Suppression in 10-Gb/s Carrier-Distributed WDM-PONs," *IEEE Photonics Technology Letters*, vol. 22, no. 18, pp. 1343-1345, Sep. 2010.
4. **J. Xu**, K. M. Chong and L.K. Chen, "Delay-interferometer Based Timing Alignment Monitoring for Data and Clock Signal in Optical RZ-DPSK and RZ-OOK Systems," *Optical Fiber Technology*, vol. 16, no. 4, pp. 236 - 239, 2010.
5. **J. Xu**, Y. Zhang, L.K. Chen and C.K. Chan, "A Delay-based Multicast Overlay Scheme for WDM Passive Optical Networks with 10-Gb/s Symmetric Two-way Traffic," *IEEE OSA Journal of Lightwave Technology*, vol. 28, no. 18, pp.2660-2666, Sep. 2010.
6. **J. Xu** and L.K. Chen, "A New Remodulation Scheme for WDM-PONs With Enhanced Tolerance to Chromatic Dispersion and Remodulation Misalignment," *IEEE Photonics Technology Letter*, vol. 22, no. 7, pp. 456 -

458, 2010.

7. **J. Xu**, M.Li, L.K. Chen and C.K. Chan, "Rayleigh Noise Suppression in 10-Gb/s Carrier-Distributed WDM-PONs using In-band Optical Filtering," **submitted to *IEEE OSA Journal of Lightwave Technology***.

CONFERENCES:

8. P.L. Li, **J. Xu**, L.K. Chen, "A Novel Time-interleaved Phase Remodulation Scheme in WDM-PON with Enhanced Tolerance to Rayleigh Backscattering," *Opto-Electronics and Communications Conference, OECC 2011, Paper 5A4-3, Kaohsiung, Taiwan, 2011*.
9. **J. Xu**, Z.X. Liu, L.K. Chen and C.K. Chan, "Time-Interleaved Phase Remodulation to Enable Broadcast Transmission in Bidirectional WDM-PONs without Additional Light Sources," *IEEE/OSA Optical Fiber Communication Conference / National Fiber Optic Engineers Conference, OFC/NFOEC 2011, Paper OThK4, Los Angeles, California, USA, 2011*.
10. W. Jia, **J. Xu**, Z.X. Liu, C.K. Chan and L.K. Chen, "Generation of 20-Gb/s RZ-DQPSK Signal using a Directly Modulated Chirp Managed Laser," *IEEE/OSA Optical Fiber Communication Conference / National Fiber Optic Engineers Conference, OFC/NFOEC 2011, Paper OThE4, Los Angeles, California, USA, 2011*.
11. **J. Xu**, Z.X. Liu, W. Jia and L.K. Chen, "A Novel Chirp-free Optical Manchester Signal Transmitter with Enhanced Dispersion Tolerance," *Asia Communications and Photonics Conference and Exhibition (ACP) 2010, Paper SA 2, Shanghai, China*.
12. Z.X. Liu, **J. Xu**, Y. Qiu and C.K. Chan, "An 80-km-Reach

- Centralized-light-source WDM PON utilizing Inverse-RZ-Duobinary Downstream Signals,” *European Conference on Optical Communications, ECOC 2010, Torino, Italy, 2010.*
13. **J. Xu**, L.K. Chen and C.K. Chan, “Enhancement of Wavelength Offset Tolerance for Downstream DPSK Signals Demodulation in 10-Gb/s WDM-PONs,” *OptoElectronics and Communications Conference, OECC 2010, Paper 6A1-4, Sapporo, Hokkaido, Japan, 2010.*
 14. W. Jia, D. Shen, K.H. Tse, **J. Xu**, M. Li and C.K. Chan, “A Novel Scheme to realize a Power-efficient WDM Passive Optical Network,” *OptoElectronics and Communications Conference, OECC 2010, Paper 8A3-4, Sapporo, Hokkaido, Japan, 2010.*
 15. **J. Xu**, L.K. Chen and C.K. Chan, “High Extinction Ratio Phase Re-modulation for 10-Gb/s WDM-PON with Enhanced Tolerance to Rayleigh Noise,” *International Conference on Optical Internet, COIN 2010, Paper P1061, Korea, Jeju, 2010.*
 16. **J. Xu** and L.K. Chen, “Optical Phase Remodulation for 10-Gb/s WDM-PON with Enhanced Tolerance to Rayleigh Noise,” *IEEE/OSA Optical Fiber Communication Conference / National Fiber Optic Engineers Conference, OFC/NFOEC 2010, Paper OThG3, San Diego, California, USA, 2010.*
 17. Z.X. Liu, Y. Qiu, **J. Xu**, C.K. Chan and L.K. Chen, “A WDM-PON Optical Multicast Overlay Scheme Using Inverse-RZ-Duobinary Signal,” *IEEE/OSA Optical Fiber Communication Conference / National Fiber Optic Engineers Conference, OFC/NFOEC 2010, Paper OThG5, San Diego, California, USA, 2010.*
 18. **J. Xu**, Y. Zhang, L.K. Chen and C.K. Chan, “A WDM-PON with 10-Gb/s

Symmetric Bit-Rates and Multicast Overlay with Delay-Based Multicast Control,” *IEEE/OSA Optical Fiber Communication Conference / National Fiber Optic Engineers Conference* , **OFC/NFOEC 2009**, Paper NME5, San Diego, USA, Mar. 2009. **(Semifinalist of Corning Outstanding Student Paper Competition)**

19. K.M.Chong, **J. Xu** and L.K. Chen, “4-wavelength 2R regeneration based on self-phase modulation and inter-channel walk-off control in bidirectional fiber configuration,” *SPIE-OSA-IEEE Asia Communications and Photonics (ACP) 2009*, *SPIE Vol. 7632*, 763203, Shanghai, China, 2009.

US Patent:

20. **J. Xu**, L.K. Chen, C.K. Chan, “Methods and Systems for Multicast Control,” filed, application number: 12/955,730.